Optimal Energy Management in Microgrids with Integrated Multi-zone Heating/Cooling Control

OPTIMAL ENERGY MANAGEMENT IN MICROGRIDS WITH INTEGRATED MULTI-ZONE HEATING/COOLING CONTROL

BY

GUOTAO LIN, B.Sc.

A THESIS

SUBMITTED TO THE DEPARTMENT OF ELECTRICAL & COMPUTER ENGINEERING

AND THE SCHOOL OF GRADUATE STUDIES

OF MCMASTER UNIVERSITY

IN PARTIAL FULFILMENT OF THE REQUIREMENTS

FOR THE DEGREE OF

MASTER OF APPLIED SCIENCE

Master of Applied Science (2014) McMaster University

(Electrical & Computer Engineering) Hamilton, Ontario, Canada

TITLE:	Optimal Energy Management in Microgrids with Integrated Multi-zone Heating/Cooling Control
AUTHOR:	Guotao Lin B.Eng., (Automation, Control Science and Engineering) Zhejiang University, Hangzhou, P.R. China
SUPERVISOR:	Dr. Shahin Sirouspour, Dr. Ali Emadi
NUMBER OF PAGES:	xvii, 105

This thesis is dedicated to my beloved parents and grandparents.

Abstract

There is a growing need for technologies that can help integrate distributed renewable energy and storage capacity into the electricity grid and increase the efficiency of its operation. Microgrids provide an effective framework for achieving these objectives. The energy consumed in buildings accounts for a significant part of the total energy demand. Space conditioning, which includes heating, ventilation and air conditioning (HVAC), is the largest contributor to the building energy consumption. Therefore, combined management of heat and power in microgrids can potentially yield substantial energy and cost savings.

This thesis presents an integrated approach to energy/power management and control of a HVAC system in a grid-connected microgrid with energy storage. The control strategy is based on an on-line optimal model predictive control philosophy. An optimization problem is formulated and solved over a rolling horizon using a model of the system and predicted microgrid load and outside temperature to obtain optimal control decisions, i.e. the energy storage charge/discharge power and HVAC control commands. The overall problem is formulated as a constrained optimization in the form of a mixed integer linear program (MILP), with the objective of minimizing energy cost subject to model and operational constraints.

First, a single temperature zone configuration is presented where only one temperature variable is controlled throughout the building. The controller maintains the

building temperature within user-defined upper and lower limits, which may also be determined based on occupancy. By employing auxiliary on-off controllable fans in the temperature zones, a multi-zone control strategy is also proposed to independently regulate the zone temperatures within their corresponding comfort limits. Several strategies for reducing real-time computations of the controller are also proposed. Simulations have been carried out under different scenarios including single-zone and multi-zone cases that demonstrate significant efficiency gains from the application of the proposed controller for energy management and HVAC control in a microgrid system. Sensitivity of the system performance with respect to modeling errors and uncertainty is examined in a number of simulations. The results demonstrate a robust behavior due to an inherent feedback mechanism in the proposed rolling horizon model predictive controller.

Acknowledgements

Foremost, I would like to express my sincere gratitude to my supervisors, Dr. Shahin Sirouspour and Dr. Ali Emadi, for their guidance and support throughout this study, for their patience, encouragement and immense knowledge.

Many thanks to Dr. Pawel Malysz for guiding my study and research for the past two years. I would like to thank my fellow colleagues in my group, Adihithya Ravichandran, Berker Bilgin, Eric Yu, Fei Peng, Ran Gu, Zhe (Jason) Sun, Jianing (Joanna) Lin, Abdul Lateef, Hao Ge, Haizhong Ye, Jin Ye, Weisheng Jiang, Yinye Yang, Chia-Hao Tu, Earl Fairall, Jing Guo, Rong Yang, Teng Guo and Yingguang Sun for their help in my research. I would like to thank Bahram Marami, Saman Rahnamaie, Mohammad Jafarifnasab, Shadi Emami, Raheleh Khodabakhsh, Fany Mendez and other colleagues in the Telerobotics, Haptics and Computational Vision laboratory for helping and encouraging me.

Special thanks to my family and my friends for their understanding, supporting and encouragement since they have made it possible for me to accomplish my graduate study.

Notation and abbreviations

Notations and abbreviations:

AEMS - Adaptive Energy Management System

AFUE - Annual Fuel Utilization Efficiency

BTU - British Thermal Unit

cfm - cubic feet per minute

CHP - Combined Heat and Power

COP - Coefficient of performance

DER - Distributed Energy Resources

DG - Distributed Generations

HP - Horsepower

HVAC - Heating, Ventilation and Air Conditioning

kW - kilowatts

kWh - kilowatts-hours

LP - Linear Program

MILP - Mixed Integer Linear Program

MPC - Model Predictive Control

PDF - Probability Distribution Function

PHEV - Plug-in Hybrid Electric Vehicle

RES - Renewable Energy Sources

RPM - Revolutions Per Minute

SHR - Sensible Heat Ratio

SP - Static Pressure

TOU- Time-of-Use

Contents

List of Figures

Chapter 1

Introduction

1.1 Motivation

A rising demand for energy has become a major concern for business, industry and government organizations. With economic development, more energy will be consumed in residential, commercial, transportation and industrial sectors. The evolution of the total energy consumption by different end-use sectors for the last 65 years in the US is shown in Figure 1.1. Primary energy consumption in the residential/commercial sectors accounts for about 40% of the total energy consumption in the year 2013 (USEIA, 2014).

The energy is supplied mostly from fossil fuels and the reliance on fossil fuels contributes to climate change due to increasing emission of greenhouse gases. Increasing temperatures have led to the rise of air conditioning costs, and increasing frequency and intensity of extreme weather events such as storm, flooding and sea level rise have challenged the current electric power systems.

Short supply of fossil fuels, more frequent power outages and climate change have led to an increasing need for renewable energy resources such as wind and solar energy

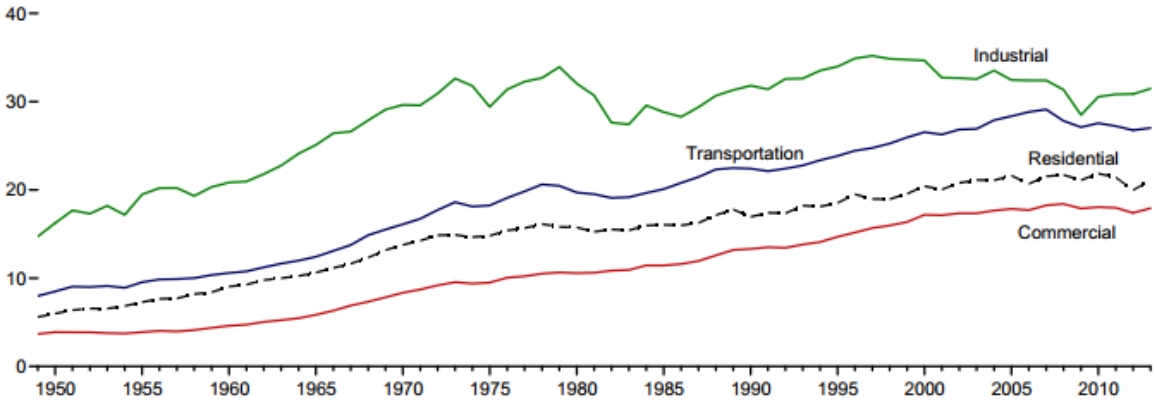

Figure 1.1: Total Energy consumption by end-use sector (quadrillion British Thermal Unit (BTU)), 1949-2013. (USEIA, 2014)

to provide more sustainable and greener energy. It has been recognized that microgrids with energy storage are one of the most effective ways to address these problems and to improve the reliability and resiliency of the power supply system with integration of renewable energy generation.

Figure 1.2 shows that the total energy consumption in U.S. homes has remained relatively stable for 30 years. This can be attributed to the increased energy efficiency that has offset the increase in the number and average size of housing units. In fact, energy consumption per household has retained a downward trend primarily thanks to improvements in efficiency for space heating, air conditioning, and other major appliances. Despite all this progress, there is still a great potential for energy and cost saving by utilizing new technologies and control strategies to improve energy efficiency.

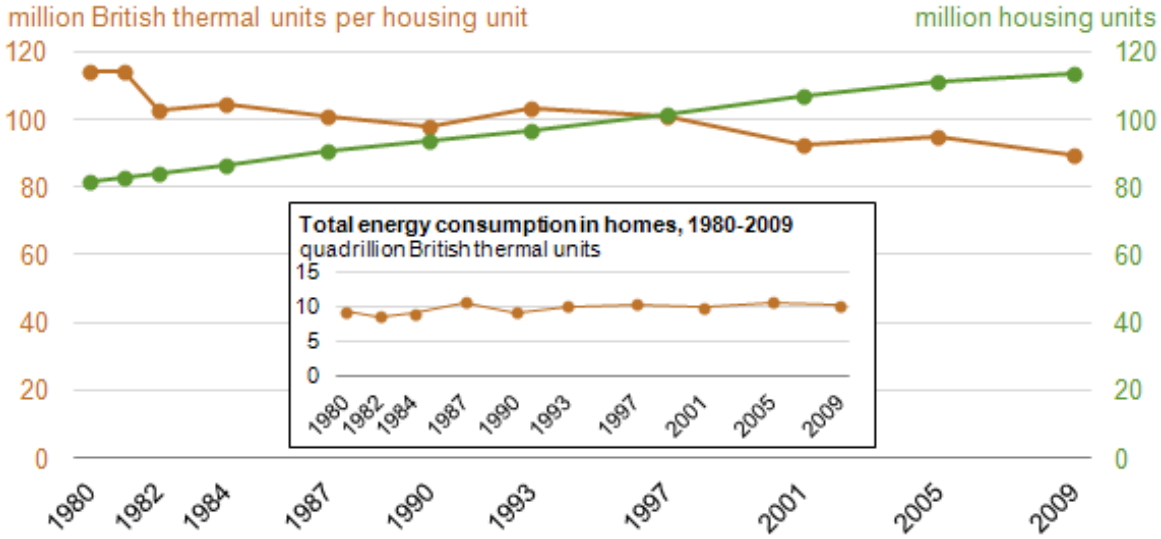

Figure 1.2: Average energy consumption per home and number of housing units, 1980-2009. (USEIA, 2009)

As illustrated in Figure 1.3, the energy consumed in households is mainly provided by electricity and natural gas. The use of electricity has grown for many years in the residential sector. Significant electricity-related losses can be observed by comparing the energy consumption on site (left) to energy consumption of primary fuels (right). Most of these losses can be attributed to long distance transmission from the generation sites to consumers. Microgrids can help integrate distributed renewable energy resources into the grid and reduce transmission losses. Energy savings can also be realized by efficiently managing electricity and natural gas uses in building microgrids.

Microgrids have emerged as one possible key to solve the problems caused by the rising energy consumption and climate change as mentioned above. They are the key to the transformation of the traditional electricity grid towards a smarter grid with distributed energy resources. Efficient integration of renewable energy through the use of electricity storage devices in microgrids can help reduce electricity loss, especially transmission loss. Microgrids can improve the reliability of the grid by adding local

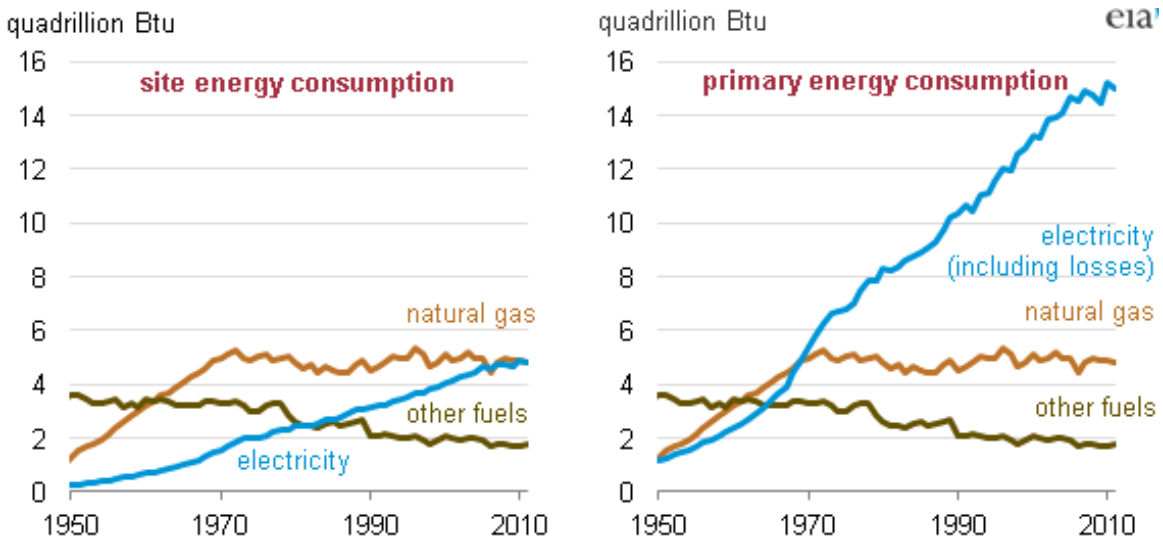

Figure 1.3: Residential energy consumption, 1950-2011. (USEIA, 2011)

inertia (storage). Microgrids can also reduce peak demand by employing demand-side control, which decreases the variation between on-peak and off-peak demand and improves the reliability of the power supply. Recognizing their potentially enormous benefits and critical role in a smarter grid of the future, substantial efforts have been devoted to developing methods and techniques for intelligent operation of microgrids within the larger electricity grid. Efficient energy management is the key to realizing many of the benefits associated with microgrids.

In residential and commercial building microgrids, the heating, ventilation and air conditioning (HVAC) systems are the largest contributor to the energy consumption. As shown in Figure 1.4, 48% of the energy consumption in U.S. homes in 2009 was for space heating and air conditioning, which is mainly consumed by HVAC systems. Therefore an integrated microgrid energy management approach which includes the HVAC control can yield potentially substantial energy savings, where the temperature control would be integrated into the energy management to provide thermal and air quality comfort in buildings.

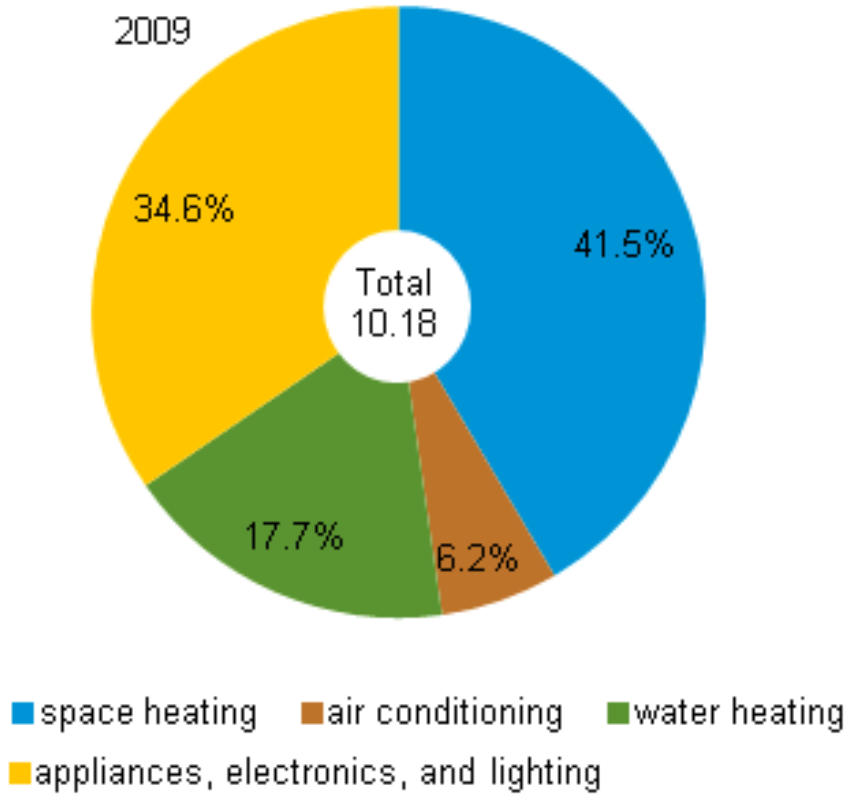

Figure 1.4: Energy consumption in homes by end uses (quadrillion BTU and percentage). (USEIA, 2009)

1.2 Problem Statement and Thesis Contributions

This thesis is concerned with integrated control of temperature and energy/power flows in grid-connected residential and commercial microgrids with local energy storage and possibly renewable energy sources.

The concept of combined heat and power - adaptive energy management system (CHP-AEMS) is depicted in Figure 1.5. The control of the HVAC system is integrated with the energy management system, which enables energy efficient operation of microgrids and HVAC system for space conditioning and heating. The idea is to

control the power flow within microgrids and in relation to the external power grid, as well as the operation of the HVAC system to maintain comfortable temperatures in the building. As an essential element of this system, the electric energy storage can be on-site dedicated storage such as a battery and/or a bi-directional plug-in hybrid electric vehicle (PHEV).

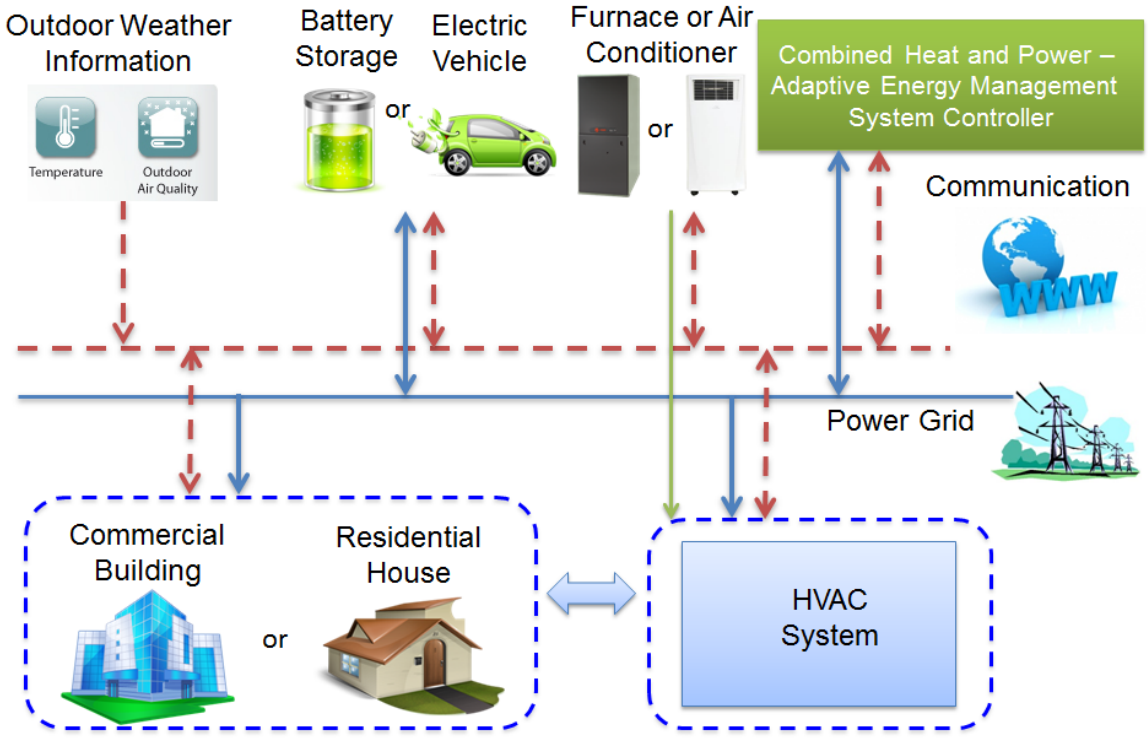

Figure 1.5: System configuration for CHP-AEMS.

An on-line optimal energy management strategy with HVAC control in grid-connected microgrids using a Mixed Integer Linear Program (MILP) based Model Predictive Control (MPC) approach is proposed in this thesis. The main objective of the control is to minimize the total energy cost, which is achieved subject to power and temperature constraints. The control decisions are energy storage charge/discharge commands as well as on-off commands for the HVAC system. Single-zone model is

studied first, where only one temperature zone is considered. Then simultaneous independent temperature control in multiple zones is proposed, where each zone has an auxiliary controllable fan in addition to the main system fan. Instead of strictly regulating the zone temperatures, the system allows for temperature variations within so-called (variable) comfort limits, which in principle could be determined based on zone occupancy. The optimal energy management controller can take advantage of this extra flexibility in temperature control by performing pre-cooling/heating with cheaper energy, whenever feasible, to reduce the cost further.

Special care has been taken to reduce the computations of the proposed controller to enable its real-time implementation. This includes posing the problem as MILP optimization as opposed to a nonlinear optimization as done in the prior work on temperature control. Fast and efficient algorithms are available for solving this particular form of optimization problems. Furthermore, the use of variable-length time steps and relaxing optimization constraints in future time steps can substantially reduce computation time with negligible impact on the system performance. The sensitivity of the system performance with respect to errors in the model parameters and uncertainty in outside temperature predictions is also studied. Simulation results under various operational scenarios including single-zone and multi-zone cases are presented to show the effectiveness of the proposed optimal control methodology.

In summary, the contributions in this thesis are:

- Temperature control is integrated with the energy management system.
- Multi-zone model for temperature control is developed by adding an auxiliary controllable fan for each thermal zone.
- Allow for temperature variations between the desired limits, which can be used to reduce cost further by performing pre-heating/cooling with cheaper energy.

- Formulate the nonlinear problem into MILP optimization problem by introducing HVAC system states.
- Variable time steps and optimization constraints relaxation are used to reduce computation time.

1.3 Thesis Organization

The rest of the thesis is organized as follows. Chapter 2 reviews the literature on microgrids and temperature control. This is followed by the system component and dynamic modelling in Chapter 3. Chapter 4 presents single-zone temperature control and energy management. The overall optimization formulation is developed and the system performance is evaluated under various operational scenarios. Chapter 5 extends the strategy to multi-zone temperature control and energy management and includes results of simulations under a number of operational scenarios to assess the system performance. The sensitivity of the system performance to modelling errors and uncertainty in outside temperature prediction is also studied in this chapter. The thesis is concluded in Chapter 6 where some possible directions for future work are discussed.

1.4 Related Publications

- Lin, Guotao, Malysz, Pawel, Sirouspour, Shahin, and Emadi, Ali. (2014, July). Optimal Microgrid Energy Management with Multi-zone Temperature Control and Energy Storage. Smart Grid, IEEE Transactions on(submitted).

Chapter 2

Literature Review

This chapter is divided into two sections. The first section presents a review of the literature on microgrid and its components modelling. Prior work on microgrid control and optimization-based control strategies of microgrids are also briefly surveyed in this chapter. The second section looks at pertinent literature on temperature control and HVAC systems control.

2.1 Microgrid Modelling and Control Strategies

Microgrids are systems that have distributed generation, energy storage and associated loads and usually operate connected to a traditional centralized grid (macrogrid). They can also be disconnected from the macrogrid to form intentional islanded grids with minimal disruption to local power system. There has been significant research on modelling and control strategies of microgrids in recent years. A number of relevant microgrid models and control strategies are briefly discussed below.

2.1.1 Off-line Energy Management Methods

Off-line optimization-based energy managements in microgrids have been explored in the literature. In off-line methods, a series of control decisions are determined by solving an optimization problem once in advance of the actual control. In (Deng *et al.*, 2011), an offline optimization approach is proposed to minimize both energy cost and emission in a microgrid, including a wind turbine, pv array and a combined heat and power (CHP) system. The optimization problem is solved by employing a genetic algorithm to achieve an operation scheme considering tariff details, weather conditions and forecasts, load details and forcasts etc. A mixed integer linear program (MILP)-based optimization of a combined heat and power (CHP) distributed generation system is proposed in (Bracco *et al.*, 2013) which considers capital and operational costs as well as carbon dioxide emissions. The work in (Stadler, 2008) investigates the impact of storage technologies on the energy management in microgrids in terms of demand response and carbon emission. It formulates a MILP optimization of distributed energy resources to determine optimal hourly operating schedules and minimize the overall energy cost. In (Handschin *et al.*, 2006), a stochastic based MILP optimization method for offline dispatch scheduling is proposed to minimize the energy cost and maximize revenue. A mathematical model integrating dispersed generations is developed and solved under the uncertainties.

In (Costa and Fichera, 2014), a method for sizing cogeneration plants in hospitals based on MILP optimization is proposed. A two-fold objective consisting of minimizing the operational cost and determining the optimal sizing of the CHP to be installed could be achieved. In (Guo *et al.*, 2013), a two-stage design and optimal planning strategy is developed for a combined cooling, heat and power (CCHP) system to determine its optimal operation scheduling and minimize the net present cost

and carbon dioxide emissions during its life circle. First, the design optimization is solved by a genetic algorithm and then a MILP optimization is formulated and solved to determine the dispatch strategy. The work in (De Oliveira *et al.*, 2011) describes a multi-layer formulation of home electricity management using MILP to minimize energy cost while meeting the occupants' comfort requirements. An optimization-based approach for the design and component sizing of microgrids is proposed in (Yu, 2014; Yu *et al.*, 2014). A MILP optimization problem is formulated with the objective of minimizing combined capital and electricity usage cost for a microgrid with energy storage and renewable generation.

From the above, the off-line control is relatively simple and easy to implement, but not so robust to modelling errors and uncertainty due to lack of in-time feedback to correct the operations in real-time. In the off-line method, the system performance is sensitive to the errors of model parameters and uncertainty.

2.1.2 On-line Energy Management Methods

There has also been significant research on online optimization-based energy management in microgrids. In on-line methods, control decisions are determined by solving an optimization problem every time step over rolling horizon, which increases the computation burden for controller. But the robustness of the system performance can be achieved by utilizing this feedback mechanism that compensates for modelling errors and uncertainty.

In (Lefort *et al.*, 2013), a hierarchical approach to energy management based on model predictive control (MPC) is proposed to minimize the energy cost considering time-varying electricity prices and local production while respecting constraints imposed by the occupants and the installations. A long time horizon MPC is solved at

the higher level. A second optimization problem with a shorter horizon is solved at the lower level. In (Mehleri *et al.*, 2012), a MILP-based MPC for microgrid design and energy management is presented, investigating cases with and without electricity storage. The optimization problem is solved for operational schedules over rolling horizon in microgrid, involving photovoltaic arrays and micro-combined heat and power (micro-CHP) system. In (Parisio *et al.*, 2014), an online MPC-MILP control scheme is proposed for minimizing overall microgrid operating costs while satisfying the operation constraints. By formulating the MILP optimization problem, improvement of solution quality and reduction of computational time could be achieved. The proposed method has been tested in an experimental microgrid in Athens, Greece. The work in (Malysz *et al.*, 2014) presents a robust formulation of the MILP optimization to account for uncertainties in load and demand prediction. Their online MILP-based energy management strategy for grid-connected microgrids simultaneously considers energy cost, battery operation cost, grid power peak reduction and power smoothing objectives (Malysz *et al.*, 2013, 2014). In (Bozchalui *et al.*, 2012), a MILP optimization-based scheduling of residential energy hubs is presented with the objectives of minimizing demand, total cost of electricity and gas, emissions and peak load. Some mathematical models of major components of a residential microgrid are also developed in this paper. Similarly, MILP optimization is used in (Kriett and Salani, 2012) to minimize the operating cost of a residential microgrid.

2.2 Temperature Control and HVAC systems

Researchers have investigated thermal energy management in microgrids using optimization-based techniques. Most of the past work formulates nonlinear optimization problems

for microgrid energy management. In (Marco *et al.*, 2014), smart home task and energy resource scheduling is proposed by using mixed integer nonlinear programming (MINLP), which deals with nonlinearities from the building thermal constraints. The overall energy cost savings and thermal requirement satisfactions could be attained. In (Zhang *et al.*, 2012), the authors present a control strategy for CCHP based on MINLP optimization for a rural microgrid with the objectives of improving energy efficiency and lessening environment problems caused by animal waste. An energy management strategy is proposed in (Pascual *et al.*, 2014) for an electro-thermal microgrid, taking into account renewable generation, hybrid electro-thermal storage system, water heater, and HVAC system, to optimize power dispatch and exchange with the grid. Optimization-based control of HVAC systems is considered in (Muratori *et al.*, 2012) and (Yang and Wang, 2012) with the aim of reducing energy cost; the resulting problem is solved using a particle swarm optimization technique. In (Anderson *et al.*, 2007), the modeling and control of HVAC system are discussed in detail, involving controlling the temperature and air flow rate.

Multi-zone control of HVAC systems has been considered in the literature before. However, the problem has usually been formulated as a nonlinear program optimization, which is difficult to solve in real time. In (Mossolly *et al.*, 2009), optimal control formulations have been developed for a multi-zone air conditioning system. The resulting optimization problems are solved by a genetic algorithm. A distributed predictive control strategy for building temperature control is proposed in (Morosan *et al.*, 2010), which is also extended for multi-zone temperature control. In (Xu *et al.*, 2013), a pre-cooling optimization approach is proposed in order to reduce peak demand and energy cost. A particle swarm optimization algorithm is used to find a near optimal solution for multi-zone temperature regulation. In (Huang *et al.*, 2013), the authors propose artificial neural networks (ANNs) modelling for temperature prediction in

multi-zone building.

From the review of the literature above, it is apparent that MINLP, MILP or MPC-based optimizations have been proposed for energy management in microgrids. However in cases where thermal management has been included as part of energy management, the focus has been mostly on single zone systems without explicit control of the temperature. The papers that have addressed temperature control using optimization-based techniques, do so by formulating nonlinear optimization problems, which are difficult and time consuming to solve and may even become infeasible.

Chapter 3

System Modelling

This chapter is divided into two sections. The first section presents the models of individual components of the microgrid including the fan, heating unit, cooling unit and electrical system. The second section develops the overall system dynamic model, where the multi-zone ventilation model is also presented. Then continuous-time temperature dynamics and their discretization in the time domain are also discussed.

3.1 Models of Individual Components

The microgrid of interest involves distributed energy resources, such as solar and wind generation, energy storage, and controllable loads. As the largest contributor to the loads, a typical HVAC system contains a supply air system, return air system, heating/cooling units, fans, air filters and dampers. A block diagram of the system including the HVAC unit is shown in Figure 3.1.

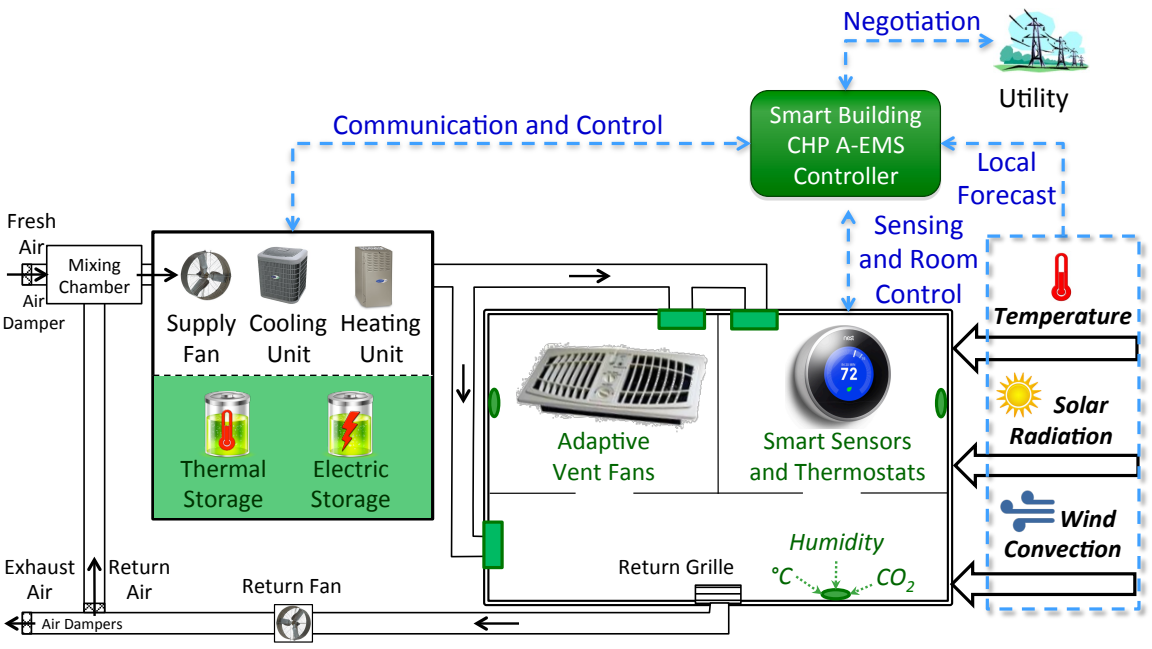

Figure 3.1: Combined heat and power microgrid for multi-room energy control.

3.1.1 Fan Model

For a constant speed fan, the power is modelled as a function of air flow rate and pressure drop (Muratori *et al.*, 2012),

$$P_{fan} = \frac{F_{volume} \Delta P_{tot}}{\eta_{fan} \eta_{motor}} \tag{3.1}$$

where P_{fan} is the power of fan (kW); ΔP_{tot} is the pressure drop (Pa); F_{volume} is the air volume flow rate (m^3/h); η_{fan}, η_{motor} are the efficiencies of fan and motor, respectively.

3.1.2 Heating Unit Model

Heating can be provided by fossil fuels, e.g. using natural gas furnace, or by electric furnace. The heating power can be modelled as (Yang and Wang, 2012)

$$P_{heat} = \frac{F_{supply} c_p (T_{supply} - T_{mix})}{\eta_{heat}} \tag{3.2}$$

where P_{heat} is the power of the heating unit, furnace (kW); η_{heat} is the efficiency of the heating unit; $c_p = 1006 J/(kgK) = \frac{1006}{3.6\times10^6} kWh/(kgK)$ is the specific heat capacity of air; F_{supply} is the mass flow rate of the supply air (kg/h); T_{supply} is the temperature of the supply air (°C).

The temperature of the mixed air from the mixing chamber can be derived as (Yang and Wang, 2012)

$$\begin{aligned} T_{mix} &= \frac{(F_{supply} - F_{return})T_{out} + F_{return}T}{F_{supply}} \\ &= (1-\lambda)T_{out} + \lambda T \end{aligned} \tag{3.3}$$

where $\lambda = \frac{F_{return}}{F_{supply}}$ is an air mixture ratio which is dependent on the design/configuration of the air dampers; F_{return} is the mass flow rate of the return air (kg/h); T_{out} is the outside temperature (°C); T is the room temperature (°C).

Basic Furnace Model

Basic features of typical existing furnaces for use in residential and commercial buildings have been investigated and their models have been discussed by (Lutz *et al.*, 2004). The fundamental characteristics of non-condensing and condensing non-weatherized gas furnaces are described in Table 3.1. These characteristics are the most common among the models on the market. We may choose $\eta_{heat} = 80\%$ *or* 90% depending on

the kind of furnace in use. Available combinations of input capacity and maximum airflow for different furnace models are shown in Table 3.2. The airflow capacity is defined as the nominal maximum airflow at 0.5 inches water gauge (in.w.g.) external static pressure. The data spans over twelve input capacities and four airflow capacity sizes. The four airflow capacities correspond to nominal air-conditioner sizes of two tons, three tons, four tons and five tons, respectively. The marked cells reflect the most common input and nominal maximum airflow capacities of commercial models.

Table 3.1: Characteristics of basic furnace models (Lutz *et al.*, 2004)

Non-Condensing Gas Furnace	**Condensing Gas Furnace**
single-stage	single-stage
80% AFUE	90-90% AFUE
permanent split capacitor (PSC) blower motor	PSC blower motor
forward-curved impeller blades	forward-curved impeller blades
up-flow or horizontal air-flow	down-flow, up-flow, or horizontal air-flow

Table 3.2: Furnace models: capacity and airflow (Lutz *et al.*, 2004)

		Input Capacity (kBtu/h)											
Maximum Airflow (at 0.5″ Static Pressure)		45	50	60	70	75	80	90	100	115	120	125	140
	800 cfm (2 tons)	x	x	x									
	1200 cfm (3 tons)	x	x	x	x	x	x	x	x				
	1600 cfm (4 tons)				x	x	x	x	x	x	x	x	
	2000 cfm (5 tons)							x	x	x	x	x	x

The fan sizes, listed as nominal diameter in inches by nominal width in inches, can be decided by the airflow capacity for the furnace model. As shown in Table 3.3,

the fan size increases with airflow capacity, but not with input capacity. The most common fan motors are six-pole permanent split capacitor (PSC) induction motors. Available motor sizes are also shown in Table 3.3. The motor size increases with the nominal maximum airflow as the fan size does.

Table 3.3: Assigned fan and motor size by airflow capacity (Lutz *et al.*, 2004)

Airflow Capacity (cfm)	**Fan Size (inches)**	**Motor Size (HP)**
2-ton models (800 cfm)	9×8	1/5
3-ton models (1200 cfm)	10×8	1/3
4-ton models (1600 cfm)	10×10	1/2
5-ton models (2000 cfm)	11×10	3/4

3.1.3 Cooling Unit Model

In summer operation, the HVAC system performs air conditioning. The cooling power can be modelled as (Yang and Wang, 2012)

$$P_{cool} = \frac{F_{supply} c_p (T_{mix} - T_{supply})}{\eta_{cool}} \tag{3.4}$$

$$\eta_{cool} = COP \tag{3.5}$$

where P_{cool} is the input power of air conditioner; η_{cool} is the efficiency of the air conditioner; COP is the coefficient of performance, defined as the thermal energy removed from the building per unit of electric energy absorbed by the HVAC system,

$$COP = \frac{EER}{3.412} \tag{3.6}$$

where EER represents the Energy Efficiency Ratio, which is the ratio of output cooling energy in BTU to input electrical energy in Wh for a particular cooling device.

3.1.4 Electrical System Model

The model here is not about the actual power circuit operation and transient events, but rather a simple active power flow model for the use in energy management. The load can be powered from grid or the storage. The power balance equation is

$$\mathbf{p}_g = \mathbf{p}_d + \mathbf{p}_s \tag{3.7}$$

where $\mathbf{p}_g$ is the grid power for buying or selling (kW), $\mathbf{p}_s$ is the battery charging/discharging power (kW), and $\mathbf{p}_d$ is the power demand (kW).

On-site electric energy storage is modelled as an integrator with discrete-time dynamics:

$$E_k = E_{k-1} + \mathbf{h}_k \mathbf{p}_{s_k} \tag{3.8}$$

where E_k is the energy level of the battery (kWh) at the k^{th} time step; p_{s_k} is the battery power (kW) at the k^{th} time step; h_k is the k^{th} time step (h).

It is noted here that more complex forms of the battery model can be developed to take into account inefficiencies, self-discharge, and asymmetry. The reader is referred to (Malysz *et al.*, 2013, 2014) for such examples where additional variables/constants would need to be introduced. The simplified model in (3.8) will be used throughout the thesis.

3.2 System Dynamic Modelling

3.2.1 Multi-zone Ventilation Modelling

A building ventilation model has been developed in (Masy, 2008) using an analogy from electric circuits. In this model, pressure and airflow rate correspond to electric

potential and current, respectively. Fan powered air flows are represented by current sources in this model.

Fan Model

An HVAC fan creates pressure differential to deliver air flow to rooms in the building. A fan can be characterized by a curve relating its flow rate (CFM) to the flow static pressure (SP) at a constant speed (rpm). The static pressure decreases with the airflow rate, as shown in Figure 3.2. The fan curve moves outward or inward depending on the speed, however the general shape of the curves remains the same.

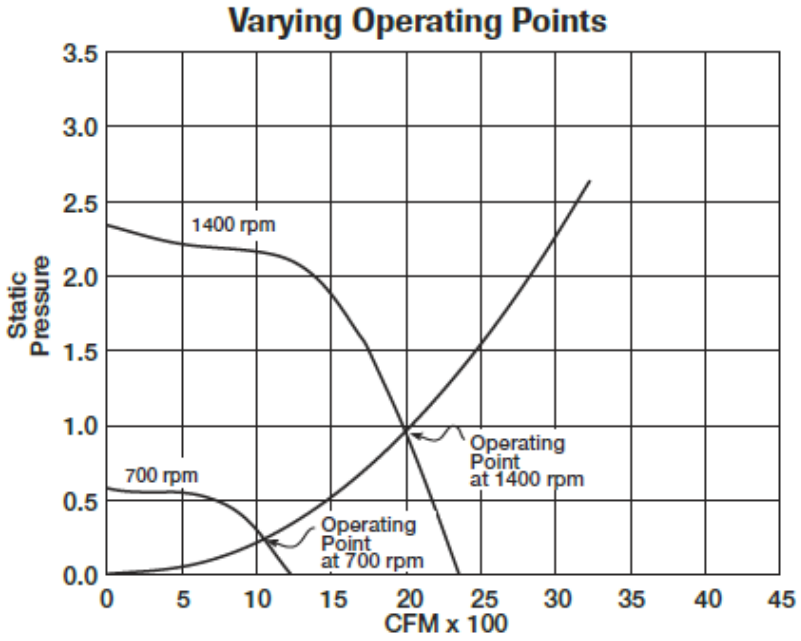

Figure 3.2: Fan curve and system resistance curve. (Dayton, 2005)

Load Resistance

For a building or a room, the airflow rate is a function of specific resistance to airflow (SP). The resistance is produced by the air distribution system, including ductwork, dampers, grills, coils and so on. All static pressure drops constitute this resistance as

air flows through the building system. The series of the static pressure and airflow rate points give the system resistance curve. As it is illustrated in Figure 3.2, the operating point is the intersection of the fan curve and system resistance curve.

The relationship between the static pressure and airflow rates for a room can be approximated as (Masy, 2008)

$$\Delta p = K \times F^2 \tag{3.9}$$

where K is the friction loss coefficient, which is related to the structure and components of the air distribution system ($Pa \cdot (h/kg)^2$), F is the air mass flow rate (kg/h), and Δp is the pressure drop (Pa).

Ventilation System Modelling

With the introduction of the system resistance, the multi-zone ventilation system can be modelled as in Figure 3.3. The resistances are produced by the air ducts, dampers, grills or orifices. The model can be further simplified by combining the resistances in each zone/room, as shown in Figure 3.4.

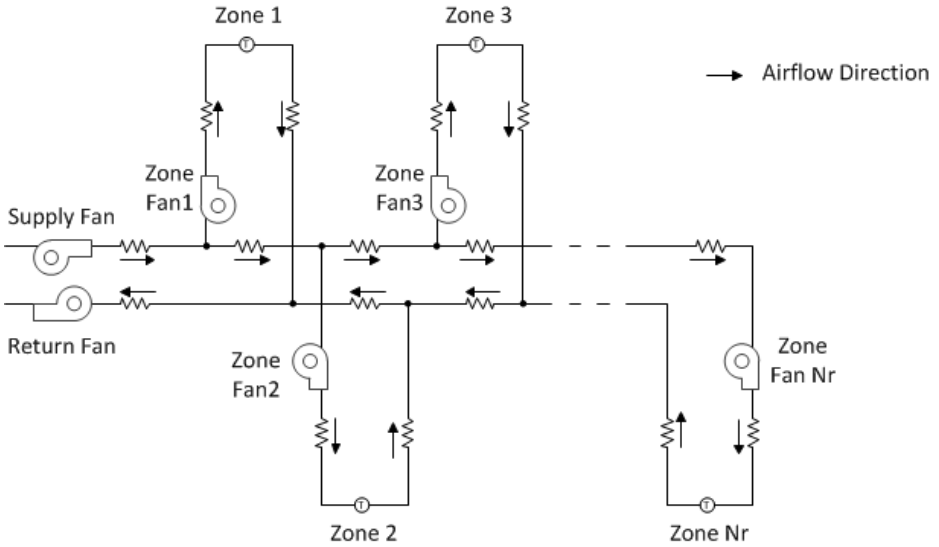

Figure 3.3: Ventilation model including supply and return air system.

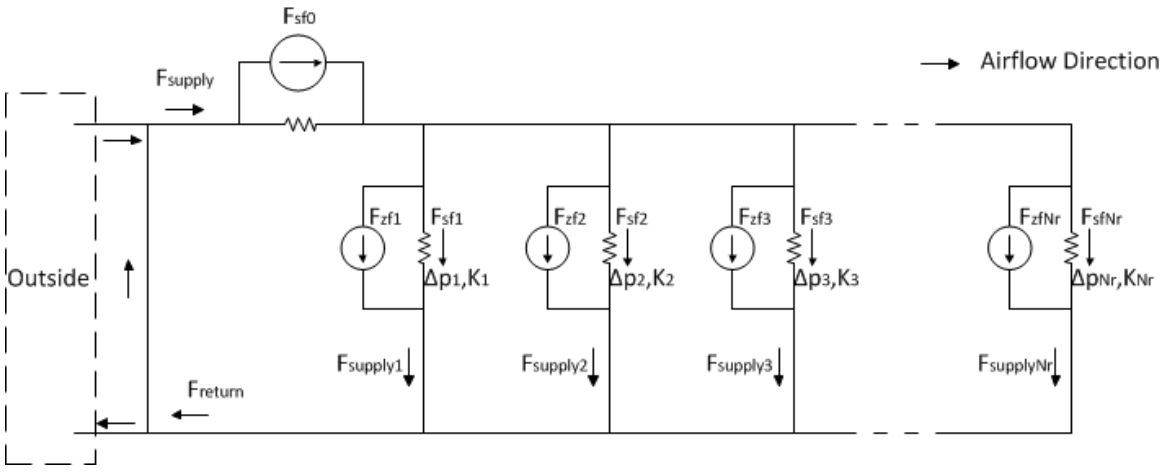

Figure 3.4: Simplified ventilation model.

The friction loss coefficient K_i stands for the friction loss level of the i^{th} path through the i^{th} room. The friction loss coefficients are constant and can be determined from the length and structure of the airflow path/ducts. Then we have

$$\Delta p_i = K_i \times (F_{supply_i})^2, \;\; i \in [1, N_r] \tag{3.10}$$

where F_{supply_i} is the air mass flow rate through the i^{th} zone/room, and N_r is the number of rooms in the building.

The rooms in the building are paralleled and the static pressures at the air entrance for each room are equal as well as the static pressure at the air exit for each room. Therefore, the static pressure drop Δp_i for each path/room should be equal. Then we can write

$$\Delta p = K_1 \times (F_{supply_1})^2 = K_2 \times (F_{supply_2})^2 = \cdots = K_{N_r} \times (F_{supply_{N_r}})^2 \tag{3.11}$$

$$\begin{aligned} F_{supply_1} : F_{supply_2} : \cdots : F_{supply_{N_r}} &= \frac{\sqrt{\Delta p}}{\sqrt{K_1}} : \frac{\sqrt{\Delta p}}{\sqrt{K_2}} : \cdots : \frac{\sqrt{\Delta p}}{\sqrt{K_{N_r}}} \\ &= \frac{1}{\sqrt{K_1}} : \frac{1}{\sqrt{K_2}} : \cdots : \frac{1}{\sqrt{K_{N_r}}} \end{aligned} \tag{3.12}$$

The air flow rate generated by the main supply fan is denoted as F_{sf_0}. Assume that the zone fans are the same. The air flow rate generated by the zone fan is F_{zf_i}, which is related to the resistance in each zone. Then the airflow distribution of the main supply airflow should be

$$F_{sf_i} = F_{sf_0} \times \frac{\frac{1}{\sqrt{K_i}}}{\sum_{j=1}^{N_r} \frac{1}{\sqrt{K_j}}}, \;\; i \in [1, N_r] \tag{3.13}$$

The airflow rate through each room could be calculated from

$$F_{supply_i} = F_{sf_i} \times \delta_{sfan} + F_{zf_i} \times \delta_{zfan_i}, \;\; i \in [1, N_r] \tag{3.14}$$

where $\delta_{sfan}, \delta_{zfan_i}$ are the main supply fan and the i^{th} zone fan on/off operation states, respectively.

3.2.2 Continuous-time Temperature Dynamics

Room temperature dynamics can be expressed as a coupled first-order dynamic system of the form (Muratori *et al.*, 2012)

$$\begin{aligned} m_i c_p \frac{dT_i}{dt} &= \kappa_{out,i}(T_{out} - T_i) + \sum_{j=1}^{N_r} \kappa_{j,i}(T_j - T_i) \\ &\quad + F_{supply_i} c_p (T_{supply} - T_i) \end{aligned} \tag{3.15}$$

where $i \in [1, N_r]$, T_i, T_{out}, and T_{supply} are the air temperatures of the i^{th} room, outside air, and HVAC supply, respectively; m_i is air mass dependent on room size, $\kappa_{j,i}$ and $\kappa_{out,i}$ are heat conductivities of room walls, and F_{supply_i} is the air flow rate into the i^{th} room.

The HVAC system supply air, as depicted in Figure 3.1, is fed by a mixture of the return air and outside air; it is then heated by a gas/electric furnace or cooled by an air conditioning unit before being distributed to the rooms. The supply air temperature can be obtained

$$\begin{aligned} T_{supply} &= (1-\lambda)T_{out} + \lambda T_{return} + \frac{\eta_{hvac} P_{hvac}}{F_{supply} c_p} \\ &= (1-\lambda)T_{out} + \lambda \sum_{i=1}^{N_r} \frac{F_{supply_i}}{F_{supply}} T_i + \frac{\eta_{hvac} P_{hvac}}{F_{supply} c_p} \end{aligned} \tag{3.16}$$

where λ is an air mixture ratio dependent on the design/configuration of the air dampers, defined earlier in (3.3). T_{return} is the return air temperature that is a linear combination of room temperatures, η_{hvac} is an efficiency/performance coefficient, P_{hvac} is HVAC power usage, and F_{supply} is the total air flow rate given by

$$F_{supply} = \sum_{i=1}^{N_r} F_{supply_i} \tag{3.17}$$

The exact values for F_{supply_i} are dependent on the HVAC supply, return, and room fans, as well as the room topology and the layout of the air duct system. It is assumed that their values can be empirically obtained for each on/off combination of system fans.

The HVAC system heating or cooling can be split into winter or summer modes

such that

$$\eta_{hvac}P_{hvac} = \begin{cases} \eta_{heat}P_{heat} & \text{Furnace on} \\ -\eta_{cool}P_{cool} & \text{AC on} \\ 0 & \text{otherwise} \end{cases} \tag{3.18}$$

where η_{heat} is the efficiency of the furnace, η_{cool} is the efficiency of the air conditioner, P_{heat} is furnace power usage, and P_{cool} is air conditioning power usage. For the case of electric-only HVAC system, P_{heat} and P_{cool} represent electric power usage that end up being combined with the other system electric loads to determine energy cost. For a natural-gas furnace P_{heat} represents heat power that is charged independently of electricity.

On/off operation is assumed for the term in (3.18) such that when the main HVAC fan is off, the furnace/AC unit is also off. Moreover, it is also assumed that when the main HVAC fan is off, all rooms fans are also off. The HVAC system can be in N_s states/configurations listed in Table 3.4 where mutually exclusive binary variables $\boldsymbol{\delta}^{state,i}$ are introduced such that $\sum_{i=1}^{N_s} \boldsymbol{\delta}^{state,i} = 1$.

Table 3.4: HVAC system states

State	Furnace or A/C	HVAC Fan	Room 1 Fan	...	Room N_r Fan
$\boldsymbol{\delta}^{state,1}$	OFF	OFF	OFF	$\cdots$	OFF
$\boldsymbol{\delta}^{state,2}$	OFF	ON	OFF	$\cdots$	OFF
$\boldsymbol{\delta}^{state,3}$	ON	ON	OFF	$\cdots$	OFF
$\boldsymbol{\delta}^{state,4}$	OFF	ON	ON	$\cdots$	OFF
$\boldsymbol{\delta}^{state,5}$	ON	ON	ON	$\cdots$	OFF
$\vdots$	$\vdots$	$\vdots$	$\vdots$	$\ddots$	$\vdots$
$\boldsymbol{\delta}^{state,N_s-1}$	OFF	ON	ON	$\cdots$	ON
$\boldsymbol{\delta}^{state,N_s}$	ON	ON	ON	$\cdots$	ON

The following vector denotes the system temperatures

$$\boldsymbol{\tau} = [T_1, T_2, \ldots, T_{N_r}]^T \tag{3.19}$$

Assuming the system is in some state $\boldsymbol{\delta}^{state,i}$, using (3.15)-(3.19), the temperature dynamics can be written as

$$\frac{d\boldsymbol{\tau}}{dt} = \mathbf{A}_i\boldsymbol{\tau} + \mathbf{b}_i T_{out} + \mathbf{c}_i, \;\; i \in [1, N_s] \tag{3.20}$$

where

$$\mathbf{A}_i = \begin{bmatrix} a_{11} & a_{12} & \cdots & a_{1N_r} \\ a_{21} & a_{22} & \cdots & a_{2N_r} \\ \vdots & \vdots & \ddots & \vdots \\ a_{N_r1} & a_{N_r2} & \cdots & a_{N_rN_r} \end{bmatrix} \tag{3.21}$$

$$a_{j_1j_1} = -\frac{1}{m_{j_1}c_p}[\kappa_{out,j_1} + \sum_{j_2=1}^{N_r}\kappa_{j_2,j_1} + F_{supply_{j_1}}c_p(1-\lambda\frac{F_{supply_{j_1}}}{F_{supply}})], j_1 \in [1, N_r] \tag{3.22}$$

$$a_{j_1j_2} = \frac{1}{m_{j_1}c_p}(F_{supply_{j_1}}c_p\lambda\frac{F_{supply_{j_2}}}{F_{supply}} + \kappa_{j_2,j_1}), \;\; j_1 \neq j_2, \;\; j_1, j_2 \in [1, N_r] \tag{3.23}$$

$$\mathbf{b}_i = \begin{bmatrix} b_{1i} \\ b_{2i} \\ \vdots \\ b_{N_ri} \end{bmatrix}, \;\; \mathbf{c}_i = \begin{bmatrix} c_{1i} \\ c_{2i} \\ \vdots \\ c_{N_ri} \end{bmatrix} \tag{3.24}$$

$$b_{ji} = \frac{1}{m_jc_p}[\kappa_{out,j} + F_{supply_j}c_p(1-\lambda)], \;\; j \in [1, N_r] \tag{3.25}$$

$$c_{ji} = \frac{1}{m_jc_p} \cdot \frac{F_{supply_j}}{F_{supply}} \cdot \eta_{hvac}P_{hvac} \tag{3.26}$$

where $F_{supply}, F_{supply_j}, j \in [1, N_r]$ are different for each state $\boldsymbol{\delta}^{state,i}, i \in [1, N_s]$. Therefore, the dynamic matrix $\mathbf{A}_i$ and the vectors $\mathbf{b}_i$, $\mathbf{c}_i$ are different for each state in Table 3.4. It is noted here that the term $\mathbf{c}_i$ is zero when $\eta_{hvac}P_{hvac}$ is zero.

3.2.3 Discrete-time Temperature Model

A subscript k is used to denote a discrete-time quantity related to the k^{th} time-step, e.g. the discrete-time temperature vector

$$\boldsymbol{\tau}_k = [T_{1,k}, T_{2,k}, \ldots, T_{N_r,k}]^T \tag{3.27}$$

A vector $\mathbf{h}$ is introduced to represent the sampling-time lengths in the prediction horizon. Assuming the control inputs are constant between the sampling time, i.e. a zero-order-hold conversion of the dynamics in (3.20) yields the discrete-time system dynamic matrices

$$\mathbf{A}_{i,k} = e^{\mathbf{A}_i \mathbf{h}_k} \tag{3.28}$$

$$\mathbf{b}_{i,k} = \mathbf{A}_i^{-1}(e^{\mathbf{A}_i \mathbf{h}_k} - \mathbf{I})\mathbf{b}_i \tag{3.29}$$

$$\mathbf{c}_{i,k} = \mathbf{A}_i^{-1}(e^{\mathbf{A}_i \mathbf{h}_k} - \mathbf{I})\mathbf{c}_i \tag{3.30}$$

Using a discrete-time binary variable $\boldsymbol{\delta}_k^{state,i}$ to select the fan, furnace or AC states at time step k, the discrete-time temperature dynamics can be written as the following nonlinear equation

$$\boldsymbol{\tau}_k = \sum_{i=1}^{N_s} \boldsymbol{\delta}_k^{state,i} \left(\mathbf{A}_{i,k}\boldsymbol{\tau}_{k-1} + \mathbf{b}_{i,k}T_{out,k} + \mathbf{c}_{i,k}\right) \tag{3.31}$$

where the variables $\boldsymbol{\delta}_k^{state,i}$ and $\boldsymbol{\tau}_k, \boldsymbol{\tau}_{k-1}$ are unknown.

Chapter 4

Single-zone Temperature Control and Energy Management

In this chapter, the temperature control and energy management for single-zone configuration is studied. The first section of this chapter discusses how the general optimization problem is formulated. The second section covers single-zone case studies. Scenarios without/with electric storage are discussed. The formulations and simulation results in single-zone configuration are presented. The last section presents a performance comparison between MILP-based model predictive control and hysteresis control in six different single-zone scenarios.

4.1 Optimization Formulation

In order to address the room temperature control and energy management problem in buildings, an optimization problem is formulated to optimize the HVAC control and power flow among microgrids and related to the external grid. The decision variables are the on/off command for the heating/cooling unit and fans in the HVAC system,

and the battery charging/discharging power rates. Based on the nonlinear character of the temperature dynamics, a mixed integer quadratic constraints linear program (MI-QCLP) optimization problem is first considered and formulated. However, such formulation is difficult and time-consuming to solve. To reduce the computations, the concepts of the HVAC system states are introduced to formulate the problem as MILP optimization as opposed to the prior nonlinear optimization.

The model predictive control (MPC) scheme is also utilized with the optimization to compensate for the uncertainty in the microgrid operations and minimize the overall operation costs. A rolling prediction horizon is employed at each time step. An optimization problem is formulated and solved at each iteration and the optimal solutions corresponding to the current time-step are used to control the operations of the HVAC system and the electric storage charging/discharging power rates over the prediction horizon. It is noted that only the value for the first time-step in the window or horizon is implemented in practice.

The rolling horizon control scheme is depicted in Figure 4.1. It can be observed that a MILP optimization problem is formulated and solved based on the current system operation states of battery usage and room temperatures by utilizing a model of outside temperature and net demand prediction. The optimized solutions of battery, grid power rates and operations of HVAC unit for the first time-step are used to control the CHP-AEMS battery and HVAC system. Then the prediction window would move forward one time-step, the MILP optimization problem based on updated information would be reformulated and solved in the next time instance.

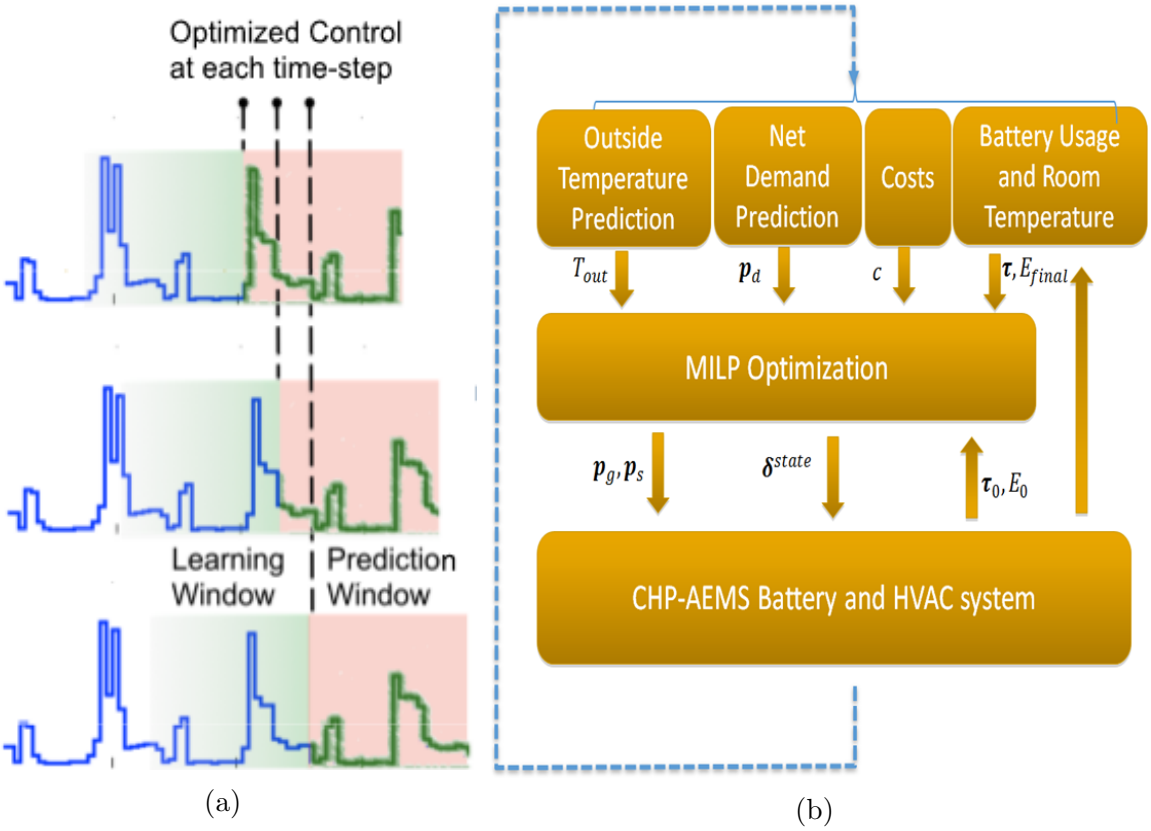

Figure 4.1: Rolling Horizon Control: a) rolling window concept (Malysz *et al.*, 2014), b) block diagram scheme.

4.1.1 MI-QCLP Formulation

The mixed integer quadratic constraints linear program (MI-QCLP) optimization problem is formulated as follows:

$$\min_{\mathbf{x}} \left(\mathbf{c}_{heat}^T \boldsymbol{\delta}_{heat} + \mathbf{c}_{fan,sc}^T \mathbf{y}_{fsc} + \mathbf{c}_{heat,sc}^T \mathbf{y}_{hsc} + \mathbf{c}_{grid}^T \mathbf{p}_g \right) \tag{4.1}$$

The vector of decision variables is

$$\mathbf{x} = [\mathbf{T}, \boldsymbol{\delta}_{heat}, \boldsymbol{\delta}_{fan}, \mathbf{y}_{fsc}, \mathbf{y}_{hsc}, \mathbf{p}_g, \mathbf{p}_s]^T \tag{4.2}$$

where

$N_h \in \mathbb{Z}$: number of time steps in horizon.

$\mathbf{c}_{heat} \in \Re^{N_h}$: cost vector for natural gas furnace ($).

$\mathbf{c}_{fan,sc}, \mathbf{c}_{heat,sc} \in \Re^{N_h}$: cost vector for the state change of fans and furnace/AC ($).

$\boldsymbol{\delta}_{heat}, \boldsymbol{\delta}_{fan} \in \mathbb{Z}^{N_h}$: binary (on/off) vector for the operation of the heater unit and fans.

$\mathbf{y}_{fsc}, \mathbf{y}_{hsc} \in \mathbb{Z}^{N_h}$: binary vectors representing operation mode changes.

$\mathbf{c}_{grid} \in \Re^{N_h}$: electricity usage cost ($/kWh).

$\mathbf{p}_g \in \Re^{N_h}$: grid buying/selling power rate (kW).

$\mathbf{p}_s \in \Re^{N_h}$: battery charging/discharging power (kW).

$\mathbf{T} \in \Re^{N_h}$: room temperature vector (℃).

Note that the term $\mathbf{c}_{heat}^T \boldsymbol{\delta}_{heat}$ represents natural gas usage cost and $\mathbf{c}_{heat} = \mathbf{0}_{N_h}$ when using an electric furnace or air conditioner. The term $\mathbf{c}_{fan,sc}^T \mathbf{y}_{fsc} + \mathbf{c}_{heat,sc}^T \mathbf{y}_{hsc}$ represents the cost of turning on/off the fans and furnace/AC. The term $\mathbf{c}_{grid}^T \mathbf{p}_g$ represents the net electricity usage cost.

The following constraints are applicable in the optimization problem.

The decision variables for the heating and the fan are binary, and the fan has to be on when the heat is on, i.e.

$$\mathbf{0}_{N_h} \leq \boldsymbol{\delta}_{heat} \leq \boldsymbol{\delta}_{fan} \leq \mathbf{1}_{N_h} \tag{4.3}$$

where $\mathbf{0}_{N_h} \in \mathbb{Z}^{N_h}$ is a vector of zeros, $\mathbf{1}_{N_h} \in \mathbb{Z}^{N_h}$ is a vector of ones.

The binary variables y_{fsc}, y_{hsc} are introduced to formulate the objective function into linear problem. Note that $y_{fsc_k} = 1$ when the fan operation state changes, $y_{hsc_k} = 1$ when the heat unit operation state changes, otherwise the values are taken

as zero. The constraints are as follows:

$$-y_{fsc_k} \leq \delta_{fan_k} - \delta_{fan_{k-1}} \leq y_{fsc_k}, \;\; k \in [1, N_h] \tag{4.4}$$

$$-y_{hsc_k} \leq \delta_{heat_k} - \delta_{heat_{k-1}} \leq y_{hsc_k}, \;\; k \in [1, N_h] \tag{4.5}$$

Instead of regulating the room temperature to a specific value, the system allows for temperature variations within so-called (variable) comfort limits. The controller can take advantage of this extra flexibility in temperature control by performing pre-heating/cooling with cheaper energy, whenever feasible, to reduce the cost further. The desired room temperature comfort limits can be written

$$\mathbf{T}_{min_{N_h}} \leq \mathbf{T} \leq \mathbf{T}_{max_{N_h}} \tag{4.6}$$

The electric power at the point of common coupling to the grid is subject to the limits

$$P_g^{min} \leq p_{g_k} \leq P_g^{max}, \;\; k \in [1, N_h] \tag{4.7}$$

where P_g^{max}, P_g^{min} are the maximum and minimum power limits, and the latter can be negative if power is allowed to be sent back to the grid, otherwise it is zero.

The power balance equality constraint is

$$\mathbf{p}_g = \mathbf{p}_d + \mathbf{p}_s + \mathbf{p}_{hvac} + \mathbf{p}_{fans} \tag{4.8}$$

where $\mathbf{p}_s$ is electric energy storage power activity, e.g. battery, $\mathbf{p}_{hvac}$ is heating/cooling electrical power load, $\mathbf{p}_{fans}$ is electrical power load of HVAC system/room fans, and $\mathbf{p}_d$ is a predicted electricity demand usage vector for other system loads.

The temperature dynamics manifest themselves as heat balance quadratic constraints of the form

$$a_1 T_{k-1}\delta_{fan_k} + a_2 T_k \delta_{fan_k} + a_3 T_{k-1} + a_4 T_k + a_5 \delta_{fan_k} + a_6 \delta_{heat_k} = a_7, \;\; k \in [1, N_h] \quad (4.9)$$

where a_{1-7} are the constant parameters that are derived from the thermal dynamics by discretizing the heat balance equation (3.15).

On-site electric energy storage has limited capacity and power capabilities, which leads to the constraints

$$E_s^{min} \leq \sum_{j=1}^{k} \mathbf{h}_j \mathbf{p}_{s_j} + E_0 \leq E_s^{max}, \;\; k \in [1, N_h] \quad (4.10)$$

$$P_s^{min} \leq \mathbf{p}_{s_k} \leq P_s^{max}, \;\; k \in [1, N_h] \quad (4.11)$$

where E_0, E_s^{min}, and E_s^{max} are initial, minimum, and maximum energies, and P_s^{max}, P_s^{min} are maximum and minimum power rates of electric energy storage; note that the latter is a negative number. Lastly, the following equality constraint is added to set a desired end-of-horizon energy level of E_{final}:

$$\mathbf{h}^T \mathbf{p}_s = E_{final} - E_0 \quad (4.12)$$

4.1.2 MILP-based Model Predictive Control Formulation

The HVAC system states are introduced to convert the above MI-QCLP optimization problem to MILP optimization in order to reduce the computations for solving this problem. In practice, in MI-QCLP the solver is often forced to quit early to meet real-time control timing constraints, resulting in suboptimal solutions. Therefore, the solution accuracy could be improved by formulating MILP optimization with

computation time reduction.

A MILP-based rolling horizon control strategy is utilized to control the microgrid electric energy storage and air temperature in the building via the HVAC system. The MPC is designed with a prediction horizon equal to $\mathbf{1}_{N_h}^T \mathbf{h}$ hours that computes an optimal control action every $\mathbf{h}_1$ hours by selecting a control state in Table 3.4. At every time step in the horizon, the following binary vectors are computed

$$\boldsymbol{\delta}^{state} = \begin{bmatrix} \boldsymbol{\delta}_1^{state} \\ \vdots \\ \boldsymbol{\delta}_{N_h}^{state} \end{bmatrix}, \quad \boldsymbol{\delta}_k^{state} = \begin{bmatrix} \boldsymbol{\delta}_k^{state,1} \\ \vdots \\ \boldsymbol{\delta}_k^{state,N_s} \end{bmatrix} \tag{4.13}$$

A MILP optimization is formulated with the objective of minimizing energy costs, i.e.

$$\min_{\mathbf{x}} \left(\underbrace{\sum_{k=1}^{N_h} \sum_{i=3, i\ odd}^{N_s} c_{gas} \mathbf{h}_k \boldsymbol{\delta}_k^{state,i}}_{\mathbf{c}_\delta^T \boldsymbol{\delta}^{state}} + \mathbf{c}_{elec}^T \mathrm{diag}(\mathbf{h}) \mathbf{p}_g \right) \tag{4.14}$$

$$\mathbf{x} = [\boldsymbol{\tau}, \boldsymbol{\delta}^{state}, \boldsymbol{\tau}^{state}, \mathbf{p}_g, \mathbf{p}_s]^T \tag{4.15}$$

where the first term represents heating costs using a natural gas furnace based on the unit time cost c_{gas} in heating operation. In cooling operation or heating using electric furnace c_{gas} equals to zero, i.e. only electricity is consumed. The second term represents electricity costs where $\mathbf{c}_{elec}$ is a time-of-day dependent price and $\mathbf{p}_g$ is the grid connection power measured at the meter. This vector is determined by the equality constraint

$$\mathbf{p}_g = \mathbf{p}_d + \mathbf{p}_s + \underbrace{\mathbf{p}_{hvac} + \mathbf{p}_{fans}}_{\mathbf{p}_\delta^T \boldsymbol{\delta}^{state}} \tag{4.16}$$

where $\mathbf{p}_s$ is electric energy storage power activity, e.g. battery, $\mathbf{p}_{hvac}$ is heating/cooling

electrical power load, $\mathbf{p}_{fans}$ is electrical power load of HVAC system/room fans, and $\mathbf{p}_d$ is a predicted electricity demand usage vector for other system loads. The last two terms can be combined into a linear function of $\boldsymbol{\delta}^{state}$ where elements of $\mathbf{p}_\delta$ satisfy

$$\mathbf{p}_{hvac_k} = \sum_{i=3,i\ odd}^{N_s} P_{hvac}\boldsymbol{\delta}_k^{state,i},\ \ k \in [1, N_h] \tag{4.17}$$

$$\mathbf{p}_{fans_k} = \sum_{i=2}^{N_s} P_{fans}^{hvac}\boldsymbol{\delta}_k^{state,i} + \mathbf{p}_{fans_k}^{room},\ \ k \in [1, N_h] \tag{4.18}$$

Here P_{fans}^{hvac} is power load of HVAC unit fans and $\mathbf{p}_{fans_k}^{room}$ is electric power usage of all the room vent fans. This term is equal to $n_{fans,on_k}^{room,i} P_{fan}^{room}$ where P_{fan}^{room} is power load of a single room vent fan, and $n_{fans,on_k}^{room,i}$ is the number of the fans that are "on" in control state $\boldsymbol{\delta}_k^{state,i}$.

To enforce mutually exclusive control states at each time-step, the following equality constraints are employed

$$\mathbf{1}_{N_s}^T \boldsymbol{\delta}_k^{state} = 1,\ \ k \in [1, N_h] \tag{4.19}$$

The temperature dynamics in (3.31) impose additional equality constraints, however these quadratic constraints in (4.9) need to be converted to linear counterparts to ensure a MILP applies. This can be achieved by introducing an additional vector

$$\boldsymbol{\tau}^{state} = \begin{bmatrix} \boldsymbol{\tau}_1^{state} \\ \vdots \\ \boldsymbol{\tau}_{N_h}^{state} \end{bmatrix},\ \ \boldsymbol{\tau}_k^{state} = \begin{bmatrix} \boldsymbol{\tau}_k^{state,1} \\ \vdots \\ \boldsymbol{\tau}_k^{state,N_s} \end{bmatrix} \tag{4.20}$$

whose subvectors are desired to be $\boldsymbol{\tau}_k^{state,i} = \boldsymbol{\delta}_k^{state,i}\boldsymbol{\tau}_{k-1}$. This simpler nonlinear

equality can be alternatively represented by the following linear inequality constraints

$$\boldsymbol{\tau}_{k-1} - T_{large}(1 - \boldsymbol{\delta}_k^{state,i})\mathbf{1}_{N_r} \leq \boldsymbol{\tau}_k^{state,i} \leq \boldsymbol{\tau}_{k-1} + T_{large}(1 - \boldsymbol{\delta}_k^{state,i})\mathbf{1}_{N_r} \tag{4.21}$$

$$-T_{large}\boldsymbol{\delta}_k^{state,i}\mathbf{1}_{N_r} \leq \boldsymbol{\tau}_k^{state,i} \leq T_{large}\boldsymbol{\delta}_k^{state,i}\mathbf{1}_{N_r}, \;\; i \in [1, N_s], k \in [1, N_h] \tag{4.22}$$

where T_{large} is a sufficiently large temperature value.

Substituting $\boldsymbol{\tau}_k^{state,i}$ into (3.31) yields linear equality constraints

$$\begin{aligned} \boldsymbol{\tau}_k \;\; = \;\; & [\mathbf{A}_{1,k}, \mathbf{A}_{2,k}, \ldots, \mathbf{A}_{N_s,k}]\boldsymbol{\tau}_k^{state} \\ & + T_{out,k}[\mathbf{b}_{1,k}, \mathbf{b}_{2,k}, \ldots, \mathbf{b}_{N_s,k}]\boldsymbol{\delta}_k^{state} \\ & + [\mathbf{c}_{1,k}, \mathbf{c}_{2,k}, \ldots, \mathbf{c}_{N_s,k}]\boldsymbol{\delta}_k^{state}, \quad k \in [1, N_h] \end{aligned} \tag{4.23}$$

A control objective is to maintain the temperature within a desired comfort range, therefore equality constraints

$$T_{min}\mathbf{1}_{N_r} \leq \boldsymbol{\tau}_k \leq T_{max}\mathbf{1}_{N_r}, \;\; k \in [1, N_h] \tag{4.24}$$

are applied where T_{min} and T_{max} are minimum and maximum desired room temperatures.

The electric power at the grid coupling point is limited and the constraints (4.7) are still applicable in the optimization problem. The electric storage energy level and charging/discharging power related constraints remain in this optimization problem, e.g. see (4.10)-(4.12).

In summary, the MILP based MPC computes vectors $\boldsymbol{\tau}, \boldsymbol{\delta}^{state}, \boldsymbol{\tau}^{state}, \mathbf{p}_g, \mathbf{p}_s$ to minimize the objective function (4.14) subject to the constraints (4.7), (4.10)-(4.12), (4.16)-(4.19), (4.21)-(4.24).

4.2 Case Studies

Simulations are performed in different scenarios to examine the performance of the proposed MILP-based MPC controller. Matlab is used with the Gurobi optimization solver (GUROBI, 2014) using an Intel(R) Core(TM) i5-2400S CPU and 8 GB RAM to solve the optimization problem and obtain the control commands. A commercial/residential setting is considered where the time of use electricity pricing is used, as shown in Table 4.1. The price of natural gas is set at $c_{ng} = \frac{22.5862¢/m^3}{10.35kWh/m^3} = 2.2¢/kWh$ (OEB, 2014), which would be used to calculate the unit time cost c_{gas}. All other costs are assumed zero. The maximum grid power rate is taken as $P_g^{max} = 16kW$. The battery parameters are given in Table 4.2. The parameters of the building are suitably chosen and given in Table 4.3. The outside temperature and electric load data of the other devices are from measurements from Weather Network Canada and Burlington Hydro, respectively. A summary of the single-zone scenarios are presented in Table 4.4.

Table 4.1: Time of use electricity pricing. (IESO, 2014)

Time Zones	Summer ($¢/kWh$)	Winter ($¢/kWh$)
7pm - 7am	7.5	7.2
7am - 11am	11.2	12.9
11am - 5pm	13.5	10.9
5pm - 7pm	11.2	12.9

Table 4.2: Battery parameters

E_s^{min}	E_s^{max}	P_s^{min}	P_s^{max}
$0\ kWh$	$25\ kWh$	$-3\ kWh$	$3\ kWh$

Table 4.3: Summary of parameters for the building

Parameter	Value	Unit
Building Size	300	m^2
R-wall (R-29)	5.11	m^2K/W
R-window	0.714	m^2K/W
Convective coefficient inside	8	W/m^2K
Convective coefficient outside	23	W/m^2K

Table 4.4: Summary of single-zone scenarios

	Scenario	Description
Single-zone Configuration 1	S1	Single room, in winter operation, heating using natural gas furnace, under TOU rates
	S2	Single room, in winter operation, heating using electric furnace, under TOU rates
	S3	Single room, in summer operation, cooling using air conditioner, under TOU rates
Single-zone Configuration 2	S4	Single room, in winter operation, heating using natural gas furnace, under TOU rates and on-site electric energy storage
	S5	Single room, in winter operation, heating using electric furnace, under TOU rates and on-site electric energy storage
	S6	Single room, in summer operation, cooling using air conditioner, under TOU rates and on-site electric energy storage

4.2.1 Single-zone Configuration 1: Single-zone Temperature Control without Electric Storage

Optimization Formulation

In this configuration, the building is modelled as one thermal zone, namely $N_r = 1$. There is no vent fan, therefore $N_s = 3$ and the first three columns and first four rows of Table 3.4 are applicable, as shown in Table 4.5. For each state $\boldsymbol{\delta}^{state,i}$, there are corresponding dynamic matrices $\mathbf{A_i}$, $\mathbf{b_i}$ and $\mathbf{c_i}$ in (3.20 - 3.26).

Table 4.5: HVAC system states in single-zone configuration 1

State	Furnace or A/C	HVAC Fan
$\boldsymbol{\delta}^{state,1}$	OFF	OFF
$\boldsymbol{\delta}^{state,2}$	OFF	ON
$\boldsymbol{\delta}^{state,3}$	ON	ON

The goal of optimization is to minimize the total energy cost, i.e.

$$\min_{\mathbf{x}} \left(\mathbf{c}_\delta^T \boldsymbol{\delta}^{state} + \mathbf{c}_e^T \mathbf{p}_g \right) \tag{4.25}$$

where the natural gas heating cost is a linear function of the HVAC control states, i.e. $\mathbf{c}_\delta^T \boldsymbol{\delta}^{state} = \sum_{k=1}^{N_h} \sum_{i=3,i\ odd}^{N_s} c_{gas} \mathbf{h}_k \boldsymbol{\delta}_k^{state,i}$, the electricity cost $\mathbf{c}_e^T = \mathbf{c}_{elec}^T \text{diag}(\mathbf{h})$, and $\mathbf{x}$ is the vector of optimization decision variables defined by

$$\mathbf{x} = \left[\boldsymbol{\tau}, \boldsymbol{\delta}^{state}, \boldsymbol{\tau}^{state}, \mathbf{p}_g \right]^T \tag{4.26}$$

where

$$\boldsymbol{\tau} = [T_1, T_2, \ldots, T_{N_h}]^T \tag{4.27}$$

$$\boldsymbol{\delta}^{state} = \begin{bmatrix} \boldsymbol{\delta}_1^{state,1} \\ \boldsymbol{\delta}_1^{state,2} \\ \boldsymbol{\delta}_1^{state,3} \\ \vdots \\ \boldsymbol{\delta}_{N_h}^{state,1} \\ \boldsymbol{\delta}_{N_h}^{state,2} \\ \boldsymbol{\delta}_{N_h}^{state,3} \end{bmatrix}, \quad \boldsymbol{\tau}^{state} = \begin{bmatrix} \boldsymbol{\tau}_1^{state,1} \\ \boldsymbol{\tau}_1^{state,2} \\ \boldsymbol{\tau}_1^{state,3} \\ \vdots \\ \boldsymbol{\tau}_{N_h}^{state,1} \\ \boldsymbol{\tau}_{N_h}^{state,2} \\ \boldsymbol{\tau}_{N_h}^{state,3} \end{bmatrix} \tag{4.28}$$

The applicable optimization constraints are as follows:

$$P_g^{min} \leq \mathbf{p}_{g_k} \leq P_g^{max}, \;\; k \in [1, N_h] \tag{4.29}$$

$$T_{min}\mathbf{1}_{N_r} \leq \boldsymbol{\tau}_k \leq T_{max}\mathbf{1}_{N_r}, \;\; k \in [1, N_h] \tag{4.30}$$

$$\mathbf{1}_{N_s}^T \boldsymbol{\delta}_k^{state} = 1, \;\; k \in [1, N_h] \tag{4.31}$$

$$\boldsymbol{\tau}_{k-1} - T_{large}(1 - \boldsymbol{\delta}_k^{state,i})\mathbf{1}_{N_r} \leq \boldsymbol{\tau}_k^{state,i} \leq \boldsymbol{\tau}_{k-1} + T_{large}(1 - \boldsymbol{\delta}_k^{state,i})\mathbf{1}_{N_r} \tag{4.32}$$

$$-T_{large}\boldsymbol{\delta}_k^{state,i}\mathbf{1}_{N_r} \leq \boldsymbol{\tau}_k^{state,i} \leq T_{large}\boldsymbol{\delta}_k^{state,i}\mathbf{1}_{N_r} \tag{4.33}$$

$$\begin{aligned} \boldsymbol{\tau}_k = [\mathbf{A}_1^k, \mathbf{A}_2^k, \ldots, \mathbf{A}_{N_s}^k]\boldsymbol{\tau}_k^{state} + T_{out,k}[\mathbf{b}_1^k, \mathbf{b}_2^k, \ldots, \mathbf{b}_{N_s}^k]\boldsymbol{\delta}_k^{state} \\ +[\mathbf{c}_1^k, \mathbf{c}_2^k, \ldots, \mathbf{c}_{N_s}^k]\boldsymbol{\delta}_k^{state}, \quad k \in [1, N_h] \end{aligned} \tag{4.34}$$

$$\mathbf{p}_g = \mathbf{p}_d + \mathbf{p}_\delta^T \boldsymbol{\delta}^{state} \tag{4.35}$$

Simulation Results

In this configuration, the time horizon used was $12h$ with the fix time-step $0.05h$ in the simulation. Figure 4.2a shows the outside temperature in a typical winter day. Figure 4.2b shows the outside temperature in a typical summer day.

The scenarios in winter operation involve heating with natural gas and electric furnace. The scenario in summer operation considers cooling with air conditioner. The simulation results are illustrated in Figure 4.3, 4.4 and 4.5. Note that the dot-dashed (red) lines indicate the desired maximum and minimum temperature limits for the room.

From these graphs, it can be seen that some of the peak load is shifted to off-peak period mainly by preheating or precooling the building.

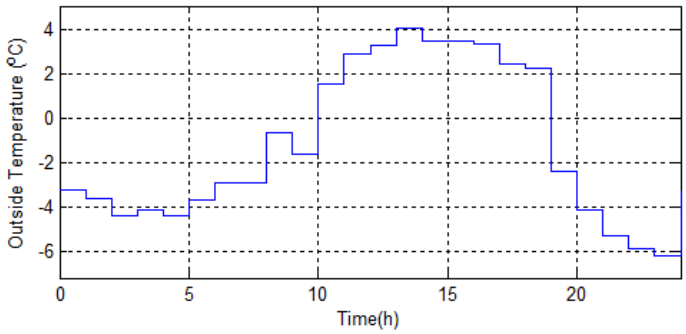

(a) In winter

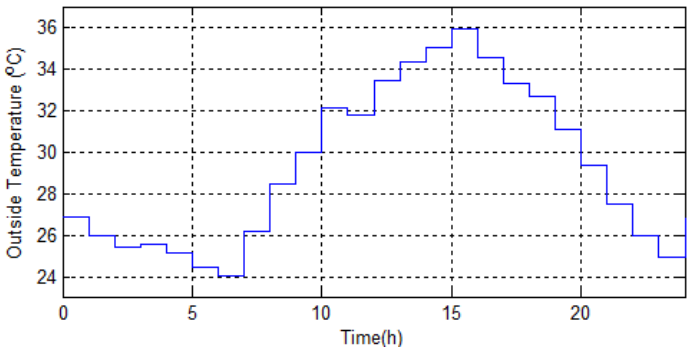

(b) In summer

Figure 4.2: Outside temperature profile in one day

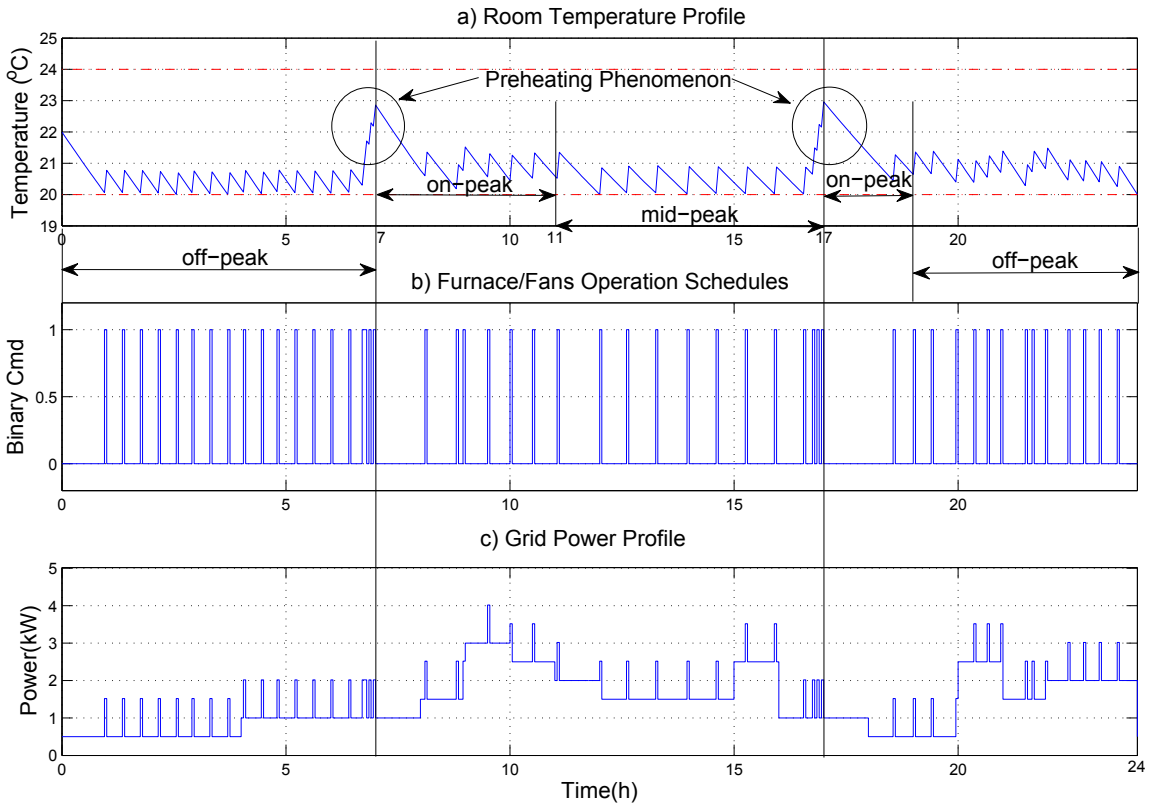

Figure 4.3: Scenario S1: single-zone, in winter operation, heating using natural gas furnace, without electric storage; a) 24-h room temperature profile, b) Furance/fans operation schedules, c) Grid power profile.

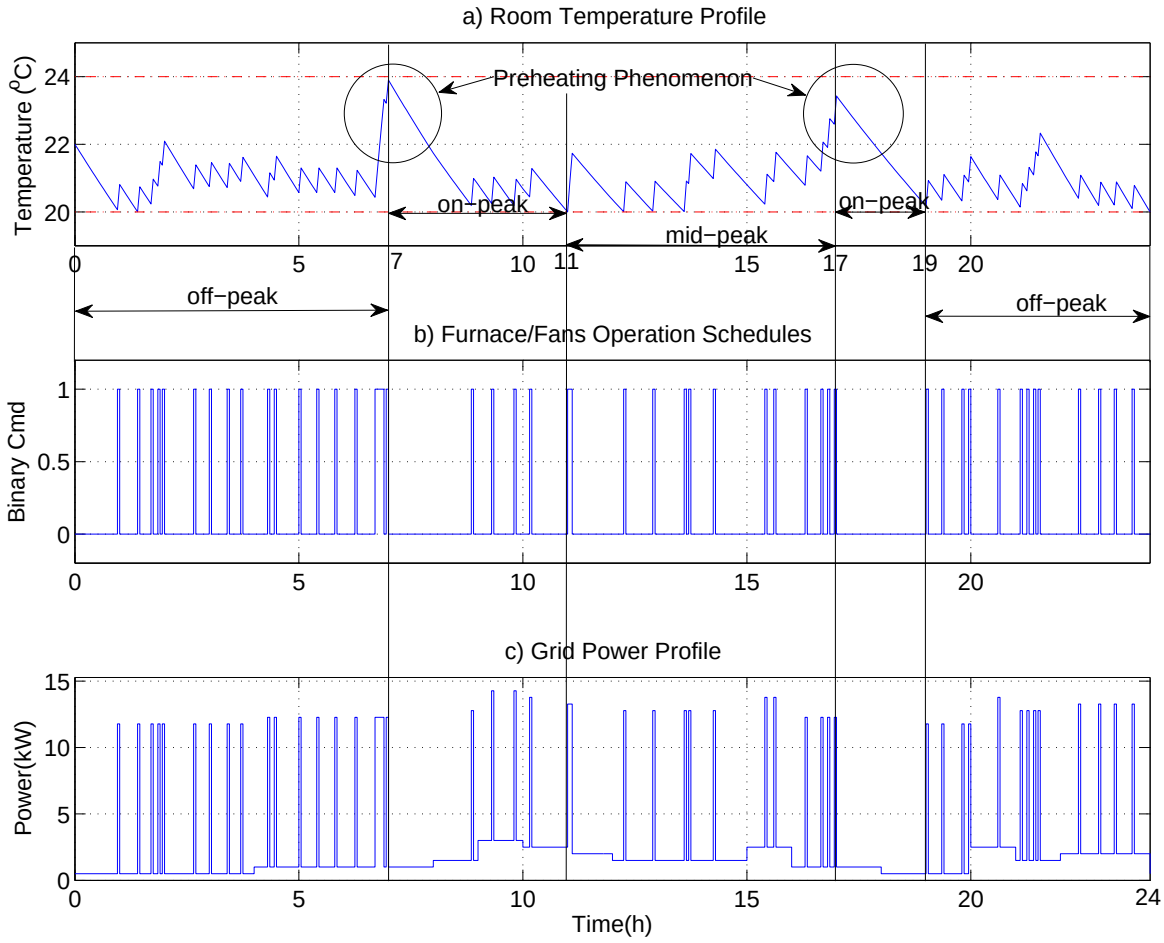

Figure 4.4: Scenario S2: single-zone, in winter operation, heating using electric furnace, without electric storage; a) 24-h room temperature profile, b) Furance/fans operation schedules, c) Grid power profile.

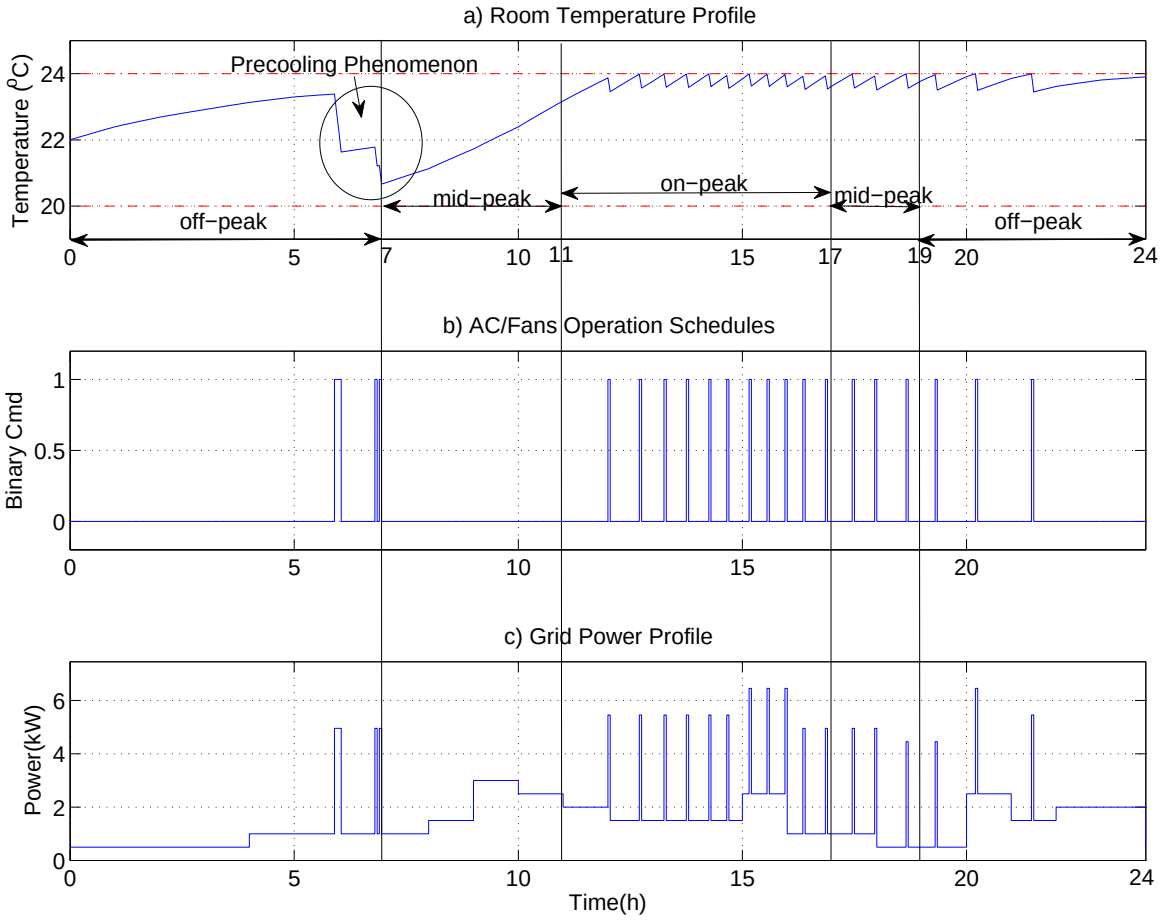

Figure 4.5: Scenario S3: single-zone, in summer operation, cooling using air conditioner, without electric storage;a) 24-h room temperature profile, b) Air conditioner/fans operation schedules, c) Grid power profile.

4.2.2 Single-zone Configuration 2: Single-zone Temperature Control with Electric Storage

Optimization Formulation

In this configuration, the electric storage is added compared to the single-zone configuration 1 in Section 4.2.1. The vector of battery charging/discharging power $\mathbf{p_s}$ is

added to the optimization variables, i.e.

$$\mathbf{x} = \left[\boldsymbol{\tau}, \boldsymbol{\delta}^{state}, \boldsymbol{\tau}^{state}, \mathbf{p}_g, \mathbf{p}_s\right]^T \tag{4.36}$$

The goal of optimization is

$$\min_{\mathbf{x}} \left(\mathbf{c}_\delta^T \boldsymbol{\delta}^{state} + \mathbf{c}_e^T \mathbf{p}_g\right) \tag{4.37}$$

where the electricity cost is $\mathbf{c}_e^T = \mathbf{c}_{elec}^T \text{diag}(\mathbf{h})$, and the term $\mathbf{c}_\delta^T \boldsymbol{\delta}^{state} = 0$ when heating using electric furnace in winter operation or cooling using air conditioner in summer operation.

The optimization constraints are:

$$P_g^{min} \leq \mathbf{p}_{g_k} \leq P_g^{max}, \;\; k \in [1, N_h] \tag{4.38}$$

$$P_s^{min} \leq \mathbf{p}_{s_k} \leq P_s^{max} \tag{4.39}$$

$$T_{min}\mathbf{1}_{N_r} \leq \boldsymbol{\tau}_k \leq T_{max}\mathbf{1}_{N_r}, \;\; k \in [1, N_h] \tag{4.40}$$

$$\mathbf{1}_{N_s}^T \boldsymbol{\delta}_k^{state} = 1, \;\; k \in [1, N_h] \tag{4.41}$$

$$\boldsymbol{\tau}_{k-1} - T_{large}(1 - \boldsymbol{\delta}_k^{state,i})\mathbf{1}_{N_r} \leq \boldsymbol{\tau}_k^{state,i} \leq \boldsymbol{\tau}_{k-1} + T_{large}(1 - \boldsymbol{\delta}_k^{state,i})\mathbf{1}_{N_r} \tag{4.42}$$

$$-T_{large}\boldsymbol{\delta}_k^{state,i}\mathbf{1}_{N_r} \leq \boldsymbol{\tau}_k^{state,i} \leq T_{large}\boldsymbol{\delta}_k^{state,i}\mathbf{1}_{N_r} \tag{4.43}$$

$$\begin{aligned}\boldsymbol{\tau}_k = [\mathbf{A}_1^k, \mathbf{A}_2^k, \ldots, \mathbf{A}_{N_s}^k]\boldsymbol{\tau}_k^{state} + T_{out,k}[\mathbf{b}_1^k, \mathbf{b}_2^k, \ldots, \mathbf{b}_{N_s}^k]\boldsymbol{\delta}_k^{state} \\ +[\mathbf{c}_1^k, \mathbf{c}_2^k, \ldots, \mathbf{c}_{N_s}^k]\boldsymbol{\delta}_k^{state}, \quad k \in [1, N_h]\end{aligned} \tag{4.44}$$

$$\mathbf{p}_g = \mathbf{p}_d + \mathbf{p}_s + \mathbf{p}_\delta^T \boldsymbol{\delta}^{state} \tag{4.45}$$

$$E_s^{min} \leq \textstyle\sum_{j=1}^{k} \mathbf{h}_j \mathbf{p}_{s_j} + E_0 \leq E_s^{max} \tag{4.46}$$

$$\mathbf{h}^T \mathbf{p}_s = E_{final} - E_0 \tag{4.47}$$

Simulation Results

In this configuration, the time horizon used was $12h$ with the fix time-step $0.05h$ in the simulation. The outside temperatures used in Single-zone Configuration 1 are employed here as well. Scenarios in winter operation include heating with natural gas and electric furnace. A scenario in summer operation considers cooling with air conditioner. The simulation results for scenarios S4-S6 are illustrated in Figure 4.6 - 4.11. Note the dot-dashed (red) lines indicate the desired maximum and minimum temperature limits for the room.

The room temperatures and the HVAC control commands in Scenario S4 are depicted in Figure 4.6. Figure 4.7 shows the charging or discharging power and energy level in the battery in a typical winter day. The room temperatures and the HVAC control commands in Scenario S5 are depicted in Figure 4.8. Figure 4.9 shows the charging or discharging power and energy level in the battery in a typical winter day. The room temperatures and the operational schedules in Scenario S6 are depicted in Figure 4.10. Figure 4.11 shows the charging or discharging power and energy level in the battery in a typical summer day.

From Figure 4.7, 4.9 and 4.11, some unnecessary battery activities can be observed. Penalizing charging/discharging activities could eliminate these unnecessary activities as in (Malysz *et al.*, 2013), and smoothen the battery power profile. In these scenarios, we can see that the proposed energy management and temperature control strategy saves cost by charging-low and discharging-high with battery.

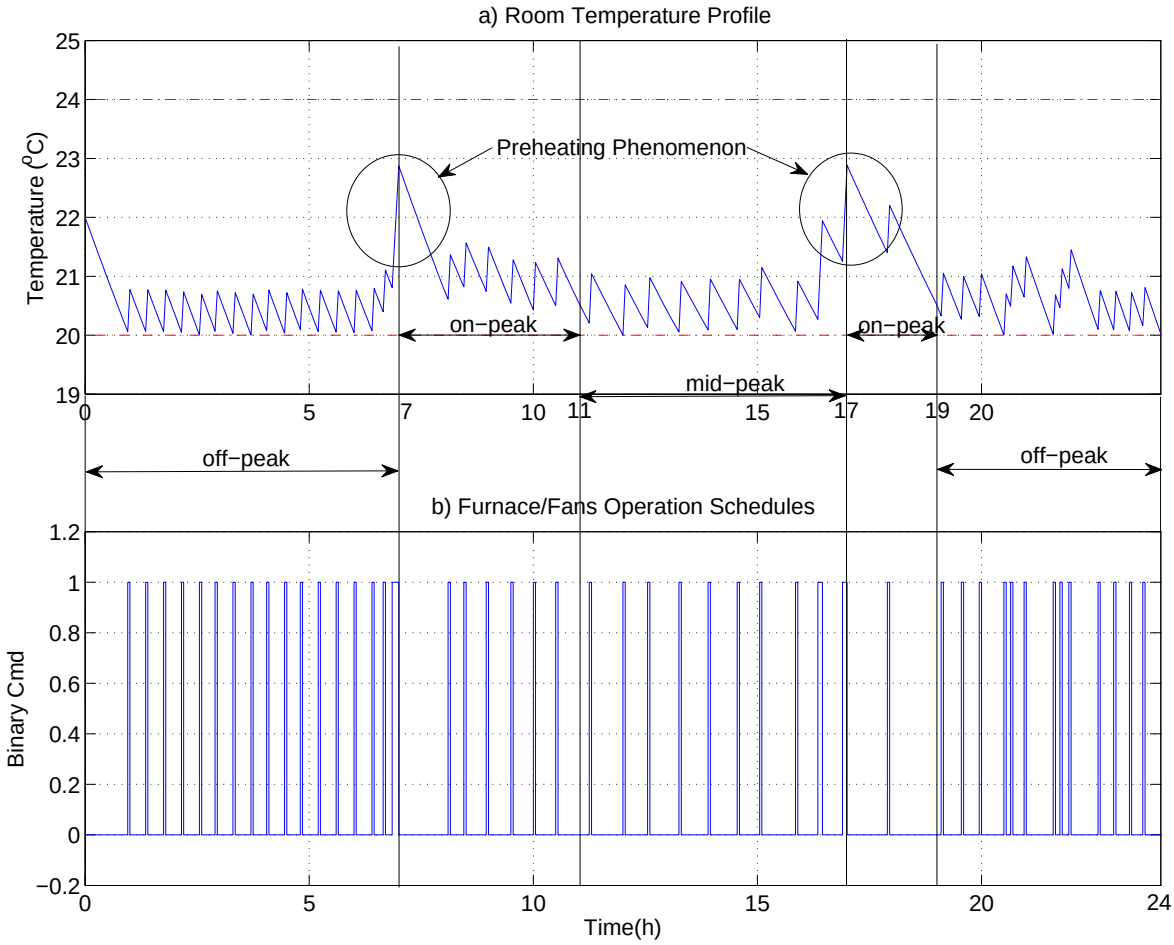

Figure 4.6: Scenario S4: single-zone, in winter operation, heating using natural gas furnace, with electric storage; a) 24-h room temperature profile, b) Furance/fans operation schedules.

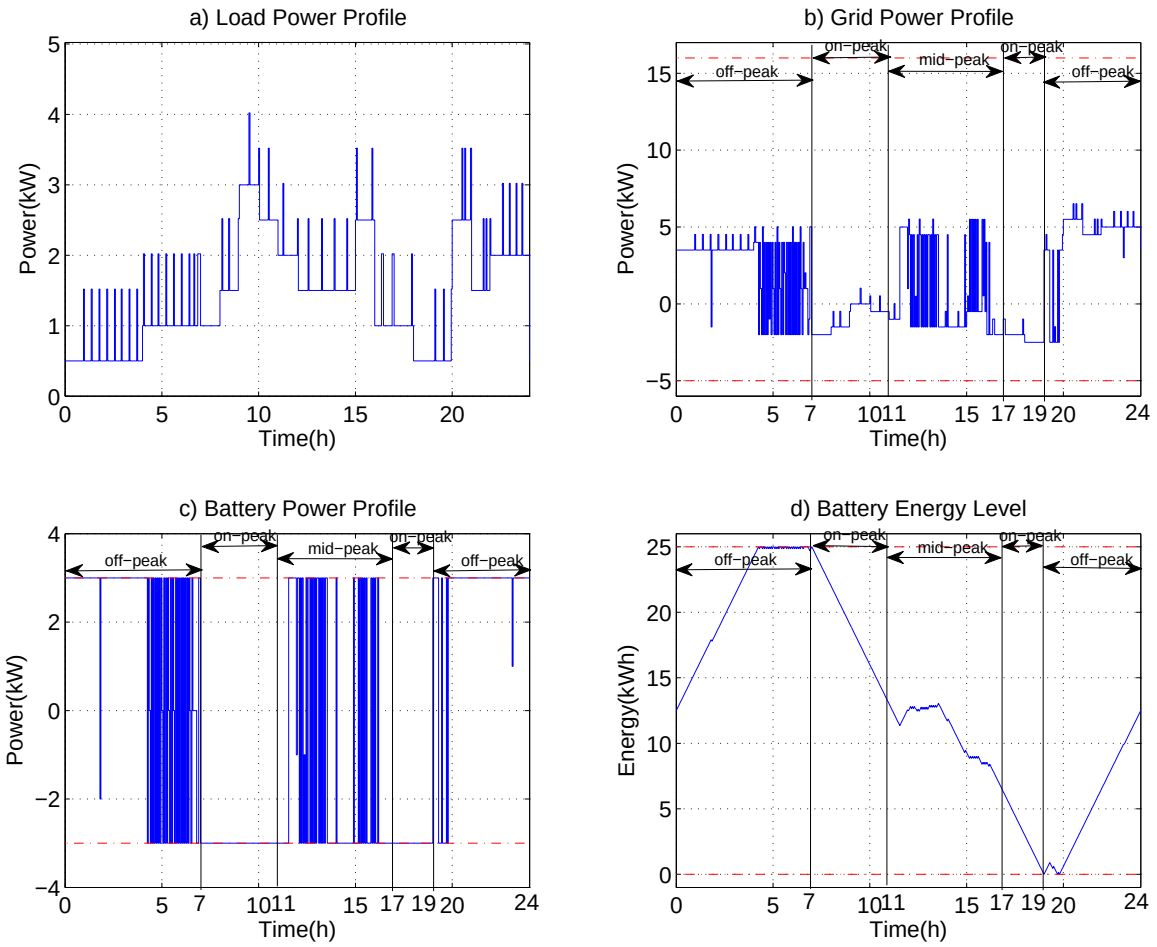

Figure 4.7: Scenario S4: single-zone, in winter operation, heating using natural gas furnace, with electric storage; a) Load power profile, b) Grid power profile, c) Battery power profile, d) Battery energy level.

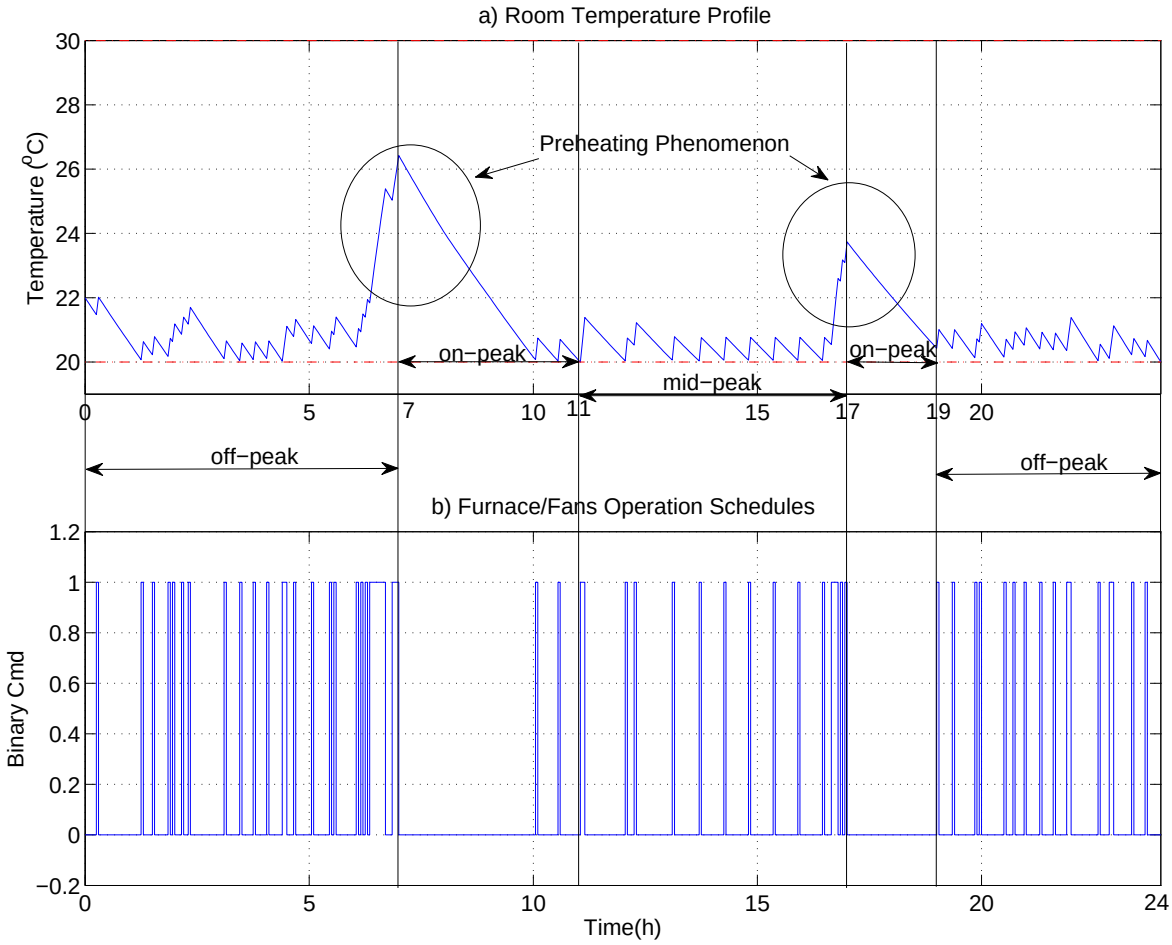

Figure 4.8: Scenario S5: single-zone, in winter operation, heating using electric furnace, with electric storage; a) 24-h room temperature profile, b) Furance/fans operation schedules.

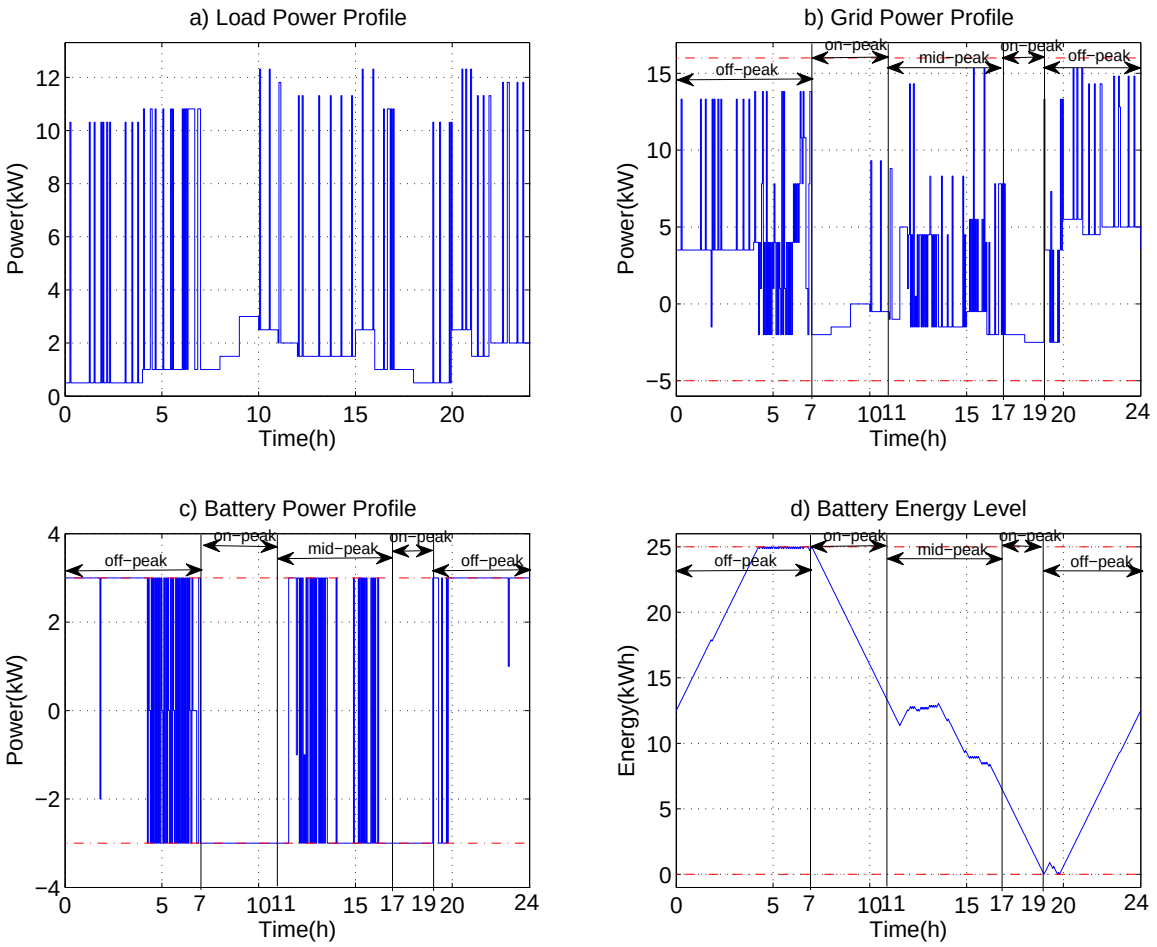

Figure 4.9: Scenario S5: single-zone, in winter operation, heating using electric furnace, with electric storage; a) Load power profile, b) Grid power profile, c) Battery power profile, d) Battery energy level.

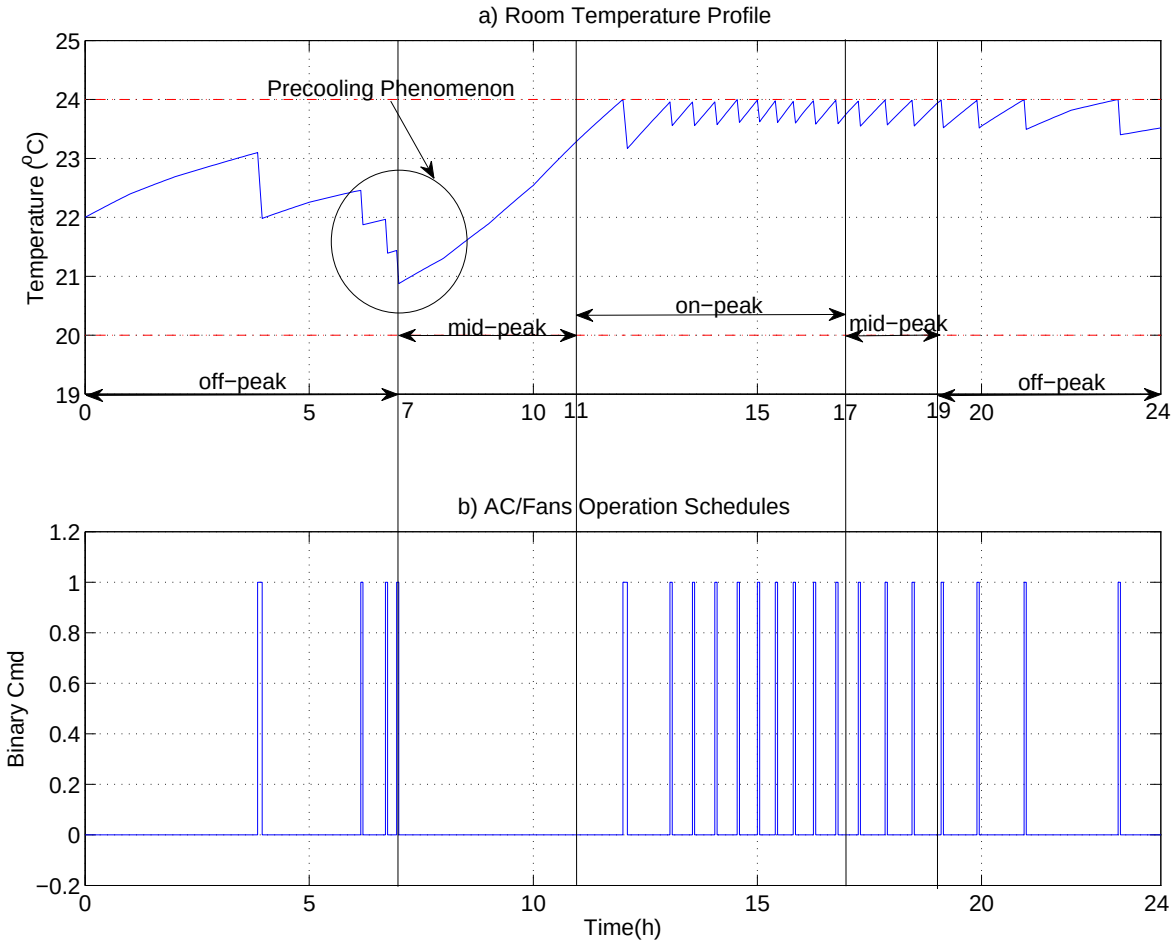

Figure 4.10: Scenario S6: single-zone, in summer operation, cooling using air conditioner, with electric storage; a) 24-h room temperature profile, b) AC/fans operation schedules.

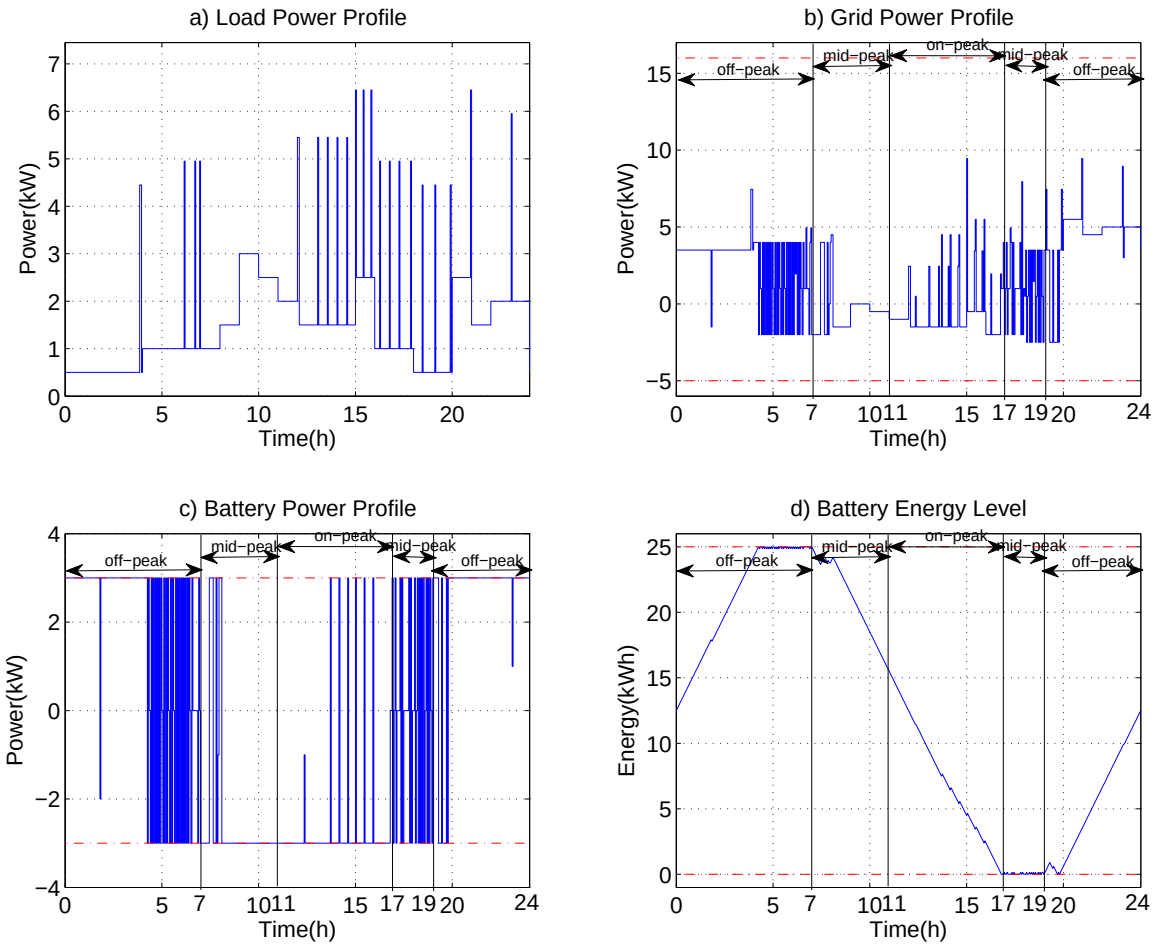

Figure 4.11: Scenario S6: single-zone, in summer operation, cooling using air conditioner, with electric storage; a) Load power profile, b) Grid power profile, c) Battery power profile, d) Battery energy level.

4.3 Comparison with Standard Control

Simulations based on a hysteresis temperature control method are conducted with the same parameters as the respective optimal MILP-based MPC case in different scenarios in Table 4.4. Electric storages are not included for this method. Hysteresis control does not use a set point but instead it uses a range for temperature control.

The temperature in hysteresis control is limited between 20-22 ℃ in winter, 22-24 ℃ in summer. That means the hysteresis controller turns the furnace on when the temperature drops below 20 ℃, but does not turn it off until the temperature rises above 22 ℃ in winter. Similarly, in summer, the hysteresis controller turns the air conditioner on when the temperature exceeds 24 ℃, and turns it off when the temperature drops below 22 ℃. Note that the temperature limits (20-24 ℃) used in MILP-based MPC control are not employed in hysteresis control. Because the proposed controller is smart and the temperature can be controlled to follow the lower temperature limit in winter and upper temperature limit in summer. Narrowing the range of temperature limits according to different seasons is more meaningful in hysteresis control. When utilizing the same temperature limits, the proposed controller can save more substantial energy cost compared with the hysteresis control. These simulation results of the hysteresis control are used for comparison with the results of MILP-based MPC control approach. Table 4.6 presents a summary of the comparison between MILP-based MPC control and hysteresis control methods in Scenario S1-S6.

It is observed that the energy cost is less in MILP-based MPC control. The scenarios without storage illustrates that the proposed method saves cost mainly by pre-heating/pre-cooling the building under time-of-use pricing, trying to use more low-price energy and less high-price energy while meeting the thermal and energy requirements of the building. In Scenario S1, the natural gas is used to heat the building, therefore the electricity energy consumed by fans is the only controllable load to benefit from pre-heating. It is negligible compared to the total consumed energy in building. That is why the saving is insignificant in Scenario S1. In Scenario S2 and S3, electric furnace and air conditioner are used, respectively. More electricity energy are consumed and can be controllable. Therefore, more low-price energy can be used by pre-heating/pre-cooling. We can see the obvious improvement in cost

saving in Scenario S2 and S3.

The scenarios with battery storage show that the proposed approach saves more by taking better advantage of the time-of-use pricing and charging-low/discharging-high. This approach makes full use of battery to store low-price energy, then supply energy to HVAC system and power demand for other devices during on-peak period. It can be seen that cost savings are more substantial in Scenario S4-S6. We can also observe that energy savings are comparatively smaller in Scenario S5. That is because the limited battery capacity has been completely employed and there is no more capacity to store low-price energy to offset the increased energy consumption in Scenario S5.

Table 4.6: Comparison results between MILP-based MPC control and Hysteresis Control methods in single-zone scenarios over 24 hours

Scenario NO.	MILP-based MPC control Energy Costs ($)	Hysteresis control Energy Costs ($)	Costs Saving Amount ($)	Costs Saving (%)
S1	4.1643	4.1930	0.0287	0.68%
S2	5.7171	6.0109	0.2938	4.89%
S3	3.7561	3.8641	0.1080	2.79%
S4	2.8793	4.1930	1.3137	31.33%
S5	4.6094	6.0109	1.4015	23.32%
S6	2.5353	3.8641	1.3288	34.39%

Chapter 5

Multi-zone Temperature Control and Energy Management

In this chapter, temperature control and energy management for multi-zone system configurations is studied. The first section describes multi-zone temperature control and energy management case studies, where scenarios without/with electric storage are considered. The formulation of optimization problem and results of simulations in a number of scenarios are presented. This is followed by a comparison with the conventional hysteresis control in six multi-zone scenarios in the second section. The third section looks at the effect of variable time-steps and optimization relaxation on system performance. The fourth section investigates the effect of the temperature limit schedules on control performance. The sensitivity of the system performance to model parameter errors and uncertainty in temperature predictions are studied in the last section.

5.1 Case Studies

A three-temperature-zone system configuration is discussed as an illustrative example and without any loss of generality. Simulations are performed in different scenarios to examine the performance of the proposed MILP-based MPC controller in multi-zone temperature control. The floor layout, room sizes and air distribution system in the building are depicted in Figure 5.1. The rest of parameter settings of the building in single-zone configurations are used in multi-zone temperature control. A battery with same characteristics as in Table 4.2 is used in multi-zone configuration 2. A summary of the multi-zone scenario studies are presented in Table 5.1.

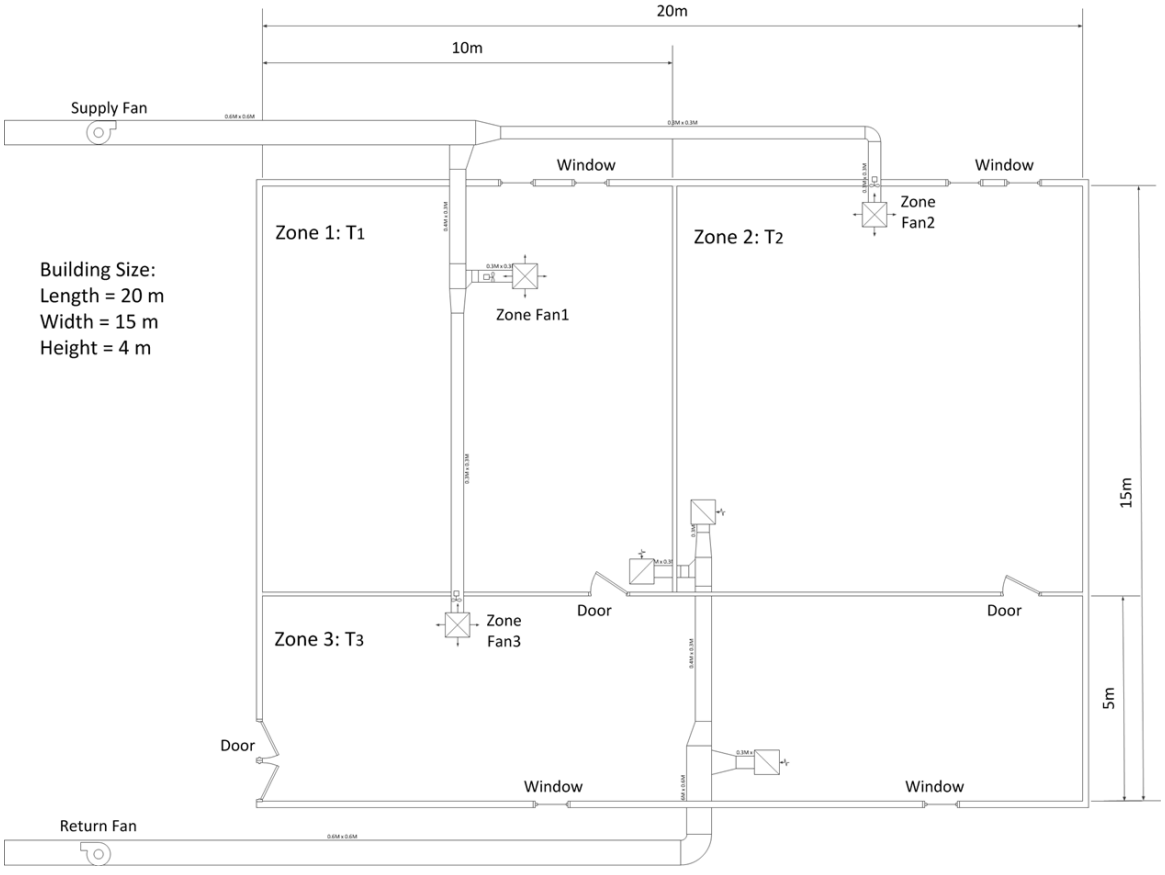

Figure 5.1: Floor layout and air distribution system in three-zone model.

Table 5.1: Summary of multi-zone scenarios

	Scenario	Description
Multi-zone Configuration 1	M1	Three rooms, in winter operation, heating using natural gas furnace, under TOU rates
	M2	Three rooms, in winter operation, heating using electric furnace, under TOU rates
	M3	Three rooms, in summer operation, cooling using air conditioner, under TOU rates
Multi-zone Configuration 2	M4	Three rooms, in winter operation, heating using natural gas furnace, under TOU rates and on-site electric energy storage
	M5	Three rooms, in winter operation, heating using electric furnace, under TOU rates and on-site electric energy storage
	M6	Three rooms, in summer operation, cooling using air conditioner, under TOU rates and on-site electric energy storage

5.1.1 Multi-zone Configuration 1: Three-room Temperature Control without Electric Storage

Optimization Formulation

In this configuration, without loss of generality, a building with three thermal zones is considered namely $N_r = 3$. The system includes one main and three vent fans, therefore $N_s = 2^{N_r+1} + 1 = 17$, e.g. see Table 3.4. The air flow rates for each room are determined by the state of the fans, as shown in Table 5.2. For each fan state $\boldsymbol{\delta}^{state,i}$, there are the corresponding dynamic matrix $\mathbf{A_i}$, $\mathbf{b_i}$ and $\mathbf{c_i}$ given in (3.21 - 3.26).

The goal here is

$$\min_{\mathbf{x}} \left(\mathbf{c}_\delta^T \boldsymbol{\delta}^{state} + \mathbf{c}_e^T \mathbf{p}_g \right) \tag{5.1}$$

where the electricity cost is $\mathbf{c}_e^T = \mathbf{c}_{elec}^T \text{diag}(\mathbf{h})$.

Table 5.2: Flow rates and room fan power for three-room system

State	F_{supply_1}	F_{supply_2}	F_{supply_3}	$\mathbf{p}_{fans_k}^{room}$
$\boldsymbol{\delta}^{state,1}$	0	0	0	0
$\boldsymbol{\delta}^{state,2}, \boldsymbol{\delta}^{state,3}$	$F_{supply_1}^{000}$	$F_{supply_2}^{000}$	$F_{supply_3}^{000}$	0
$\boldsymbol{\delta}^{state,4}, \boldsymbol{\delta}^{state,5}$	$F_{supply_1}^{100}$	$F_{supply_2}^{100}$	$F_{supply_3}^{100}$	P_{fan}^{room}
$\boldsymbol{\delta}^{state,6}, \boldsymbol{\delta}^{state,7}$	$F_{supply_1}^{010}$	$F_{supply_2}^{010}$	$F_{supply_3}^{010}$	P_{fan}^{room}
$\boldsymbol{\delta}^{state,8}, \boldsymbol{\delta}^{state,9}$	$F_{supply_1}^{001}$	$F_{supply_2}^{001}$	$F_{supply_3}^{001}$	P_{fan}^{room}
$\boldsymbol{\delta}^{state,10}, \boldsymbol{\delta}^{state,11}$	$F_{supply_1}^{110}$	$F_{supply_2}^{110}$	$F_{supply_3}^{110}$	$2P_{fan}^{room}$
$\boldsymbol{\delta}^{state,12}, \boldsymbol{\delta}^{state,13}$	$F_{supply_1}^{101}$	$F_{supply_2}^{101}$	$F_{supply_3}^{101}$	$2P_{fan}^{room}$
$\boldsymbol{\delta}^{state,14}, \boldsymbol{\delta}^{state,15}$	$F_{supply_1}^{011}$	$F_{supply_2}^{011}$	$F_{supply_3}^{011}$	$2P_{fan}^{room}$
$\boldsymbol{\delta}^{state,16}, \boldsymbol{\delta}^{state,17}$	$F_{supply_1}^{111}$	$F_{supply_2}^{111}$	$F_{supply_3}^{111}$	$3P_{fan}^{room}$

The optimization variables are

$$\mathbf{x} = \left[\boldsymbol{\tau}, \boldsymbol{\delta}^{state}, \boldsymbol{\tau}^{state}, \mathbf{p}_g\right]^T \tag{5.2}$$

where

$$\boldsymbol{\tau} = \begin{bmatrix} T_{1,1} \\ \vdots \\ T_{N_r,1} \\ \vdots \\ T_{1,N_h} \\ \vdots \\ T_{N_r,N_h} \end{bmatrix}, \boldsymbol{\delta}^{state} = \begin{bmatrix} \boldsymbol{\delta}_1^{state,1} \\ \vdots \\ \boldsymbol{\delta}_1^{state,N_s} \\ \vdots \\ \boldsymbol{\delta}_{N_h}^{state,1} \\ \vdots \\ \boldsymbol{\delta}_{N_h}^{state,N_s} \end{bmatrix}, \boldsymbol{\tau}^{state} = \begin{bmatrix} \boldsymbol{\tau}_1^{state,1} \\ \vdots \\ \boldsymbol{\tau}_1^{state,N_s} \\ \vdots \\ \boldsymbol{\tau}_{N_h}^{state,1} \\ \vdots \\ \boldsymbol{\tau}_{N_h}^{state,N_s} \end{bmatrix} \tag{5.3}$$

The following constraints are applicable in this optimization:

$$P_g^{min} \leq \mathbf{p}_{g_k} \leq P_g^{max}, \;\; k \in [1, N_h] \tag{5.4}$$

$$T_{min}\mathbf{1}_{N_r} \leq \boldsymbol{\tau}_k \leq T_{max}\mathbf{1}_{N_r}, \;\; k \in [1, N_h] \tag{5.5}$$

$$\mathbf{1}_{N_s}^T \boldsymbol{\delta}_k^{state} = 1, \;\; k \in [1, N_h] \tag{5.6}$$

$$\boldsymbol{\tau}_{k-1} - T_{large}(1 - \boldsymbol{\delta}_k^{state,i})\mathbf{1}_{N_r} \leq \boldsymbol{\tau}_k^{state,i} \leq \boldsymbol{\tau}_{k-1} + T_{large}(1 - \boldsymbol{\delta}_k^{state,i})\mathbf{1}_{N_r} \tag{5.7}$$

$$-T_{large}\boldsymbol{\delta}_k^{state,i}\mathbf{1}_{N_r} \leq \boldsymbol{\tau}_k^{state,i} \leq T_{large}\boldsymbol{\delta}_k^{state,i}\mathbf{1}_{N_r} \tag{5.8}$$

$$\begin{aligned}\boldsymbol{\tau}_k = [\mathbf{A}_1^k, \mathbf{A}_2^k, \ldots, \mathbf{A}_{N_s}^k]\boldsymbol{\tau}_k^{state} + T_{out,k}[\mathbf{b}_1^k, \mathbf{b}_2^k, \ldots, \mathbf{b}_{N_s}^k]\boldsymbol{\delta}_k^{state} \\ +[\mathbf{c}_1^k, \mathbf{c}_2^k, \ldots, \mathbf{c}_{N_s}^k]\boldsymbol{\delta}_k^{state}, \quad k \in [1, N_h]\end{aligned} \tag{5.9}$$

$$\mathbf{p}_g = \mathbf{p}_d + \mathbf{p}_\delta^T \boldsymbol{\delta}^{state} \tag{5.10}$$

Simulation Results

In theses simulations a time horizon $6h$ with the fix time-step $0.1h$ are used. Each room has the same volume ($400m^3$). The heat conductivities of the rooms are assumed different to simulate rooms with different number of windows. For winter operation, scenarios involving heating with natural gas and electric furnace have been studied. For summer operation, cooling with air conditioner is considered.

The room temperatures, outside temperature and the associated HVAC operational schedules in Scenario M1-M3 are depicted in Figure 5.2 - 5.7. Note that the dot-dashed (red) lines indicate maximum and minimum set temperature limits for each room.

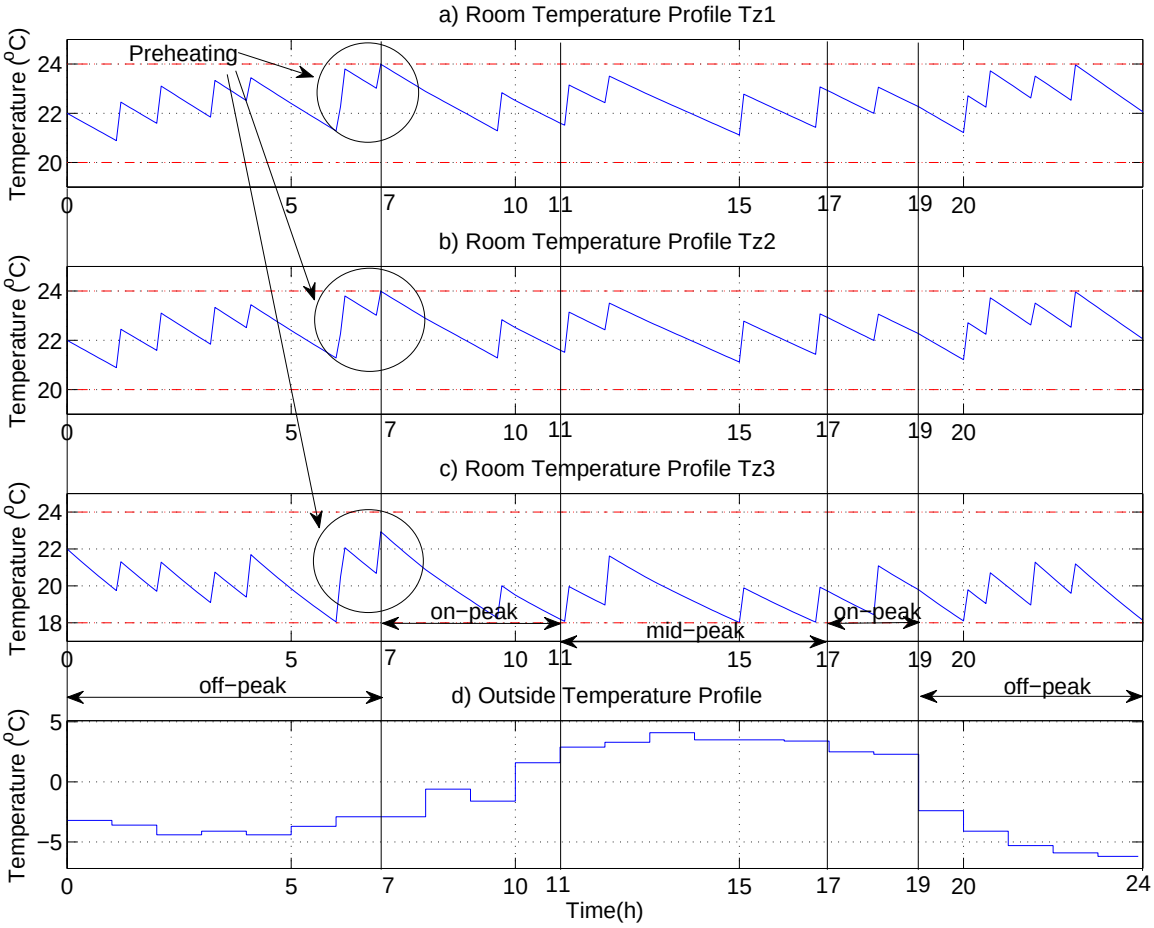

Figure 5.2: Scenario M1: three rooms, in winter operation, heating using natural gas furnace, without electric storage; a) 24-h Room 1 temperature profile Tz1, b) Room 2 temperature profile Tz2, c) Room 3 temperature profile Tz3, d) Outside temperature profile.

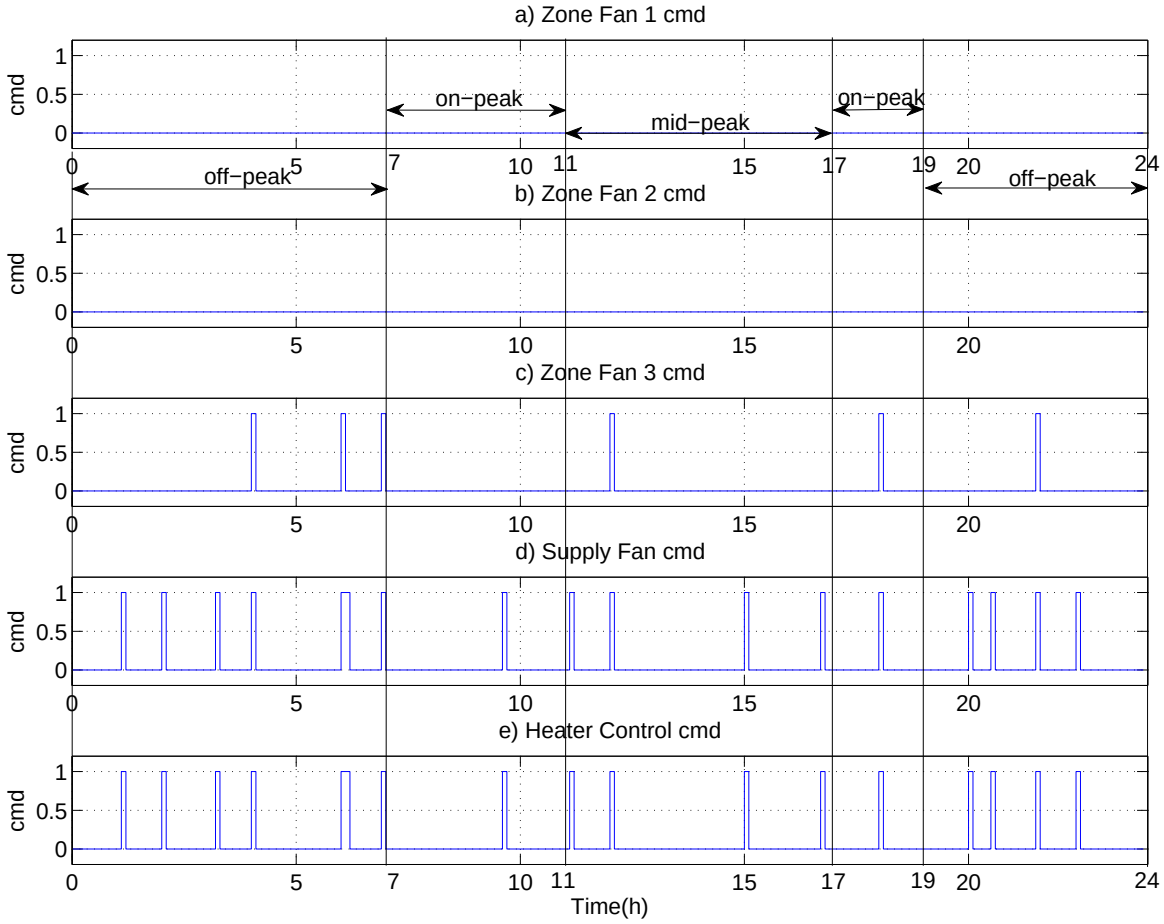

Figure 5.3: Scenario M1: three rooms, in winter operation, heating using natural gas furnace, without electric storage; a) Room 1 fan command, b) Room 2 fan command, c) Room 3 fan command, d) Supply fan command, e) Heater unit control command.

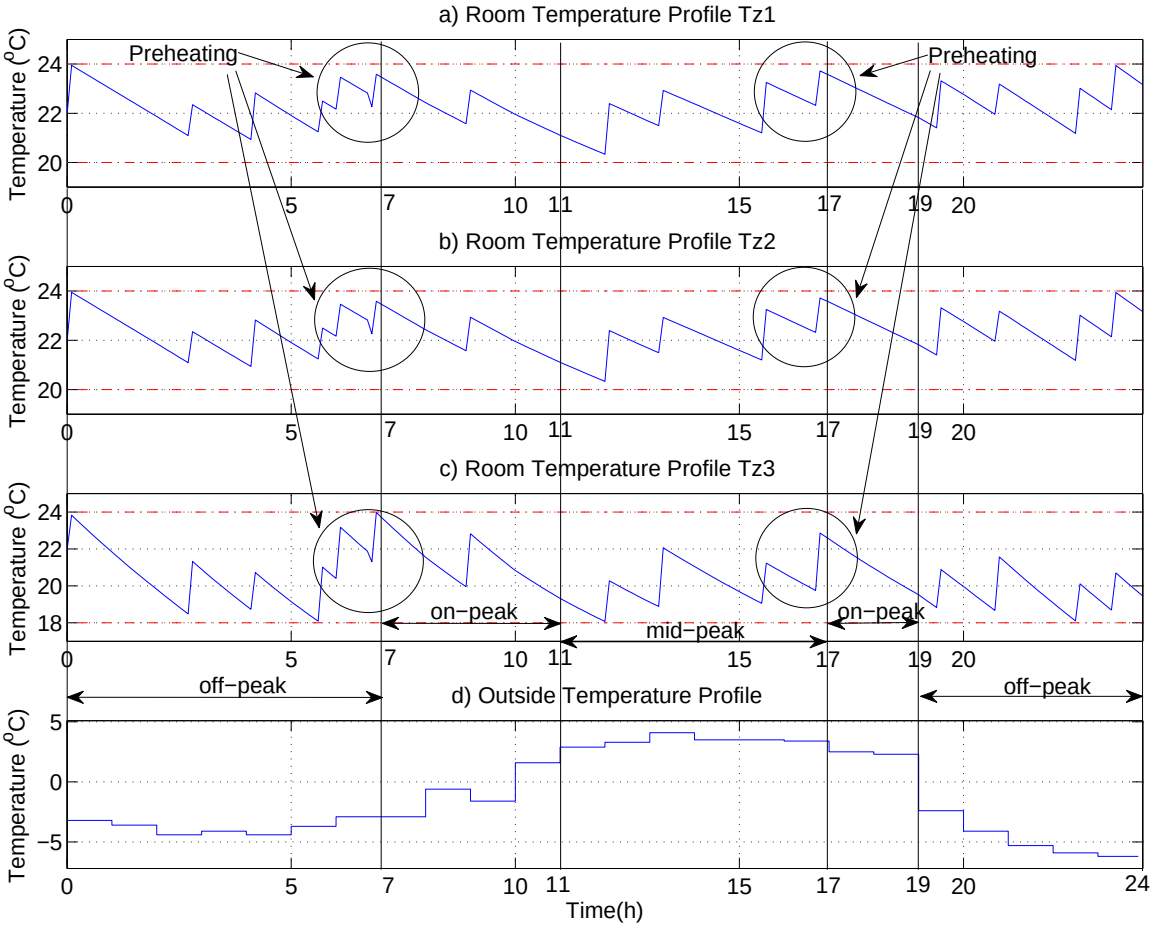

Figure 5.4: Scenario M2: three rooms, in winter operation, heating using electric furnace, without electric storage; a) 24-h Room 1 temperature profile Tz1, b) Room 2 temperature profile Tz2, c) Room 3 temperature profile Tz3, d) Outside temperature profile.

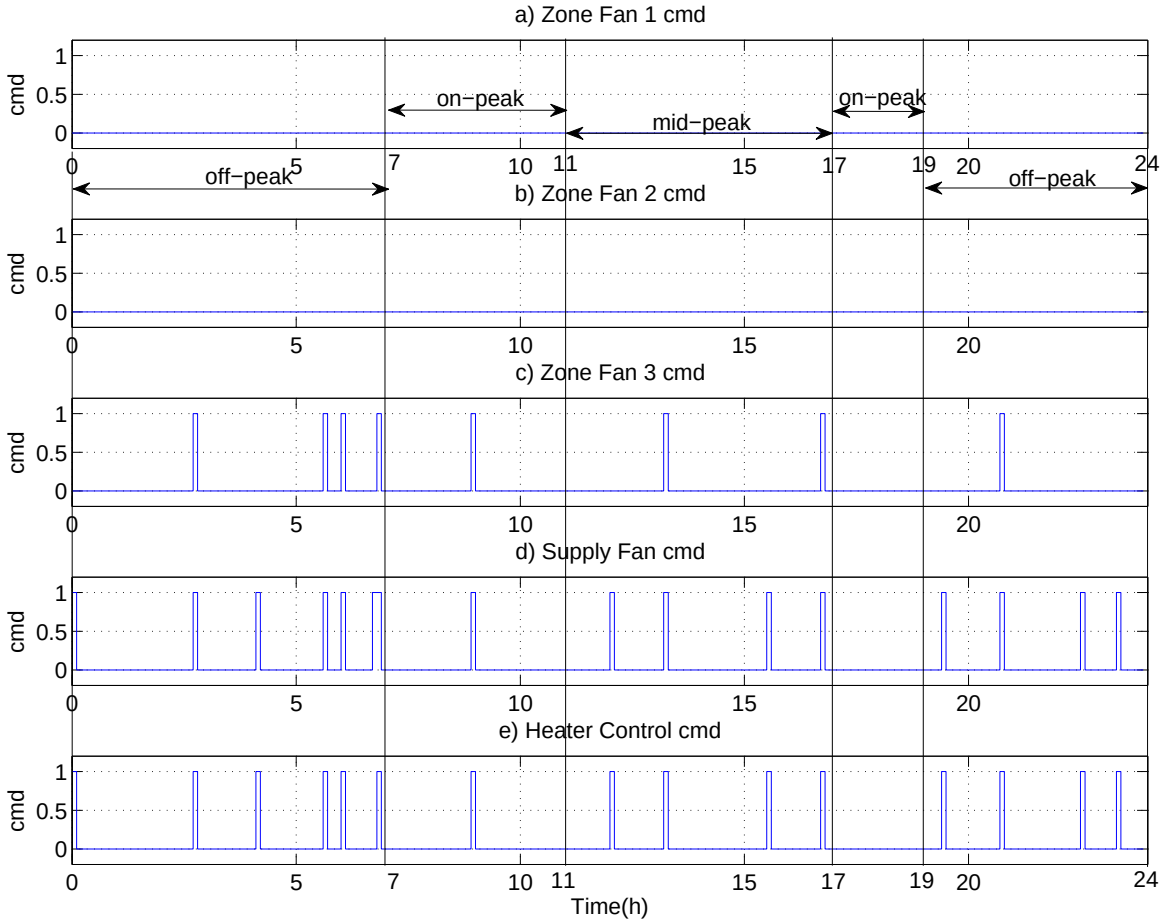

Figure 5.5: Scenario M2: three rooms, in winter operation, heating using electric furnace, without electric storage; a) Room 1 fan command, b) Room 2 fan command, c) Room 3 fan command, d) Supply fan command, e) Heater unit control command.

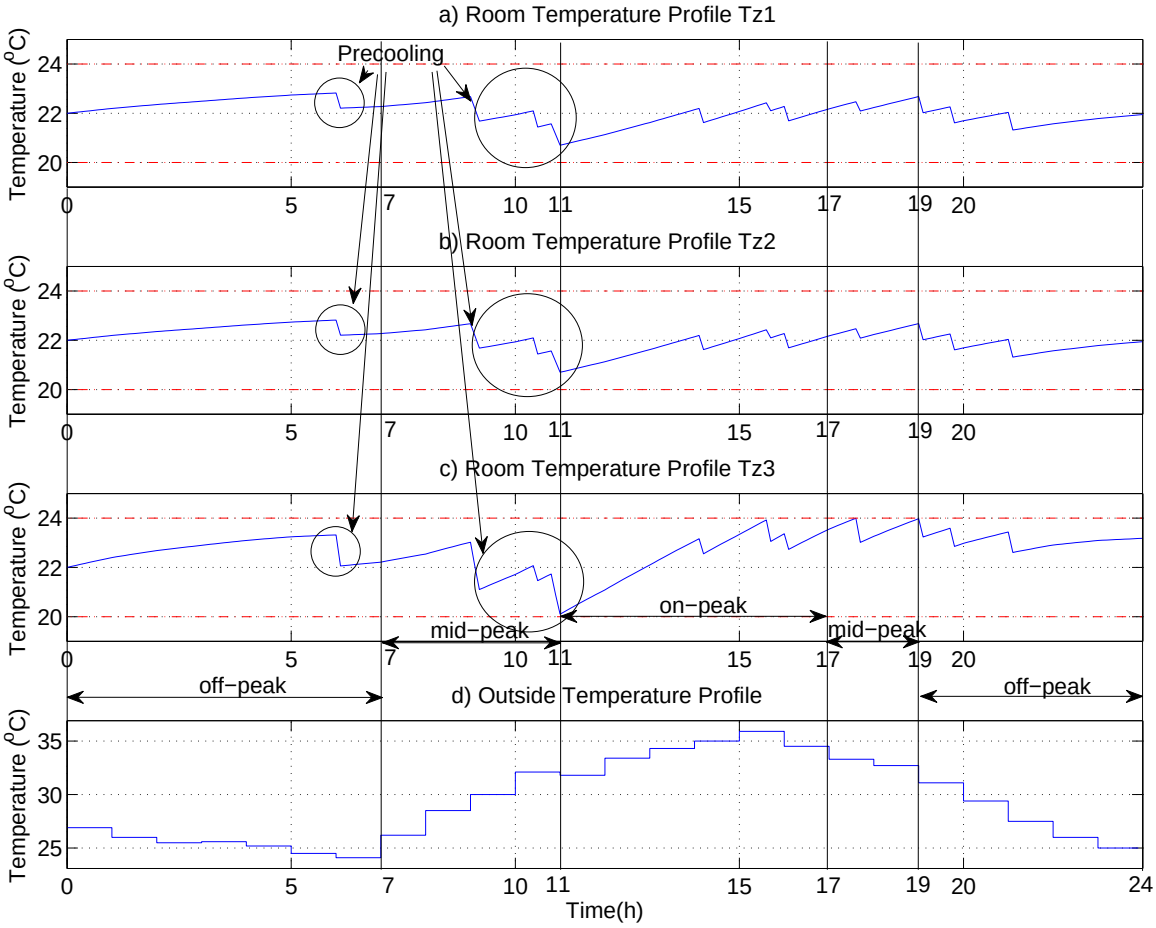

Figure 5.6: Scenario M3: three rooms, in summer operation, cooling using air conditioner, without electric storage; a) 24-h Room 1 temperature profile Tz1, b) Room 2 temperature profile Tz2, c) Room 3 temperature profile Tz3, d) Outside temperature profile.

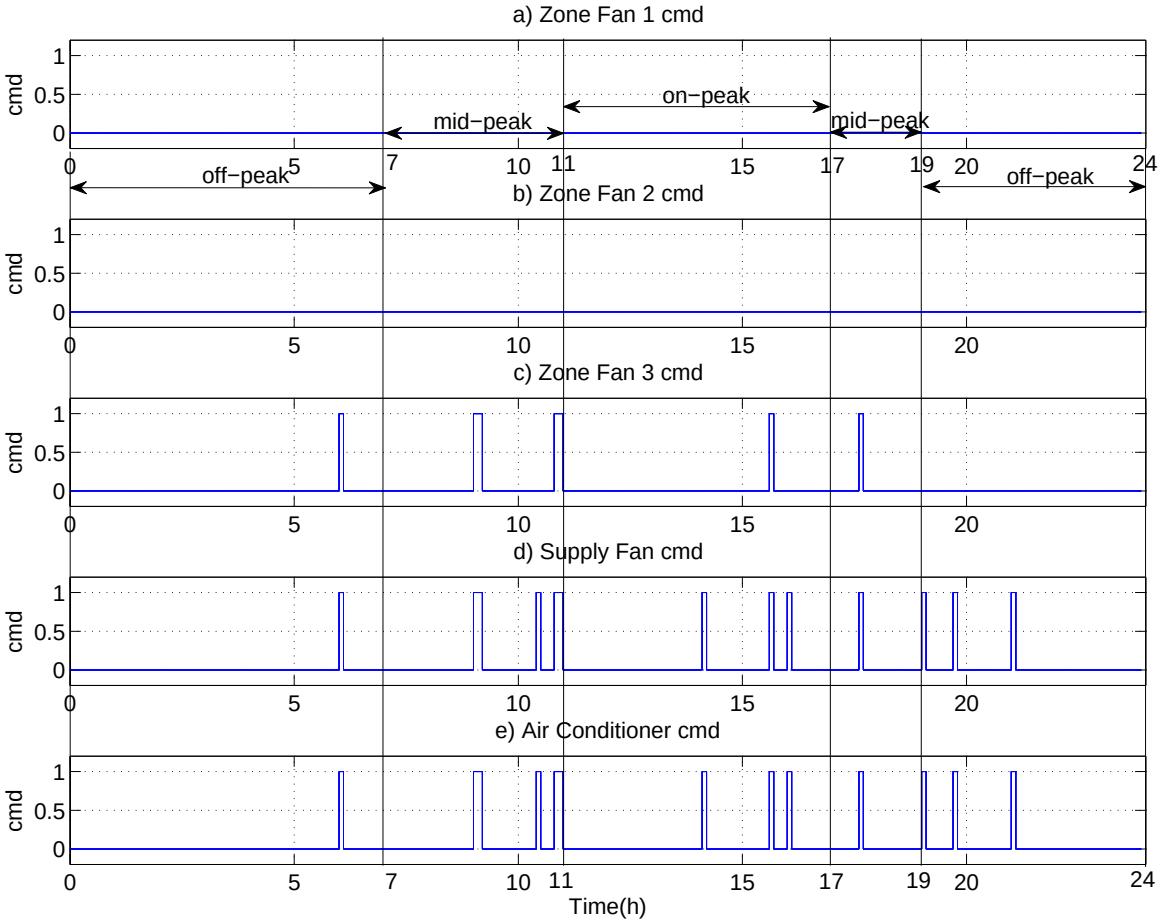

Figure 5.7: Scenario M3: three rooms, in summer operation, cooling using air conditioner, without electric storage; a) Room 1 fan command, b) Room 2 fan command, c) Room 3 fan command, d) Supply fan command, e) Air conditioner control command.

5.1.2 Multi-zone Configuration 2: Three-room Temperature Control with Electric Storage

Optimization Formulation

In this configuration, the electric storage is considered compared to the multi-zone configuration 1 in Section 5.1.1 that had no storage. The extra variable, battery

charging/discharging power $\mathbf{p}_s \in \Re^{N_h}$ is added to the optimization variables vector, i.e.

$$\mathbf{x} = \left[\boldsymbol{\tau}, \boldsymbol{\delta}^{state}, \boldsymbol{\tau}^{state}, \mathbf{p}_g, \mathbf{p}_s\right]^T \tag{5.11}$$

The goal is to minimize the energy cost, i.e.

$$\min_{\mathbf{x}} \left(\mathbf{c}_\delta^T \boldsymbol{\delta}^{state} + \mathbf{c}_e^T \mathbf{p}_g\right) \tag{5.12}$$

where $\mathbf{c}_e^T = \mathbf{c}_{elec}^T \text{diag}(\mathbf{h})$ is the electricity cost, $\mathbf{c}_\delta^T \boldsymbol{\delta}^{state}$ is the natural gas cost, and $\mathbf{c}_\delta^T \boldsymbol{\delta}^{state} = 0$ when heating using electric furnace in winter operation or cooling in summer operation.

The optimization constraints in this configuration are:

$$P_g^{min} \leq \mathbf{p}_{g_k} \leq P_g^{max}, \;\; k \in [1, N_h] \tag{5.13}$$

$$P_s^{min} \leq \mathbf{p}_{s_k} \leq P_s^{max} \tag{5.14}$$

$$T_{min}\mathbf{1}_{N_r} \leq \boldsymbol{\tau}_k \leq T_{max}\mathbf{1}_{N_r}, \;\; k \in [1, N_h] \tag{5.15}$$

$$\mathbf{1}_{N_s}^T \boldsymbol{\delta}_k^{state} = 1, \;\; k \in [1, N_h] \tag{5.16}$$

$$\boldsymbol{\tau}_{k-1} - T_{large}(1 - \boldsymbol{\delta}_k^{state,i})\mathbf{1}_{N_r} \leq \boldsymbol{\tau}_k^{state,i} \leq \boldsymbol{\tau}_{k-1} + T_{large}(1 - \boldsymbol{\delta}_k^{state,i})\mathbf{1}_{N_r} \tag{5.17}$$

$$-T_{large}\boldsymbol{\delta}_k^{state,i}\mathbf{1}_{N_r} \leq \boldsymbol{\tau}_k^{state,i} \leq T_{large}\boldsymbol{\delta}_k^{state,i}\mathbf{1}_{N_r} \tag{5.18}$$

$$\begin{aligned}\boldsymbol{\tau}_k = [\mathbf{A}_1^k, \mathbf{A}_2^k, \ldots, \mathbf{A}_{N_s}^k]\boldsymbol{\tau}_k^{state} + T_{out,k}[\mathbf{b}_1^k, \mathbf{b}_2^k, \ldots, \mathbf{b}_{N_s}^k]\boldsymbol{\delta}_k^{state} \\ +[\mathbf{c}_1^k, \mathbf{c}_2^k, \ldots, \mathbf{c}_{N_s}^k]\boldsymbol{\delta}_k^{state}, \quad k \in [1, N_h]\end{aligned} \tag{5.19}$$

$$\mathbf{p}_g = \mathbf{p}_d + \mathbf{p}_s + \mathbf{p}_\delta^T \boldsymbol{\delta}^{state} \tag{5.20}$$

$$E_s^{min} \leq \textstyle\sum_{j=1}^{k} \mathbf{h}_j \mathbf{p}_{s_j} + E_0 \leq E_s^{max}, \;\; k \in [1, N_h] \tag{5.21}$$

$$\mathbf{h}^T \mathbf{p}_s = E_{final} - E_0 \tag{5.22}$$

Simulation Results

In these simulations, the control time horizon is $6h$ with a fix time-step of $0.1h$. For scenarios in winter operation, heating with natural gas and electric furnace has been studied. For summer operation, cooling with air conditioner is considered. The room temperatures and the operational schedules in Scenario M4-M6 are depicted in Figure 5.8,5.9, Figure 5.11,5.12, Figure 5.14,5.15. Figures 5.10, 5.13, 5.16 show the load power profile, grid buying or selling power, charging or discharging power and energy level in the battery in a typical winter/summer day. Note that the dot-dashed (red) lines indicate maximum and minimum temperature limit set for the corresponding room.

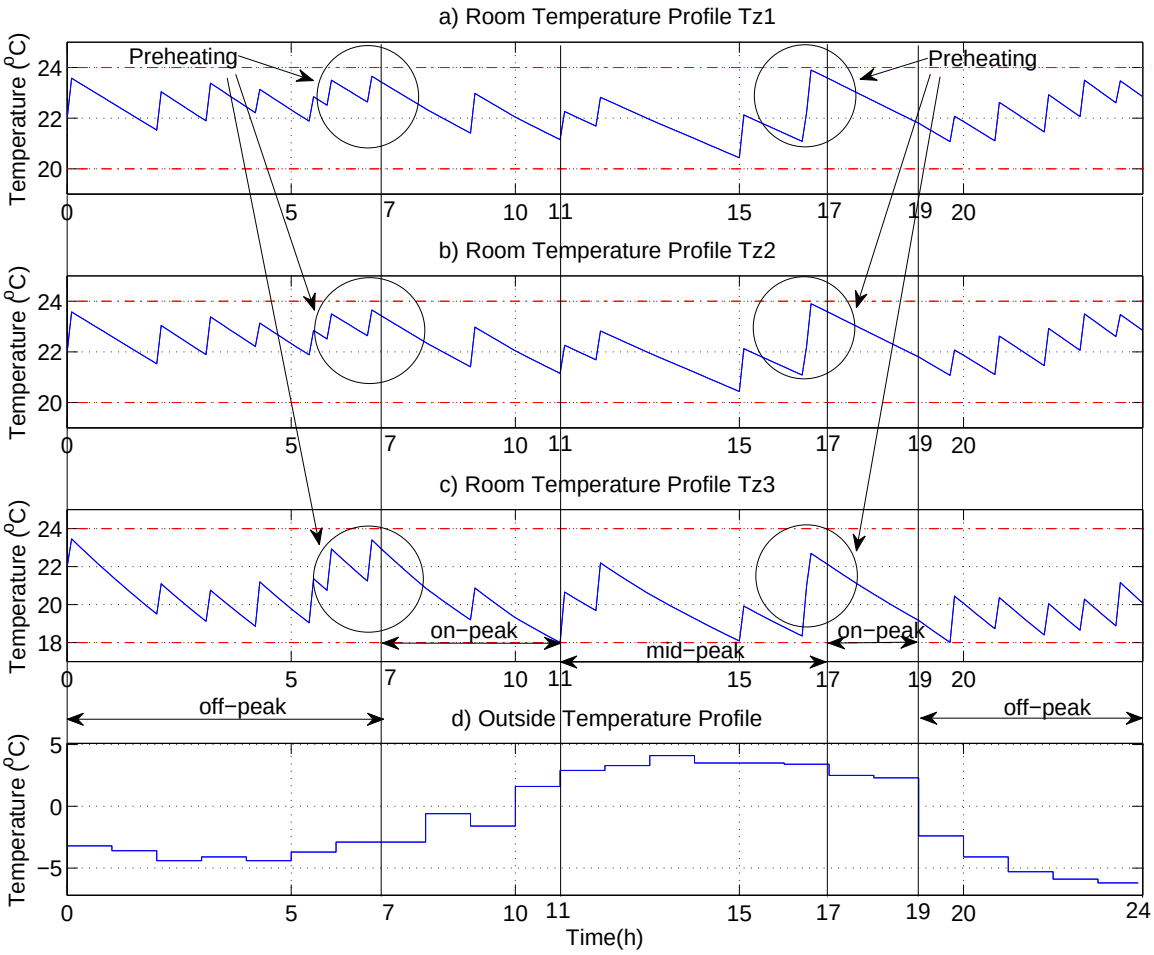

Figure 5.8: Scenario M4: three rooms, in winter operation, heating using natural gas furnace, with electric storage; a) 24-h Room 1 temperature profile Tz1, b) Room 2 temperature profile Tz2, c) Room 3 temperature profile Tz3, d) Outside temperature profile.

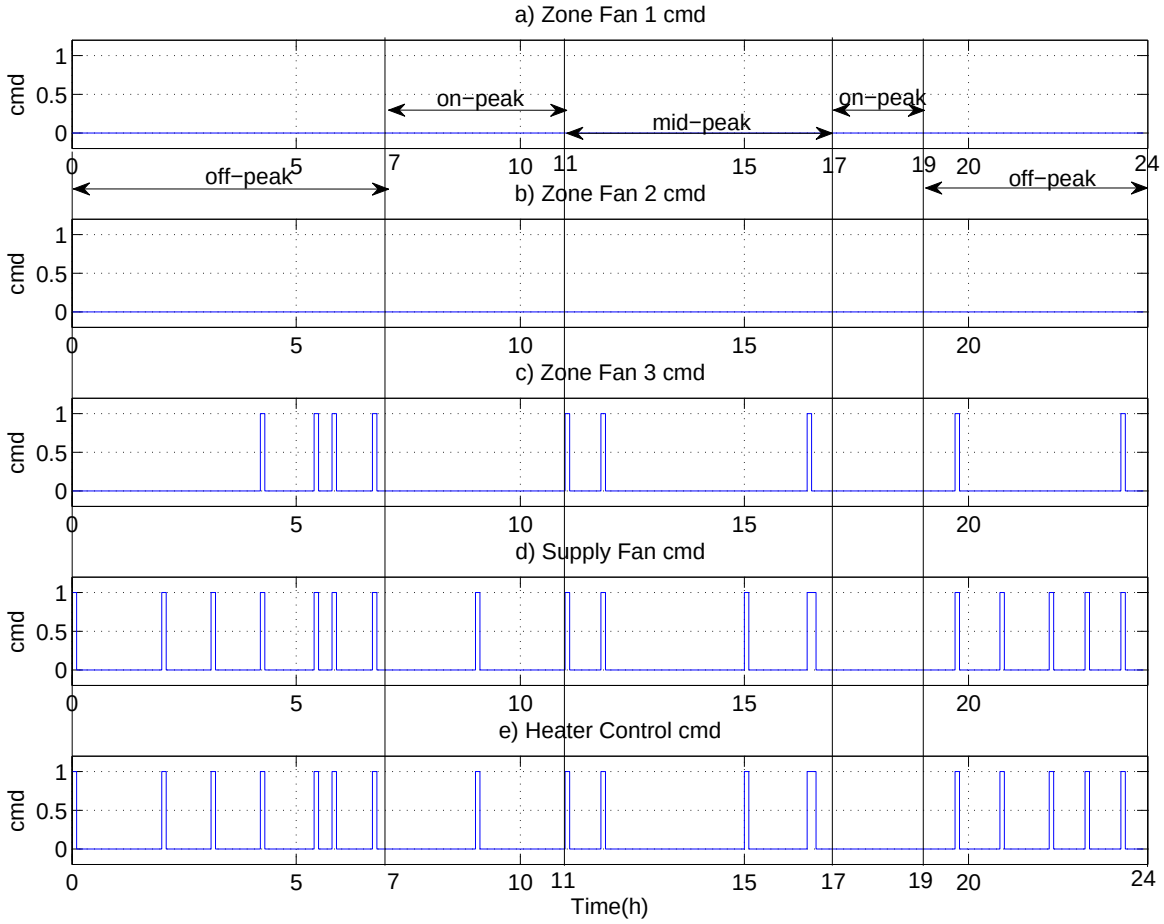

Figure 5.9: Scenario M4: three rooms, in winter operation, heating using natural gas furnace, with electric storage; a) Room 1 fan command, b) Room 2 fan command, c) Room 3 fan command, d) Supply fan command, e) Heater unit control command.

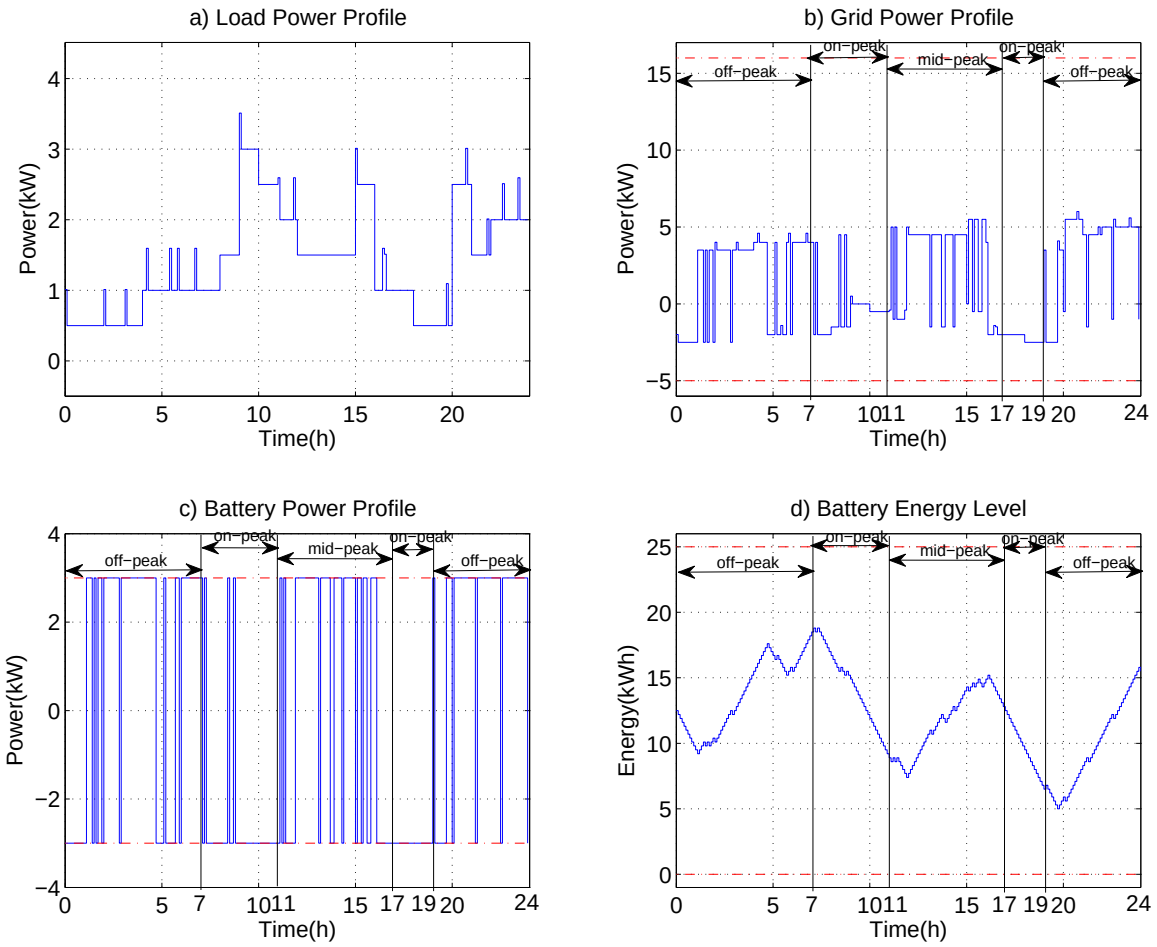

Figure 5.10: Scenario M4: three rooms, in winter operation, heating using natural gas furnace, with electric storage; a) Load power profile, b) Grid power profile, c) Battery power profile, d) Battery Energy Level.

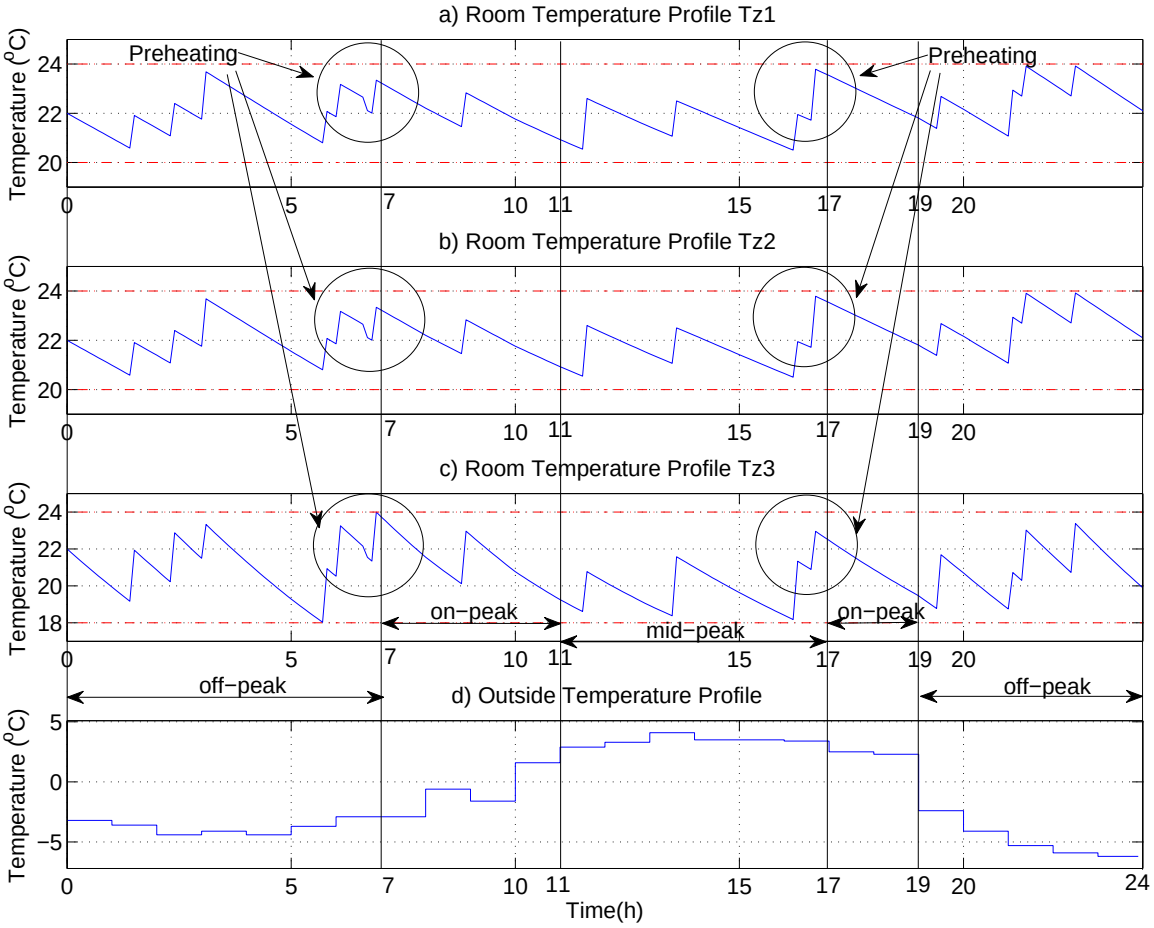

Figure 5.11: Scenario M5: three rooms, in winter operation, heating using electric furnace, with electric storage; a) 24-h Room 1 temperature profile Tz1, b) Room 2 temperature profile Tz2, c) Room 3 temperature profile Tz3, d) Outside temperature profile.

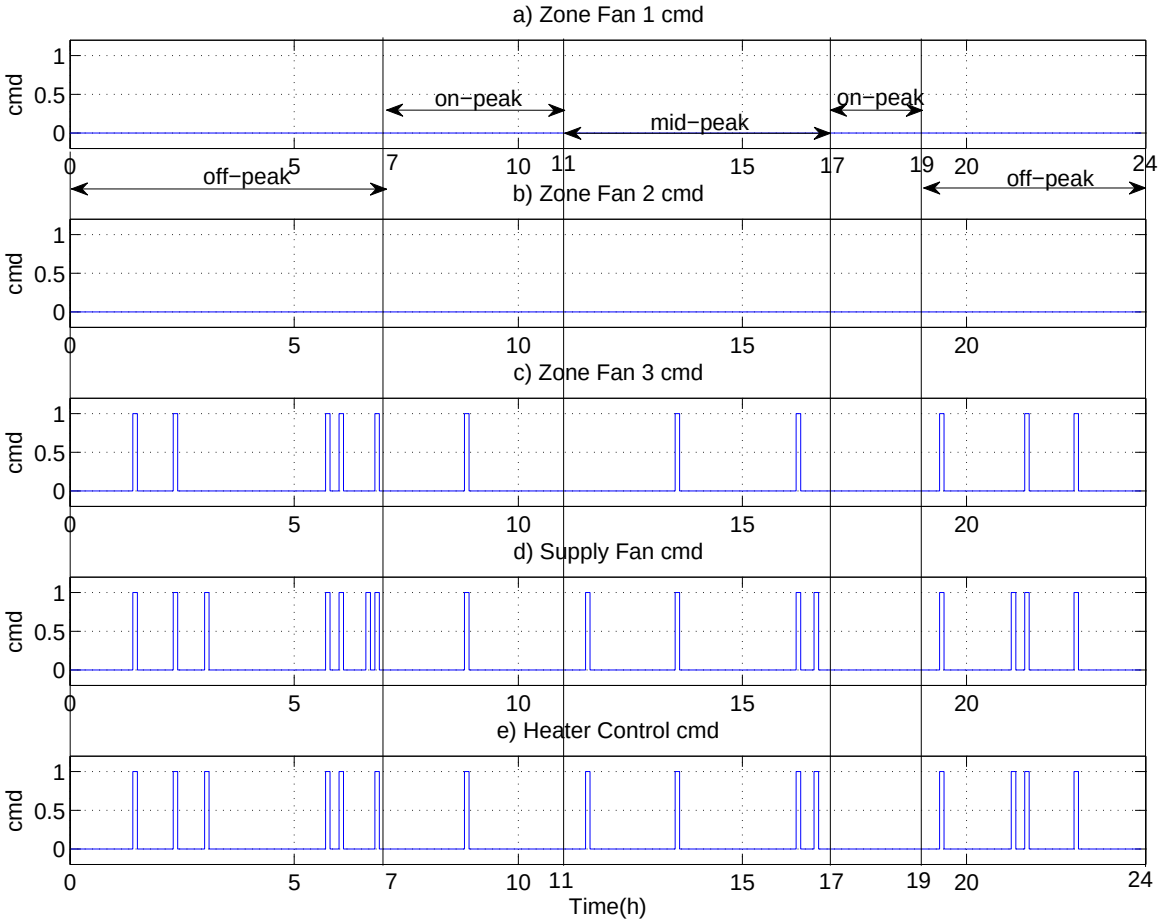

Figure 5.12: Scenario M5: three rooms, in winter operation, heating using electric furnace, with electric storage; a) Room 1 fan command, b) Room 2 fan command, c) Room 3 fan command, d) Supply fan command, e) Heater unit control command.

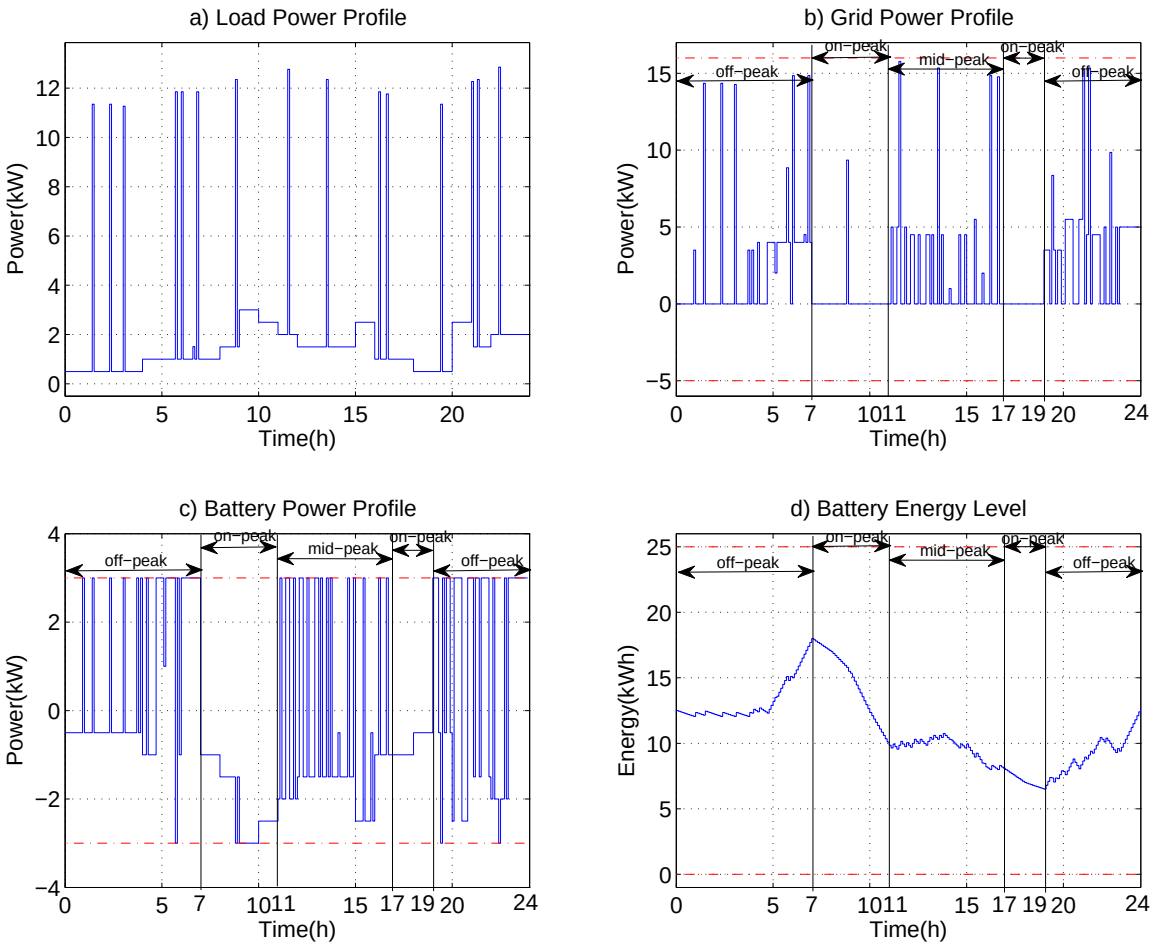

Figure 5.13: Scenario M5: three rooms, in winter operation, heating using electric furnace, with electric storage; a) Load power profile, b) Grid power profile, c) Battery power profile, d) Battery energy level.

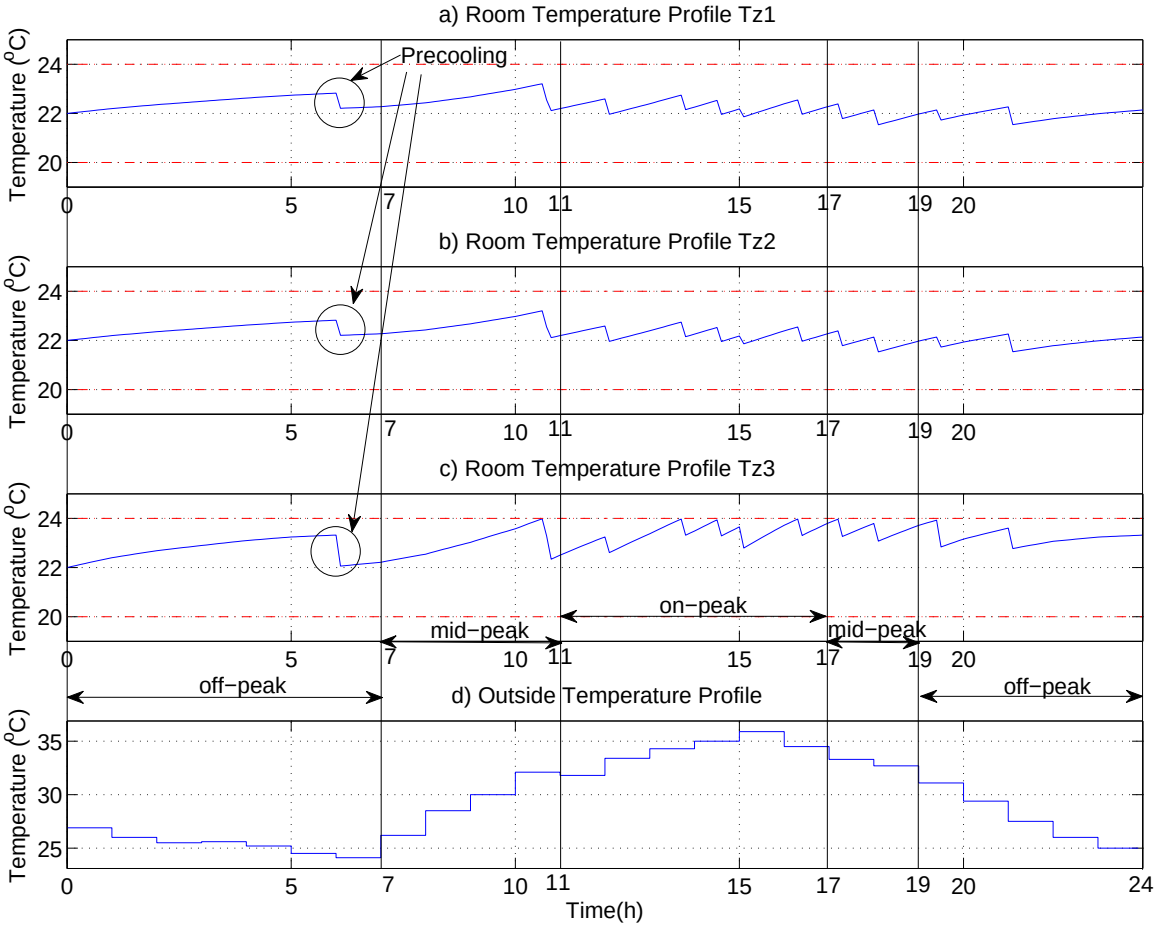

Figure 5.14: Scenario M6: three rooms, in summer operation, cooling using air conditioner, with electric storage; a) 24-h Room 1 temperature profile Tz1, b) Room 2 temperature profile Tz2, c) Room 3 temperature profile Tz3, d) Outside temperature profile.

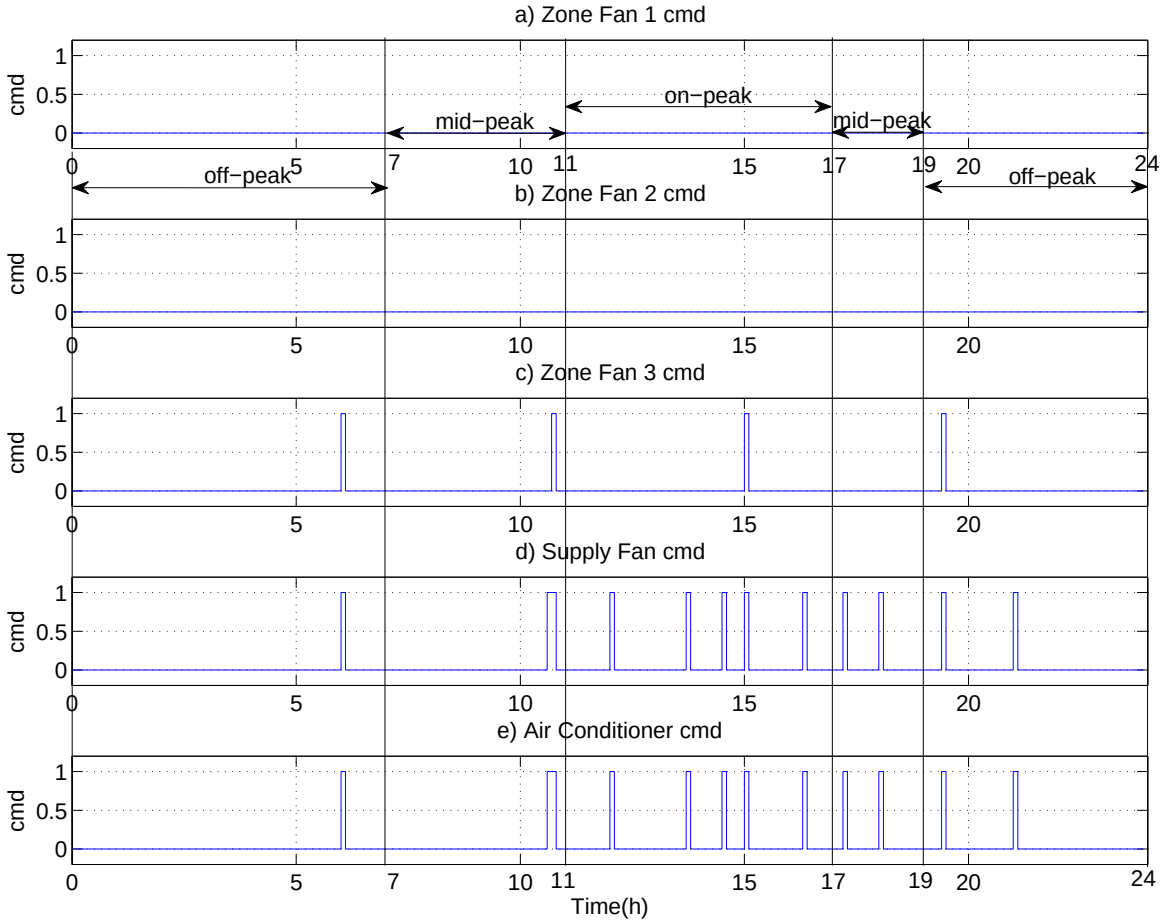

Figure 5.15: Scenario M6: three rooms, in summer operation, cooling using air conditioner, with electric storage; a) Room 1 fan command, b) Room 2 fan command, c) Room 3 fan command, d) Supply fan command, e) Air conditioner control command.

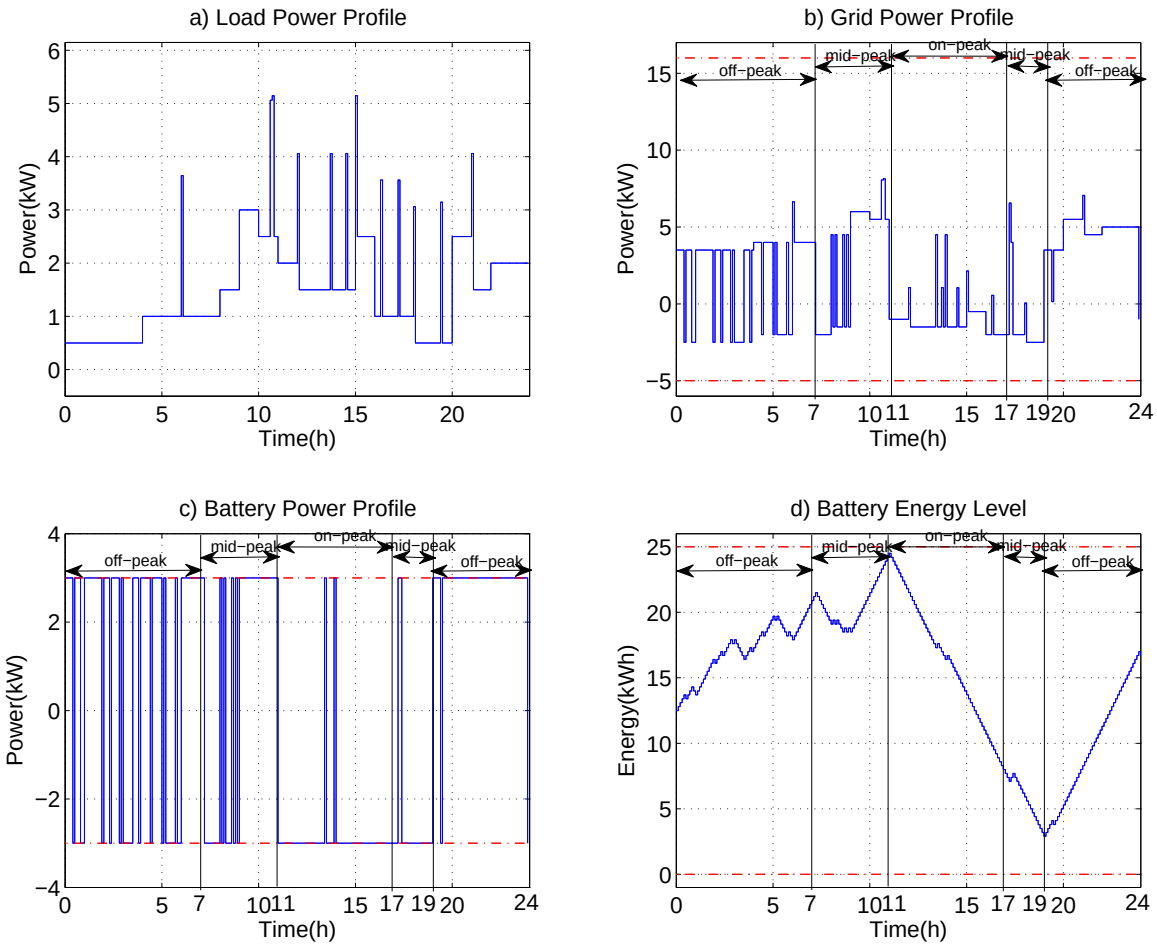

Figure 5.16: Scenario M6: three rooms, in summer operation, cooling using air conditioner, with electric storage; a) Load power profile, b) Grid power profile, c) Battery power profile, d) Battery energy level.

5.2 Comparison With Hysteresis Control

Simulations based on a hysteresis control method are conducted with the same parameters as those in the respective optimal MILP-based MPC case in different scenarios in Table 5.1. The temperature in hysteresis control are limited within 20-22 ℃ in winter, and 22-24 ℃ in summer. These simulation results are compared with those

from the proposed MILP-based MPC control approach. Table 5.3 presents a summary of the comparison between MILP-based MPC control and hysteresis control methods in Scenarios M1-M6. It should be noted that since the hysteresis controller does not utilize the energy storage, its results are not impacted by the presence or absence of storage.

It is observed that the energy cost is less in MILP-based MPC control. The scenarios without storage M1-M3 illustrate that the proposed control method saves cost mainly by pre-heating/pre-cooling the building under time-of-use pricing, trying to use more low-price energy and less high-price energy while meeting the thermal and energy requirements of the building. The scenarios with battery storage M4-M6 show increased savings by better exploiting time-of-use pricing, charging-low/discharging-high.

Table 5.3: Comparison results between MILP-based MPC Control and Hysteresis Control methods in multi-zone scenarios over 24 hours

Scenario NO.	MILP-based MPC control Energy Costs ($)	Hysteresis control Energy Costs ($)	Costs Saving Amount ($)	Costs Saving (%)
M1	3.7449	4.1438	0.3989	9.63%
M2	4.6808	5.5200	0.8392	15.20%
M3	3.6442	3.9982	0.3540	8.85%
M4	2.8323	4.1438	1.3115	31.65%
M5	4.0785	5.5200	1.4415	26.11%
M6	2.9333	3.9982	1.0649	26.63%

5.3 Effect of Variable Time Steps and Optimization Relaxation

The settings in Scenario M2 are used to examine the performance of the proposed controller with variable time-step and optimization relaxation. The room temperatures are maintained between 15 ℃ and 30 ℃ during the unoccupied period, and between 20 ℃ and 24 ℃ during the occupied period. It is assumed that both occupied and on-peak/mid-peak periods occur simultaneously from 7:00 to 19:00. The time horizon is still 6 h, however the time-step vector $\mathbf{h}$ is adjusted. For uniform time steps, the elements of $\mathbf{h}$ are all 0.1 h, namely $\mathbf{h} = 0.1 * ones(60, 1)$, where $ones(N_h, 1) \in \mathbf{Z}^{N_h}$ is used to denote a vector of ones. For variable time steps, the vector is modified to $\mathbf{h} = [0.1 * ones(10, 1); 0.2 * ones(10, 1); 0.3 * ones(10, 1)]$. For opt-relaxation, the time-step vector is still $\mathbf{h} = 0.1 * ones(60, 1)$ with relaxing the binary constraints for all but the first one hour in the rolling horizon window. Similarly, for variable time steps and opt-relaxation case, all the binary constraints are relaxed except for the first one hour in the rolling horizon window based on the variable time-step setting. Table 5.4 summarizes the effects of the variable time-steps and optimization relaxation on computation time and system performance.

It can be seen that the use of variable time steps and optimization relaxation dramatically reduces the computation time. In fact, in the vast majority of control time steps, the rolling horizon computations can be carried out in less than 10 seconds; see the distribution of the computation time Figure 5.17. For the uniform time-step case, suboptimal solutions are found because the solver is forced to quit early due to time constraints. For the variable time-step case, long control time steps and limited computation time both force suboptimal planning. With the use of variable time-steps and optimization relaxation, the computations can be completed in reasonable

Table 5.4: Effect of variable time steps and opt-relaxation in Scenario M2

	MILP-based CHP control		Hysteresis control	
Cases	Ave-Computation Time Per Opt (s)	Energy Cost ($)	Energy Cost ($)	Cost Saving (%)
Uniform Time-steps	> 7200	4.7394	5.1642	8.23%
Variable Time-steps	537.9571	4.8167	5.1642	6.73%
Opt-Relax	153.393	4.7032	5.1642	8.93%
Var Time-Steps & Opt-Relax	49.05	4.7032	5.1642	8.93%

time and optimal solution under this condition can be obtained, which also improves the accuracy of the solutions. That is why we observe a little improvement in energy cost for variable time steps and opt-relaxation case.

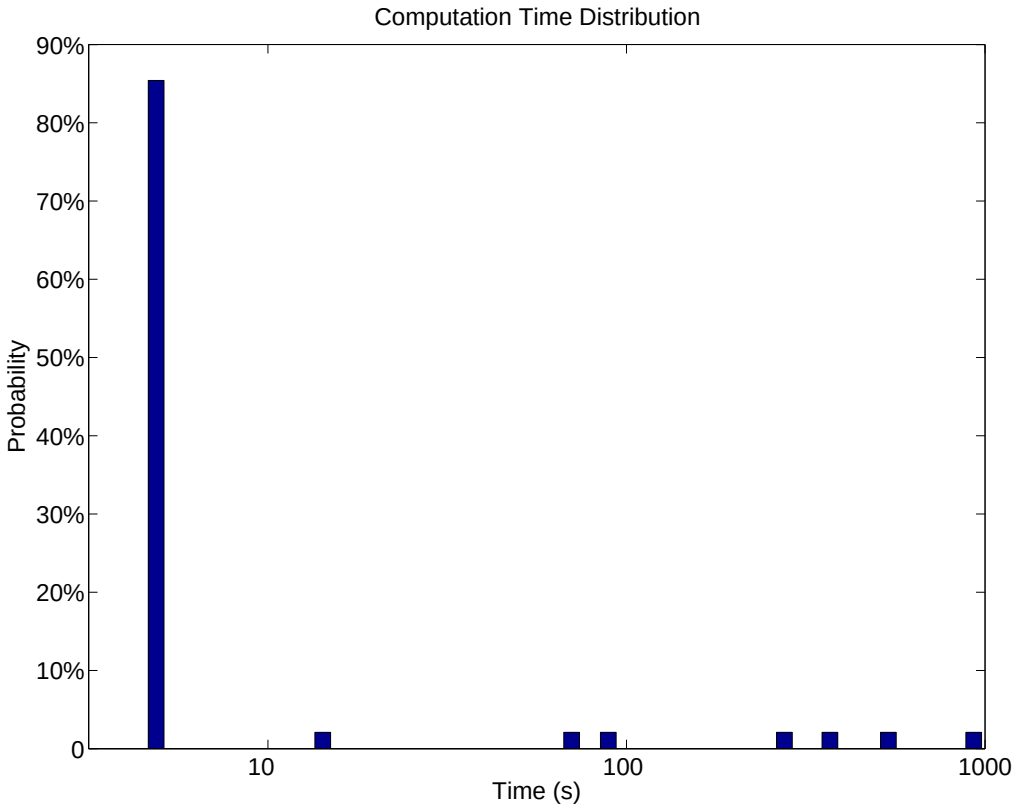

Figure 5.17: Computation time distribution for variable time-steps & opt-relax case in Scenario M2.

As comparative case, the room temperature profile and operation schedules in uniform time steps in Scenario M2 are presented in Figures 5.18, 5.19. The room temperature profile and operation schedules in variable time step and opt-relaxation in Scenario M2 are depicted in Figures 5.20, 5.21. Note that the dot-dashed (red) lines indicate maximum and minimum temperature limit set for the corresponding rooms.

It can be seen that the performance is not affected any more when energy cost decreases by the use of variable time steps and optimization relaxation. The room temperatures can be still controlled within the desired limits, although some changes on the operations of heater unit and fans are caused by utilizing the variable time-step

and optimization relaxation strategy. Considering the computation time constraints, the use of variable time steps and relaxation of some of the binary constraints make real-time control implementation of the proposed controller feasible.

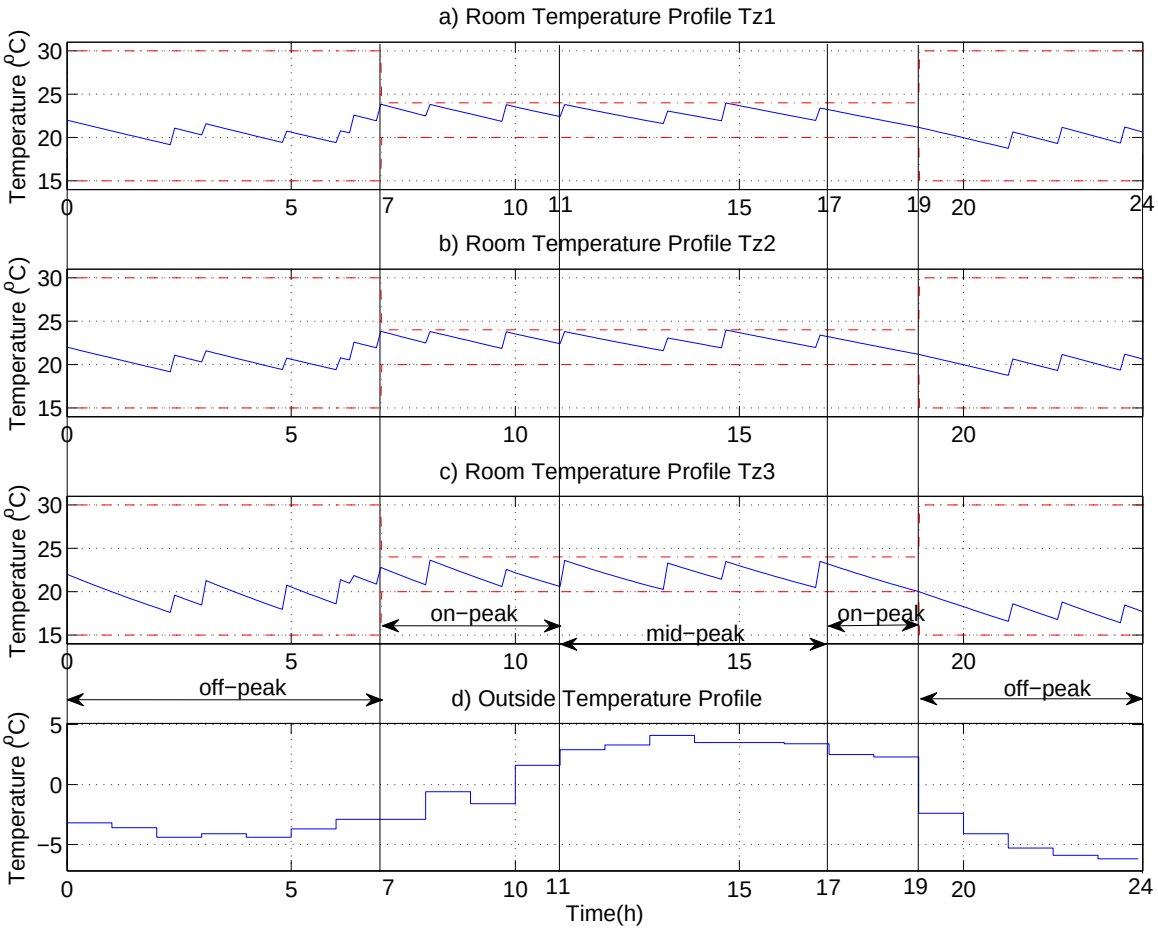

Figure 5.18: Comparative case with uniform time-step in Scenario M2: a) 24-h Room 1 temperature profile Tz1, b) Room 2 temperature profile Tz2, c) Room 3 temperature profile Tz3, d) Outside temperature profile.

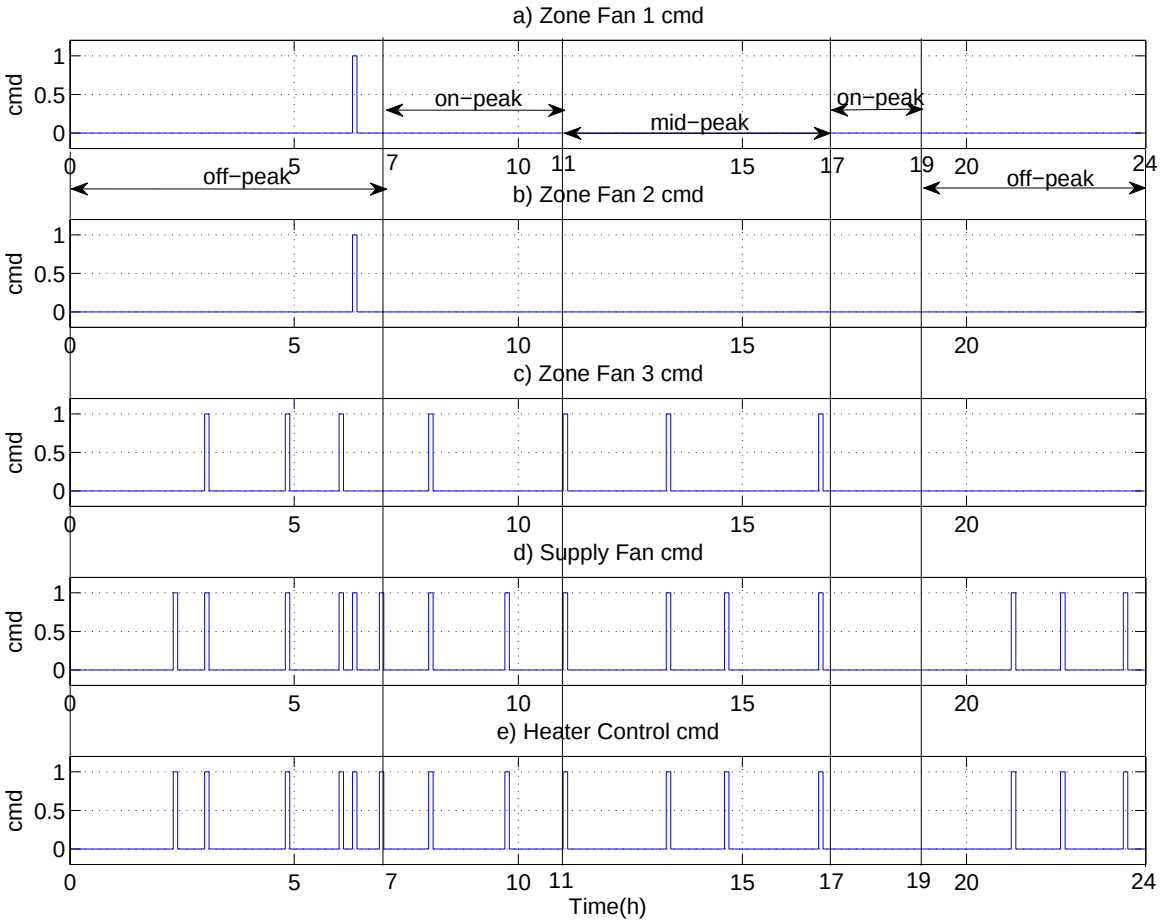

Figure 5.19: Comparative case with uniform time-step in Scenario M2: a) Room 1 fan command, b) Room 2 fan command, c) Room 3 fan command, d) Supply fan command, e) Heater unit control command.

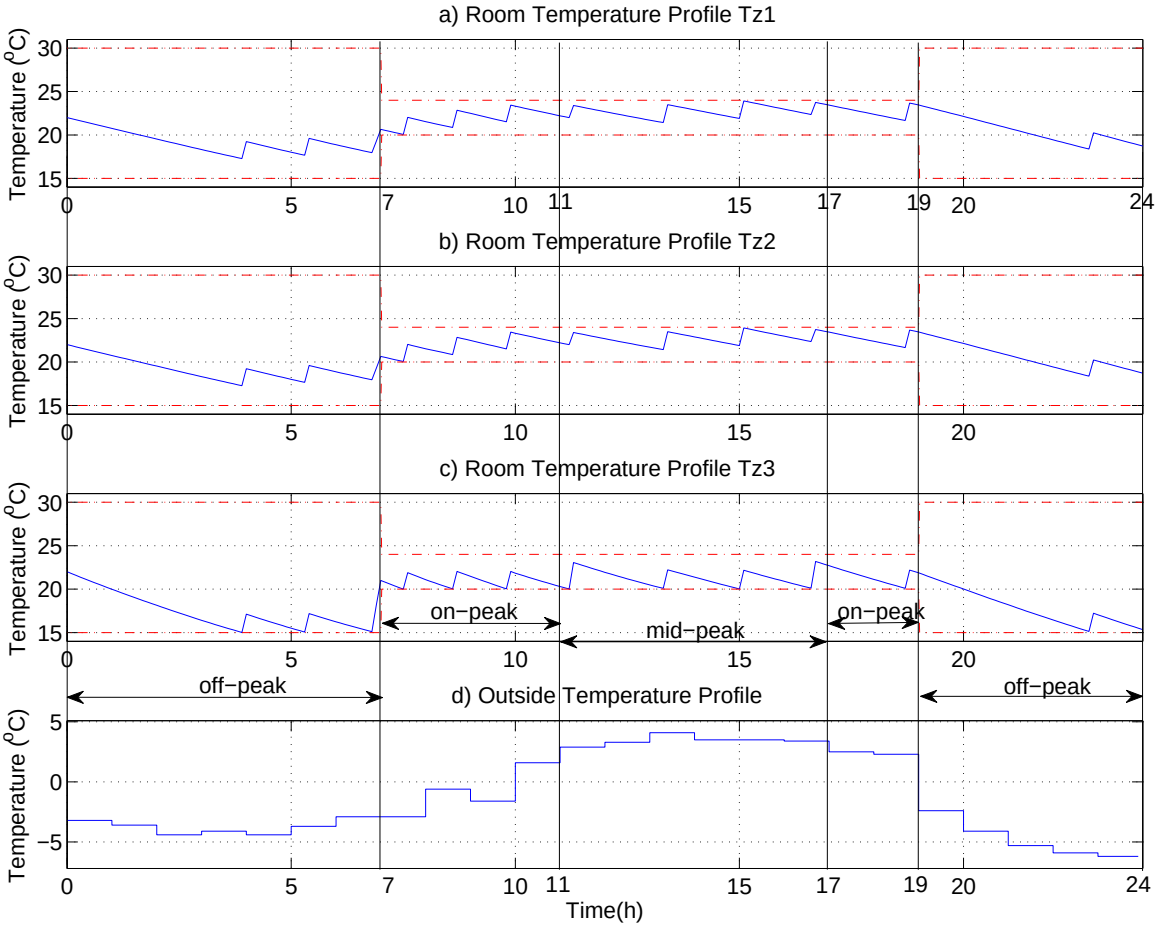

Figure 5.20: Effect of variable time-steps & opt-relax in Scenario M2: a) 24-h Room 1 temperature profile Tz1, b) Room 2 temperature profile Tz2, c) Room 3 temperature profile Tz3, d) Outside temperature profile.

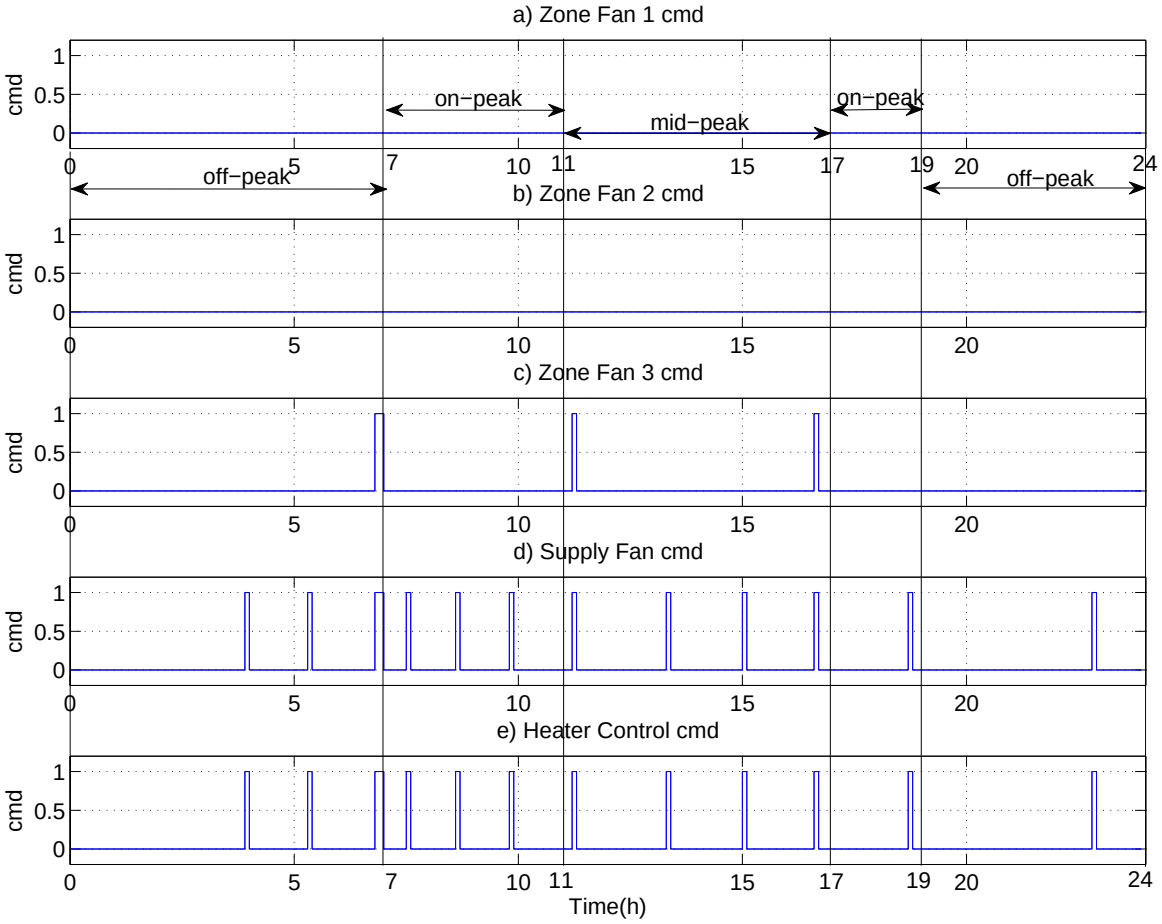

Figure 5.21: Effect of variable time-steps & opt-relax in Scenario M2: a) Room 1 fan command, b) Room 2 fan command, c) Room 3 fan command, d) Supply fan command, e) Heater unit control command.

5.4 Effect of Temperature Limit Schedules

The case in scenario M2 is used to examine the performance of the proposed MILP-based MPC control under different temperature limit schedules, as shown in Figures 5.22, 5.23. Variable time steps and optimization relaxation are utilized in these simulations. The other settings used in the previous section are also employed here,

however the temperature limit schedules are adjusted. It can be seen that the room fans can help maintain the temperatures between their desired limits even during transitions in the limits.

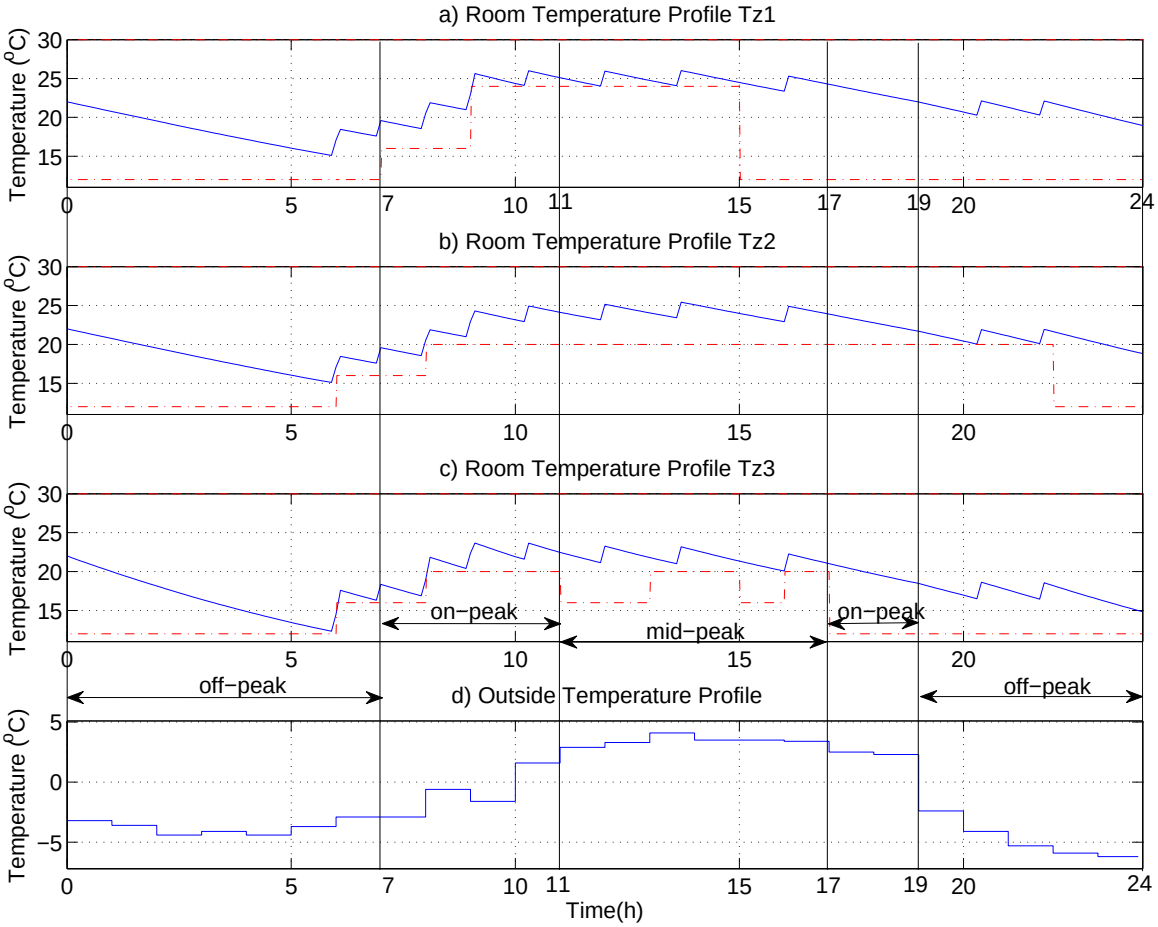

Figure 5.22: Effect of variable temperature limit schedule in Scenario M2: a) 24-h Room 1 temperature profile Tz1, b) Room 2 temperature profile Tz2, c) Room 3 temperature profile Tz3, d) Outside temperature profile.

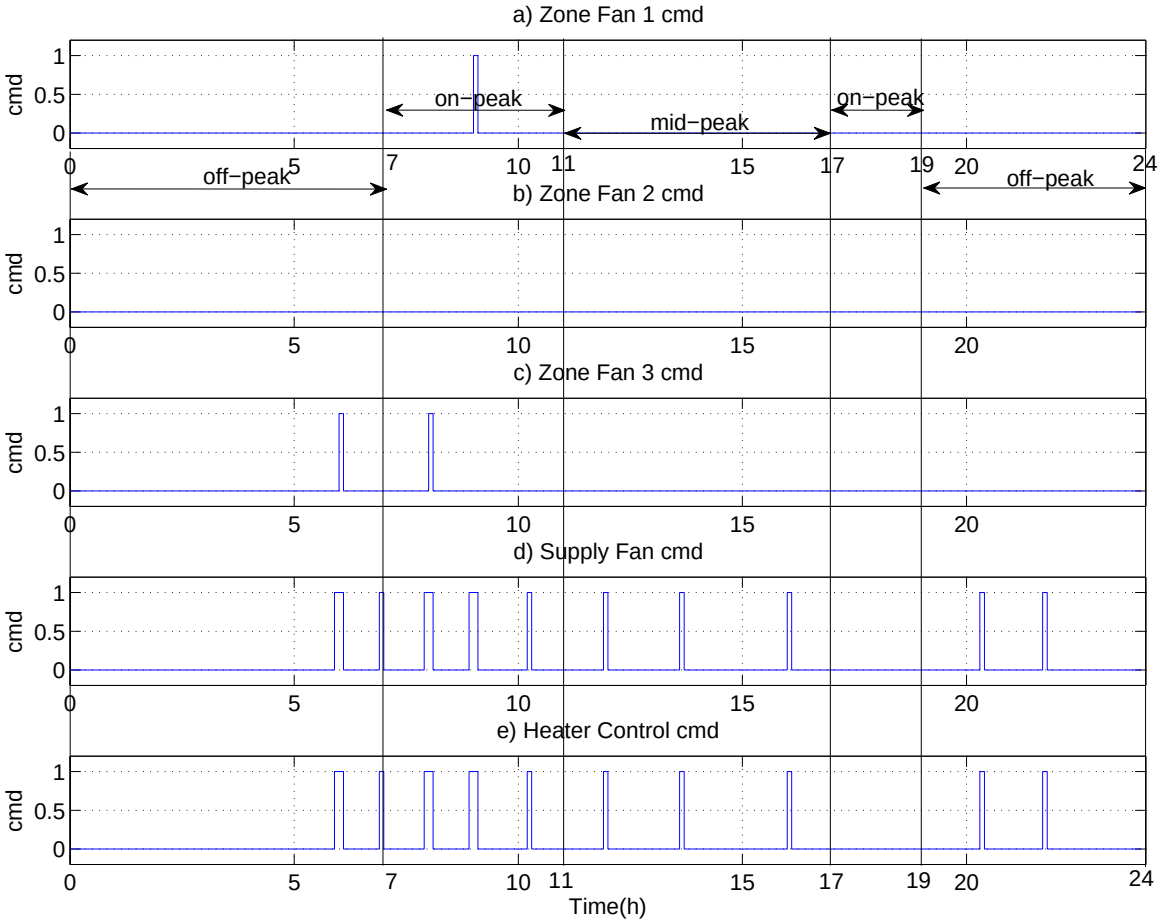

Figure 5.23: Effect of variable temperature limit schedule in Scenario M2: a) Room 1 fan command, b) Room 2 fan command, c) Room 3 fan command, d) Supply fan command, e) Heater unit control command.

5.5 Sensitivity and Uncertainty Analysis

There are many factors that affect the performance of the proposed optimal energy management control system. In this section, we investigate the effect of uncertainty in three parameters, namely heat conductivity, air mass and outside temperature, on the performance of the system. This is achieved by introducing errors in the values

of the parameters used in the optimal control calculations.

5.5.1 Heat Conductivity

The first study focuses on heat conductivity (κ) of the building. The percentage error of the heat conductivity ϕ_{HC} is defined as

$$\phi_{HC} = \frac{\kappa_{usedInPrediction} - \kappa_{actual}}{\kappa_{actual}} \tag{5.23}$$

We introduce the Constraint Satisfaction Ratio (CSR) as the ratio of the number of the sampling points at which the temperatures meet the constraints to the total number of sampling points, as a measure of how well the temperature constraints are satisfied.

Table 5.5 summarizes results of simulations with different error ratios ϕ_{HC}. When the optimal controller underestimates the heat conductivity, the errors are negative ($\phi_{HC} = -30\% \sim 0$). We can observe that the energy cost does not change in these four cases. But some drops in Constraint Satisfaction Ratio (CSR) can be observed, which means the performance is affected due to the mismatch of the predicted heat conductivity. When the optimal controller overestimates the heat conductivity, the error ϕ_{HC} is set as positive. It can been seen from the cases $\phi_{HC} = 0$ and 10% that error in heat conductivity causes more energy consumption without any impact on Constraint Satisfaction Ratio. As the error increases further, the control performance would be affected. However in these cases, the temperature constraints are only violated in a very small fraction of time by the mismatch of the heat conductivity. This robustness can be attributed to the model predictive control strategy in this thesis. The system employs a feedback mechanism by measuring and using the actual room temperatures in the control optimization at every time step to minimize the

impact of the mismatched parameters on system performance.

Table 5.5: Sensitivity of system performance to errors in heat conductivity

	MILP-based MPC control			Hysteresis control				
ϕ_{HC}	Ave-Computation Time Per Opt (s)	Energy Consumption (kWh)	Energy Cost ($)	Energy Consumption (kWh)	Energy Cost ($)	Energy Saving (%)	Cost Saving (%)	Constraint Satisfaction Ratio (CSR)
-30%	6.2470	47.0313	4.7032	50.3162	5.1642	6.53%	8.93%	98.75%
-20%	4.8778	47.0313	4.7032	50.3162	5.1642	6.53%	8.93%	98.89%
-10%	53.9471	47.0313	4.7032	50.3162	5.1642	6.53%	8.93%	99.72%
0	49.05	47.0313	4.7032	50.3162	5.1642	6.53%	8.93%	100%
10%	41.6584	48.1590	4.7486	50.3162	5.1642	4.29%	8.05%	100%
20%	48.8947	48.0995	4.7410	50.3162	5.1642	4.41%	8.19%	99.17%
30%	92.0296	48.0995	4.7410	50.3162	5.1642	4.41%	8.19%	99.17%

The performance of temperatures control and energy cost are also analysed by plotting and comparing the results in three of the cases. Figure 5.24 compares the actual temperature profiles for cases with different error ratios of the heat conductivity. Figure 5.25 shows that the daily energy consumption, cost and the associated savings. It can be seen that overestimation of heat conductivity ($\phi_{HC} = 10\%$) has a more obvious impact on the actual temperature response and energy cost than its underestimation. The reliability and effectiveness would decrease when the error increases.

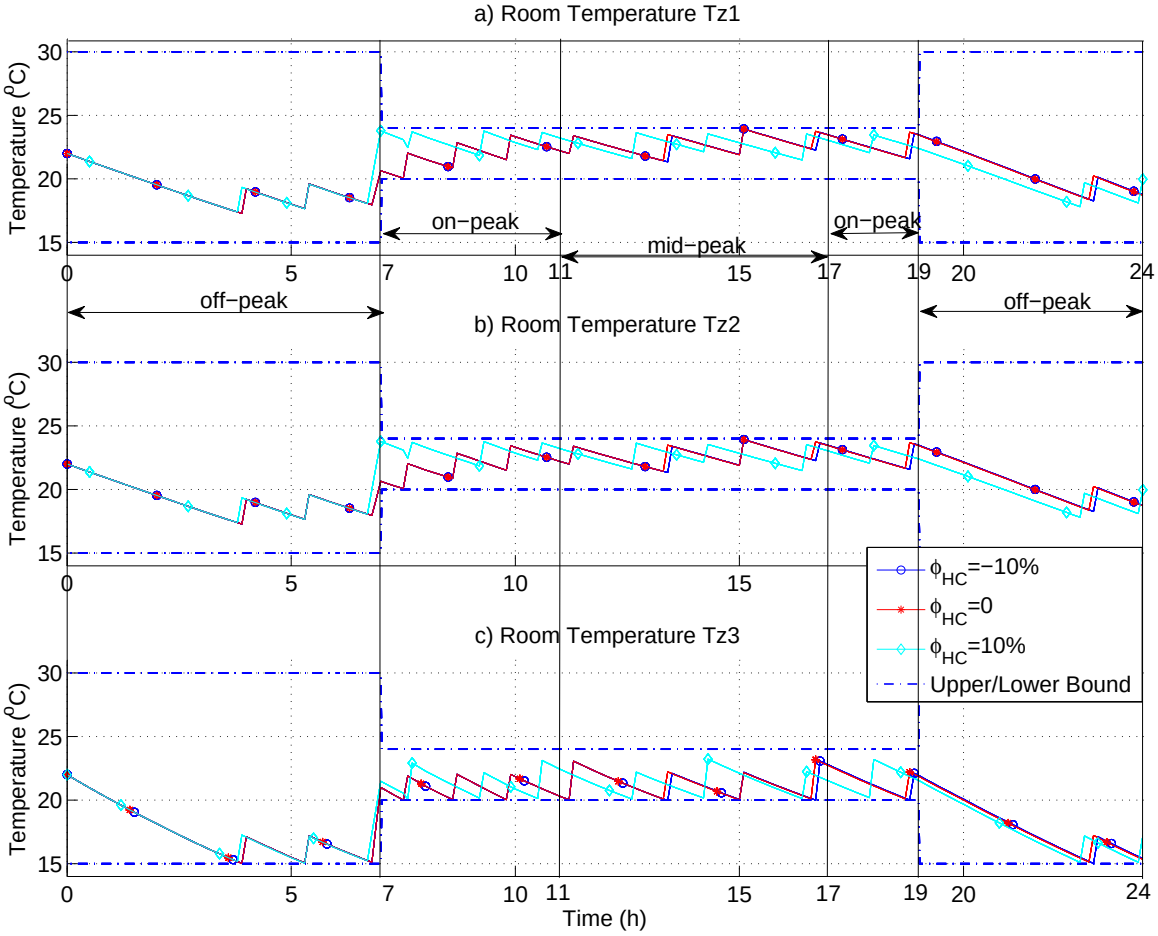

Figure 5.24: Sensitivity of performance with respect to errors in heat conductivity: 24-hour temperature profiles for various ϕ_{HC} in Scenario M2.

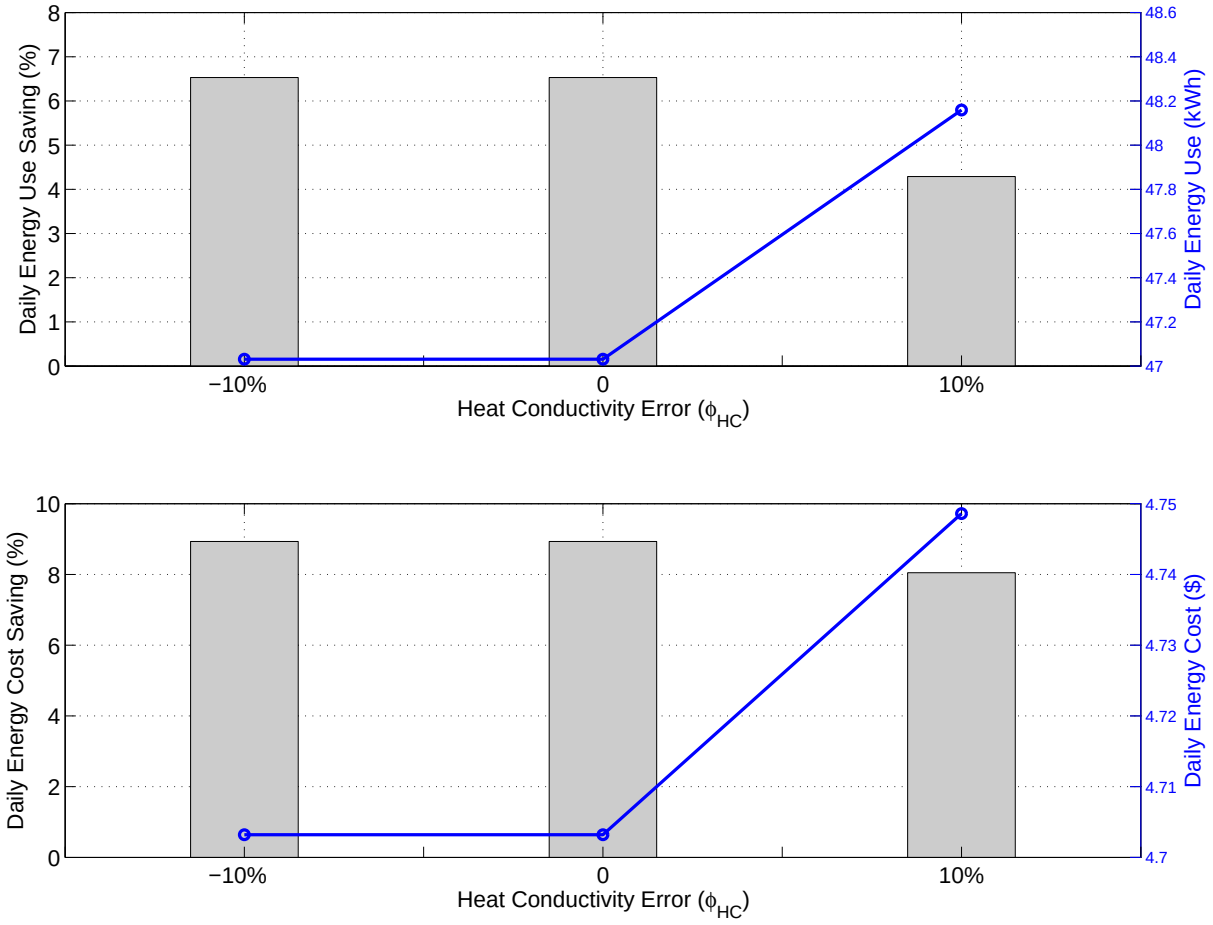

Figure 5.25: Sensitivity of performance with respect to errors in heat conductivity: Daily energy consumption and cost for various ϕ_{HC} in Scenario M2.

5.5.2 Air Mass

In this section, we analyse the sensitivity of the performance of the energy management control system to uncertainty in the building air mass. The percentage error in the air mass ϕ_{AM} is defined as

$$\phi_{AM} = \frac{m_{usedInPrediction} - m_{actual}}{m_{actual}} \tag{5.24}$$

Table 5.6 summarizes the results of simulations with different error ratios ϕ_{AM}. When the building air mass is underestimated by the proposed optimal energy management system, namely $\phi_{AM} = -30\% \sim 0$, it can be observed that system performances are not affected, but energy cost increases as the error increases. Because the underestimation of air mass leads to underestimate the thermal inertia in the building, the room temperatures would be thought to change faster than they actually do. The controller tends to heat more to maintain room temperatures within desired limits when in winter operation. When the optimal controller overestimates the building air mass ($\phi_{AM} = 0 \sim 30\%$), it can be seen that system performance is slightly affected. In these cases, the increasing of energy cost and violations of temperature constraints are negligible when the errors of the building air mass are small ($\phi_{AM} = -20\% \sim 20\%$). There would be an obvious impact on the system performance when the errors increase further. The feedback mechanism of MPC considerably improves the robustness of the proposed energy management system compared to off-line control strategies.

Table 5.6: Sensitivity of system performance to errors in air mass.

	MILP-based MPC control			Hysteresis control				
ϕ_{AM}	Ave-Computation Time Per Opt (s)	Energy Consumption (kWh)	Energy Cost ($)	Energy Consumption (kWh)	Energy Cost ($)	Energy Saving (%)	Cost Saving (%)	Constraints Satisfaction Ratio (CSR)
-30%	106.3296	52.1452	5.2713	50.3162	5.1642	-3.64%	-2.07%	100%
-20%	12.4580	47.0398	4.7048	50.3162	5.1642	6.51%	8.90%	100%
-10%	52.8079	47.0398	4.7043	50.3162	5.1642	6.51%	8.91%	100%
0	49.05	47.0313	4.7032	50.3162	5.1642	6.53%	8.93%	100%
10%	120.5788	47.0228	4.6634	50.3162	5.1642	6.55%	9.70%	99.03%
20%	30.9864	47.0228	4.6629	50.3162	5.1642	6.55%	9.71%	99.03%
30%	20.0539	47.0228	4.6631	50.3162	5.1642	6.55%	9.70%	96.67%

To further demonstrate the impact of error in the air mass on the system performance, the temperature profiles and energy cost are plotted in three of these cases. Figure 5.26 compares the room temperatures for these cases. Figure 5.27 shows the daily energy consumption, cost and the associated savings. We can see that performance of the temperature control is affected more obviously by positive parameter errors than negative parameter errors. Because the overestimation (positive errors) of air mass leads to overestimate the thermal inertia in the building, the room temperatures would be thought to change slower than they do in practice for controller. Under this condition, it is easier for room temperatures to go out of the temperature limits, and the controller tends to heat less to maintain room temperatures within so-called desired limits when in winter operation. That is why the system performance is impaired more obviously in the cases with positive parameter errors.

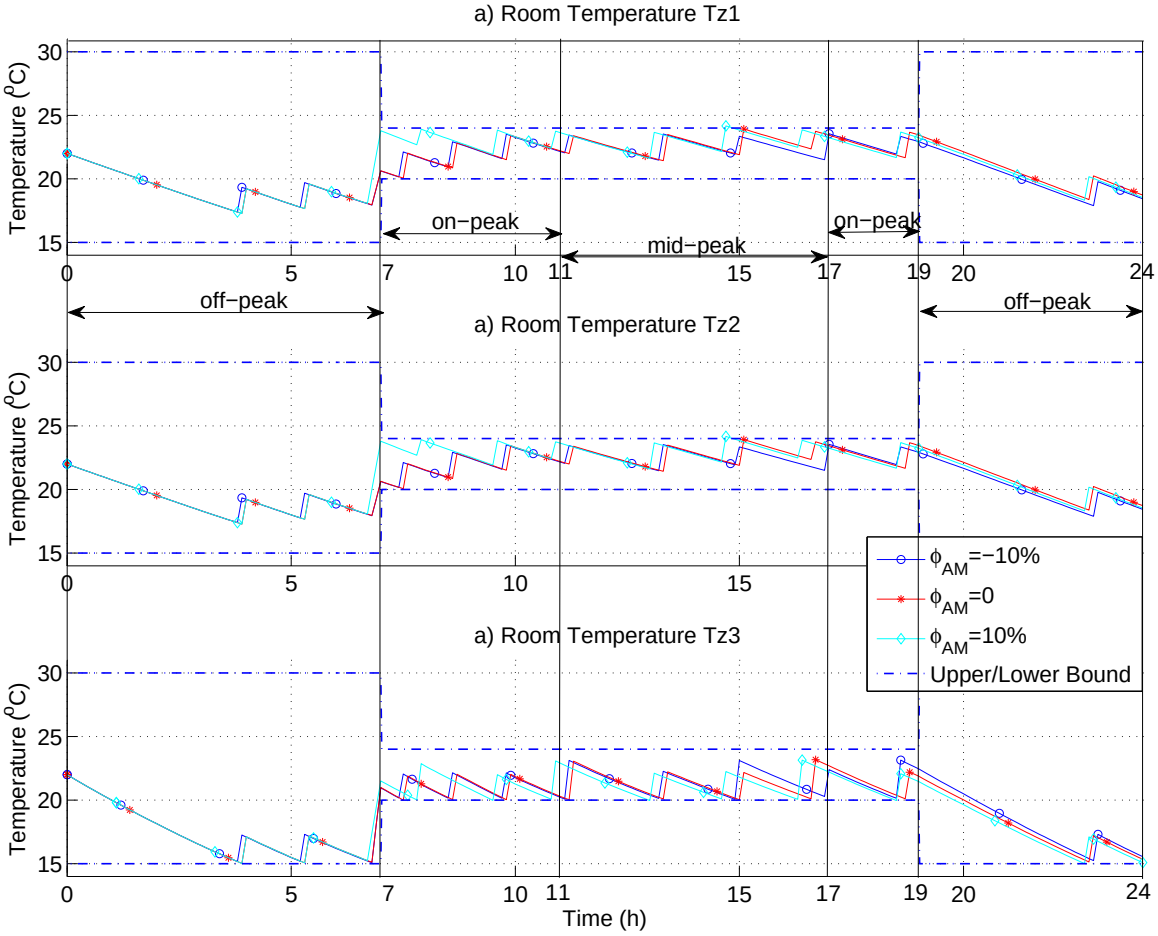

Figure 5.26: Sensitivity of performance with respect to errors in air mass: 24-hour temperature profiles for various ϕ_{AM} in Scenario M2.

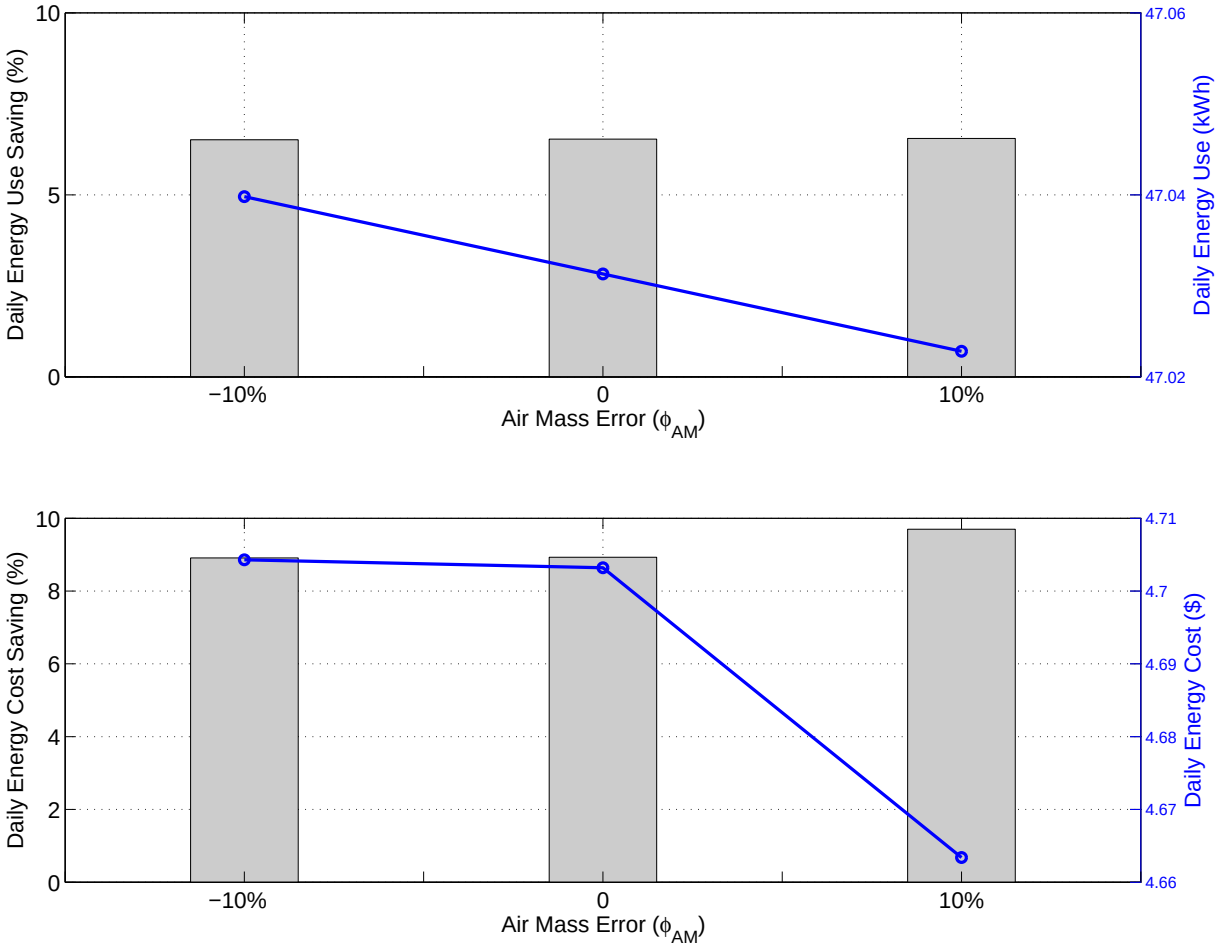

Figure 5.27: Sensitivity of performance with respect to errors in air mass: Daily energy consumption and cost for various ϕ_{AM} in Scenario M2.

5.5.3 Outside Temperature

In this case, the sensitivity of the system performance to errors in outside temperature prediction is studied. Scenario M2 is considered for this analysis. Random temperature errors with mean of 0℃ and standard deviation of 1℃ are added to the temperature predictions, i.e. see Figure 5.28.

Table 5.7 demonstrates the performance of the energy management control system

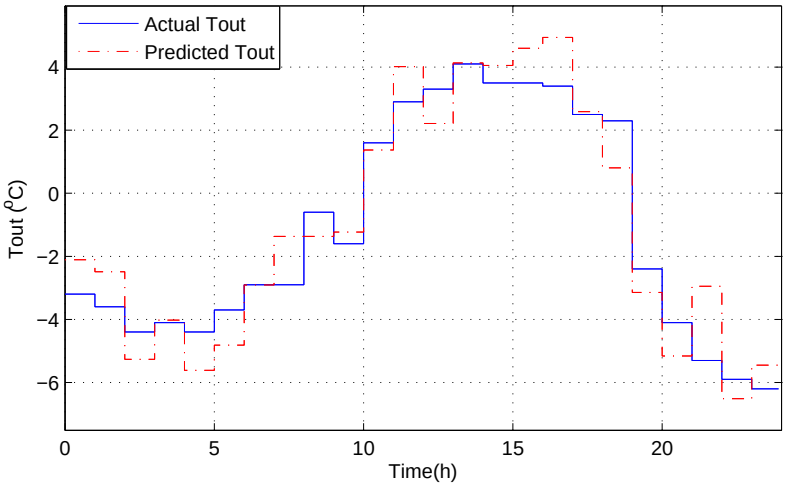

Figure 5.28: 24-hour temperature profile for outside temperatures

in the presence of uncertainty in the outside temperature prediction. As evident from the results in this table, the proposed controller is fairly robust to errors in temperature predictions, although there is a very small degree of temperature limit violation. The room temperature profiles are also presented in Figure 5.29 to show the robustness of the proposed controller. We can see that temperature profile has a very small change when the errors are added to the outside temperature prediction.

Table 5.7: Sensitivity of system performance to uncertainty in outside temperature prediction.

	MILP-based MPC control		Hysteresis control		
Cases	Ave-Computation Time Per Opt (s)	Energy Cost ($)	Energy Cost ($)	Cost Saving (%)	Constraints Satisfaction Ratio (CSR)
Error Added	141.3703	4.7032	5.1642	8.93%	99.86%
Reference Case	49.05	4.7032	5.1642	8.93%	100%

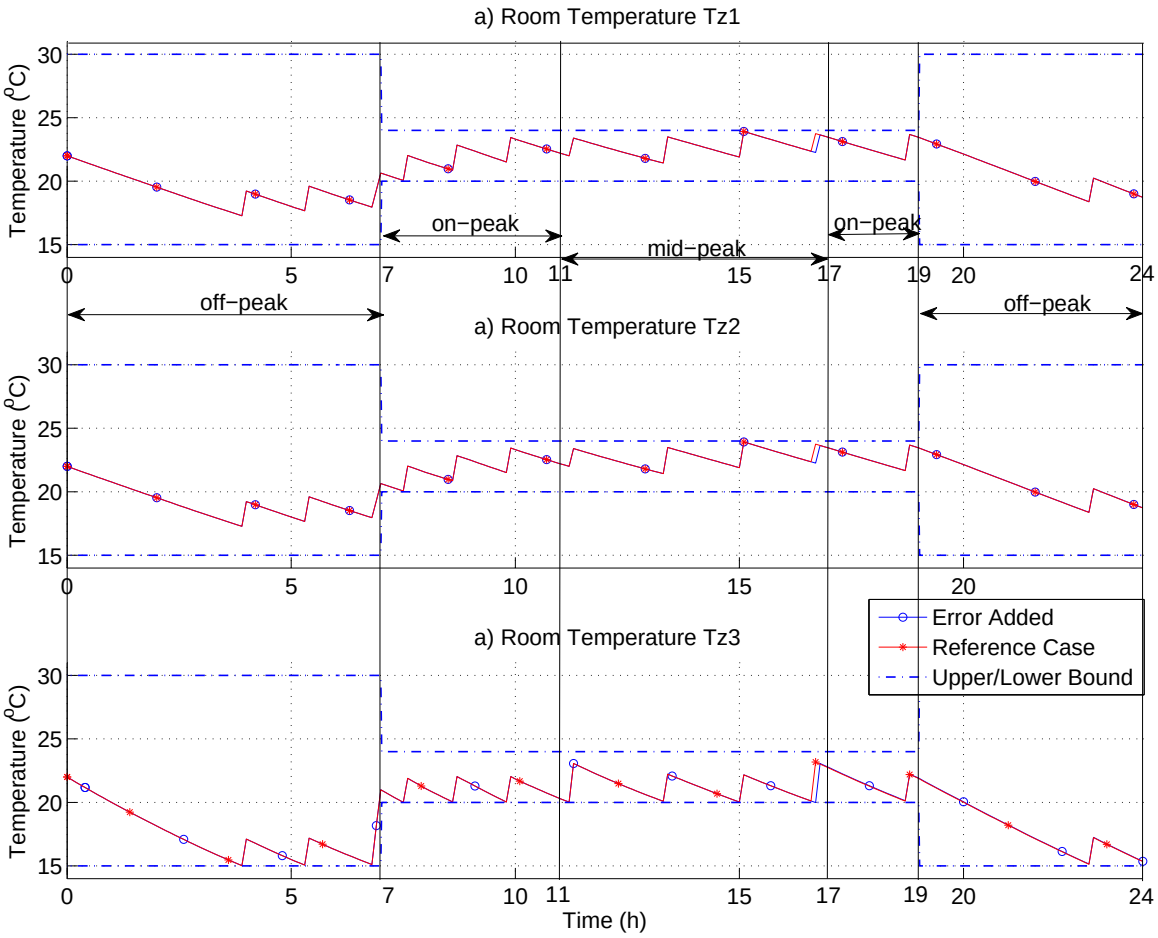

Figure 5.29: Sensitivity of performance with respect to uncertainty in outside temperature prediction: 24-hour temperature profiles in Scenario M2.

Chapter 6

Conclusion and Future Work

6.1 Conclusion

This thesis was concerned with energy management in microgrids with single-zone and multi-zone heating/cooling control. An optimal on-line MPC-type control method was proposed for integrated energy management and HVAC control in a grid-connected microgrid with energy storage. The continuous-time dynamics and discrete-time system models were developed and presented first. Using the discrete-time model of the system, a MILP optimization problem was formulated and solved over the control horizon using a model of the system dynamics and predictions of demand and outside temperature in order to select the optimal values of the control variables, including the fan control commands and battery charge/discharge activities. Only the values corresponding to the first time step, or first finite time steps if applicable, were used to operate the system, and the optimization problem was reformulated and solved in the next time instance by utilizing a rolling horizon mechanism.

Single-zone configuration was studied first, and then was extended to multi-zone control by using auxiliary on-off controllable fans in the so-called temperature zones.

The control strategy maintained temperatures in the zones within upper and lower comfort limits that could be determined based on zone occupancy instead of strictly regulating the zone temperatures. This flexibility of the temperature control was utilized to reduce energy cost by pre-heating/pre-cooling with lower-price electricity energy.

The performance of the system was evaluated in single-zone and multi-zone simulation scenarios. The results of the simulation studies were discussed and presented. Significant energy cost savings and efficiency gains were observed from the application of the proposed controller under the simulated operation scenarios when compared with conventional hysteresis temperature control. The scenarios without storage showed energy cost savings were realized mainly by pre-heating/pre-cooling the building under time-of-use pricing. The proposed optimal energy management system would attempt to use more low-price energy and less high-price energy while meeting the thermal and energy requirements of the building. The scenarios with battery storage illustrated further cost savings for the proposed approach by taking better advantage of the time-of-use pricing and charging-low/discharging-high. The battery was fully used to store low-price energy, then supply energy to HVAC system and other devices during on-peak period.

Some strategies were proposed to reduce the computation time of the proposed controller. The formulation of the optimization problem into a MILP problem, application of variable time steps, and relaxation of some of the binary constraints all contributed to a significant reduction in computation time, making the method suitable for real-time control. The case with variable temperature limit schedules was also studied. It could be observed that temperatures in different zones were maintained within the comfortable temperature ranges, even at the changing points in the limits. Finally, an analysis of the sensitivity of the proposed controller to uncertainty in

some of the major model parameters, including heat conductivity, building air mass and outside temperature was carried out. The system performance was found to be fairly robust with respect to modelling uncertainty from the results of the sensitivity analysis.

6.2 Future Work

There are some possibilities for future research based on the work presented in this thesis as discussed below.

- Other storage elements, such as thermal storage can be considered in problem formulation.
- The islanding mode of the microgrid can be studied, and extension to multiple micro-grid scenarios could be explored.
- Methods can be developed for adaption of the temperature comfort limits and the inclusion of weather related thermal effects such as solar radiation and wind convection.
- On-line estimation of system parameters and their use in the control is another possible direction for future work.
- Finally, a microgrid testbed can be developed to evaluate the performance of the proposed controller in experiment. This is currently a work in-progress in our group.

Bibliography

Anderson, M., Buehner, M., Young, P., Hittle, D., Charles, A., Tu, J., and Hodgson, D. (2007). An experimental system for advanced heating, ventilating and air conditioning (hvac) control. *Energy and Buildings*, pages 136–147.

Bozchalui, M. C., Hashmi, S. A., Hassen, H., Cañizares, C. A., and Bhattacharya, K. (2012). Optimal operation of residential energy hubs in smart grids. *Smart Grid, IEEE Transactions on*, **3**(4), 1755–1766.

Bracco, S., Dentici, G., and Siri, S. (2013). Economic and environmental optimization model for the design and the operation of a combined heat and power distributed generation system in an urban area. *Energy*, **55**, 1014–1024.

Costa, A. and Fichera, A. (2014). A mixed-integer linear programming (milp) model for the evaluation of chp system in the context of hospital structures. *Applied Thermal Engineering*.

Dayton (2005). Ventilation fundamentals. Technical report, Dayton Electric Manufuring Co.

De Oliveira, G., Jacomino, M., Ha, D. L., and Ploix, S. (2011). Optimal power control for smart homes. In *18th IFAC World Congress, elsevier, Ed.*

Deng, Q., Gao, X., Zhou, H., and Hu, W. (2011). System modeling and optimization of microgrid using genetic algorithm. In *Intelligent Control and Information Processing (ICICIP), 2011 2nd International Conference on*, pages 540–544. IEEE.

Guo, L., Liu, W., Cai, J., Hong, B., and Wang, C. (2013). A two-stage optimal planning and design method for combined cooling, heat and power microgrid system. *Energy Conversion and Management*, **74**, 433–445.

GUROBI (2014). Gurobi optimization solver. `http://www.gurobi.com/`.

Handschin, E., Neise, F., Neumann, H., and Schultz, R. (2006). Optimal operation of dispersed generation under uncertainty using mathematical programming. In *International Journal of Electrical Power and Energy Systems*, volume 28, pages 618–626.

Huang, H., Chen, L., Mohammadzaheri, M., Hu, E., and Chen, M. (2013). Multi-zone temperature prediction in a commercial building using artificial neural network model. In *Control and Automation (ICCA), 2013 10th IEEE International Conference on*.

IESO (2014). Time-of-use price periods. `http://ieso.ca/imoweb/siteShared/options.asp?sid=ic`.

Kriett, P. O. and Salani, M. (2012). Optimal control of a residential microgrid. *Energy*, **42**, 321–330.

Lefort, A., Bourdais, R., Ansanay-Alex, G., and Guéguen, H. (2013). Hierarchical control method applied to energy management of a residential house. *Energy and Buildings*, **64**, 53–61.

Lutz, J., Dunham-Whitehead, C., Lekov, A., and McMahon, J. (2004). Modeling energy consumption of residential furnaces and boilders in u.s. homes. Technical report, Energy Analysis Department, Environmental Energy Technologies Division, Ernest Orlando Lawrence Berkeley National Laboratory, University of California.

Malysz, P., Sirouspour, S., and Emadi, A. (2013). Milp-based rolling horizon control for microgrids with battery storage. In *Industrial Electronics Society, IECON 2013-39th Annual Conference of the IEEE*, pages 2099–2104. IEEE.

Malysz, P., Sirouspour, S., and Emadi, A. (2014). An optimal energy storage control strategy for grid-connected microgrids. *Smart Grid, IEEE Transaction on*, **5**(4), 1785–1796.

Marco, S., Squartini, S., Surace, G. P., and Piazza, F. (2014). Smart home task and energy resource scheduling based on nonlinear programming. In *Recent Advances of Neural Network Models and Applications*, pages 175–185. Springer.

Masy, G. (2007-2008). *Definition and validation of a simplified multizone dynamic building model connected to heating system and HVAC unit.* Ph.D. thesis, Ingenieur Civil Architecte.

Mehleri, E., Papageorgiou, L., Markatos, N., and Sarimveis, H. (2012). A model predictive control framework for residential microgrids. In *22nd European Symposium on Computer Aided Process Engineering*, volume 30, page 327. Elsevier.

Morosan, P.-D., Bourdais, R., Dumur, D., and Buisson, J. (2010). A dynamic horizon distributed predictive control approach for temperature regulation in multi-zone buildings. In *Control and Automation (MED), 2010 18th Mediterranean Conference on.*

Mossolly, M., Ghali, K., and Ghaddar, N. (2009). Optimal control strategy for a multi-zone air conditioning system using a genetic algorithm. *Energy*.

Muratori, M., Marano, V., Sioshansi, R., and Rizzoni, G. (2012). Energy consumption of residential hvac systems: a simple physically-based model. In *Power and Energy Society General Meeting, 2012 IEEE*, pages 1–8. IEEE.

OEB (2014). Natural gas rates. `http://www.ontarioenergyboard.ca/OEB/Consumers/Natural+Gas/Natural+Gas+Rates`.

Parisio, A., Rikos, E., and Glielmo, L. (2014). A model predictive control approach to microgrid operation optimization. *Control Systems Technology, IEEE Transaction on*.

Pascual, J., Sanchis, P., and Marroyo, L. (2014). Implementation and control of a residential electrothermal microgrid based on renewable energies, a hybrid storage system and demand side management. *Energies*, **7**(1), 210–237.

Stadler, M. (2008). Distributed energy resources on-site optimization for commercial buildings with electric and thermal storage technologies.

USEIA (2009). Residential energy consumption survey (recs). `http://www.eia.gov/todayinenergy/detail.cfm?id=6570`. U.S. Energy Information Administration.

USEIA (2011). Annual energy review. `http://www.eia.gov/todayinenergy/detail.cfm?id=10251`. U.S. Energy Information Administration.

USEIA (2014). Monthly energy review. `http://www.eia.gov/totalenergy/data/monthly/`. U.S. Energy Information Administration.

Xu, Y., Ji, K., Lu, Y., Yu, Y., and Liu, W. (2013). Optimal building energy management using intelligent optimization. In *Automation Science and Engineering (CASE), 2013 IEEE International Conference on*.

Yang, R. and Wang, L. (2012). Optimal control strategy for hvac system in building energy management. *IEEE*.

Yu, X. (2014). *Optimization and Control of an Energy Management System for Microgrids*. Master's thesis, McMaster University.

Yu, X., Malysz, P., Sirouspour, S., and Emadi, A. (2014). Optimization-based components sizing for microgrid. In *Transportation Electrification Conference and Expo (ITEC), 2014 IEEE*. IEEE.

Zhang, X., Sharma, R., and He, Y. (2012). Optimal energy management of a rural microgrid system using multi-objective optimization. In *Innovative Smart Grid Technologies (ISGT), 2012 IEEE PES*, pages 1–8. IEEE.